On the Modelling and Design of Environmentally Friendly Biochar Production for Soil Application

Thesis by

Yize Li

Submitted in fulfilment of the requirement for
the Degree of Doctor of Philosophy

James Watt School of Engineering
College of Science and Engineering
University of Glasgow

Date of Submission
December 2023

Abstract

Biochar production through pyrolysis of various agricultural wastes has the potential to effectively reduce waste disposal issues and mitigate the potential impact of global warming. This thesis firstly provided a comprehensive review of the state-of-the-art knowledge on the pyrolysis processing of agricultural waste, its influencing factors, and the multifunctional application of biochar. Meanwhile, machine learning modelling, life cycle assessment, multiple-objective optimization are reviewed in the context of advancing biochar production and applications, providing more effective means of optimising processes and assessing environmental impacts. However, existing studies tend to be targeted at individual machine learning models or environmental assessment approaches. From a time- and cost-saving perspective, the process operating parameters and the type of biomass must be appropriately selected to obtain the desired product yield and characteristics. It is necessary to determine the environmental performance of the process before deciding to apply the technology on a large scale. Thus, this thesis has innovatively developed a framework containing life cycle assessment method, machine learning modelling, multi-objective optimisation and multi-criteria decision making. Key aspects of the study included the comparison of machine learning methods for predicting the influences of agricultural waste compositions and process conditions on biochar production. Specifically, Multi-layer Perceptron Neural Network and Gaussian Process Regression models were compared in terms of their accuracy in predicting biochar yields and properties. An environmental impact assessment framework was developed by combining Machine Learning and Life Cycle Assessment to assess the carbon footprint of biochar production and soil application, highlighting the potential of biochar soil application to achieve negative carbon emissions. By combining Multi-Objective Optimization and Multi-Criteria Decision-Making techniques with Life Cycle Assessment, this study also developed a novel

framework to optimise the biochar production process and analysis its environmental impact. Together, this research aimed to support the development of application-oriented biochar process pathways for agricultural waste management and low carbon development, promoting sustainable agricultural practices.

Contents

List of Tables

List of Figures

List of Publications

Publications included in thesis:

1. **Yize Li**, Rohit Gupta, Siming You. "Machine learning assisted prediction of biochar yield and composition via pyrolysis of biomass." Bioresource Technology 359 (2022): 127511.
2. **Yize Li**, Rohit Gupta, Qiaozhi Zhang, Siming You. "Review of biochar production via crop residue pyrolysis: Development and perspectives." Bioresource Technology (2022): 128423.
3. **Yize Li**, Siming You. "Biochar soil application: soil improvement and pollution remediation." Biochar in Agriculture for Achieving Sustainable Development Goals. Academic Press, 2022. 97-102.
4. **Yize Li**, Asam Ahmed, Ian Watson, Siming You. "Waste-to-biofuel and carbon footprints." Waste Biorefinery. Elsevier, 2020. 579-597

Other publications:

1. Yi Fang, Xian Li, Simon Ascher, **Yize Li**, Leilei Dai, Roger Ruan, Siming You. "Life cycle assessment and cost benefit analysis of concentrated solar thermal gasification of biomass for continuous electricity generation." Energy 284 (2023): 128709.
2. Yujie Yang, Enming Huang, Panchan Dansawad, **Yize Li**, Yashi Qing, Changzheng Lv, Lixia Cao, Siming You, Yanxiang Li, Wangliang Li. "Superhydrophilic and underwater superoleophobic PVDF-PES nanofibrous membranes for highly efficient surfactant-stabilized oil-in-water emulsions separation." Journal of Membrane Science (2023): 122044.
3. Panchan Dansawad, Yanxiang Li, **Yize Li**, Jingjie Zhang, Siming You, Wangliang Li, Shouliang Yi. "Machine learning toward improving the performance of membrane-based wastewater treatment: A review." Advanced Membranes (2023): 100072
4. Yi Fang*, **Yize Li***, Asam Ahmed, Siming You. "Development, economics and global warming potential of lignocellulose biorefinery." Biomass, Biofuels, Biochemicals (2021): 1-13.

Acknowledgements

Firstly, I would like to express my deepest gratitude to my supervisor, Dr. Siming You, who has not only been my academic advisor, but also my life mentor during my journey towards my PhD degree. On the road of research, it was his wisdom that lit up my way forward, and it was his patience and support that gave me the courage to stand up again in every scientific confusion. Whether it is his subtle insights in academic discussions or generous guidance in life choices, his words and deeds have deeply influenced me and benefited me for the rest of my life.

I would like to thank my wife, who has been the strongest support in my life. During the years of my studies, she was the one who silently supported me behind the scenes, no matter in the details of life or emotional comfort, she was always my best partner. I am grateful for her selfless love, as well as her understanding and support for my academic pursuits.

To my parents and family, I carry the deepest gratitude. Your love is as silent as spring rain, and it is your support and encouragement that has built my solid spiritual pillar. Since I was a child, you have taught me how to face challenges and how to grow up in the face of adversity. You have been present at every milestone of my PhD career, and I thank you for everything.

I must express my deepest gratitude to my colleagues. It was your support and encouragement that enabled me to overcome many difficulties during the long road of research. I would like to express my special thanks to Dr. Rohit Gupta, whose expertise and invaluable advice have helped me immensely in my research work. Our discussions often led to new ideas and his critical perspective made my research more rigorous.

I must also mention my three cats, Lil High, Luca and Jimo, who have brought endless laughter and soothing moments to my life in their own unique way. They are my most faithful companions during the long days and nights of research, and their company allows me to find a moment of peace even under stress.

No one is alone in their endeavours, and I am grateful for all the visible and invisible help and companionship, which have been the source of strength for this academic journey. I would like to dedicate this achievement to all those who have given me support and encouragement. Thank you.

Declaration

I declare that this thesis is the result of original work done by myself under the supervision of Dr. Siming You, James Watt School of Engineering, University of Glasgow, Glasgow, Scotland.

Printed Name: Yize Li

Signature:

Elements of this research have previously been published in the following places:

1. **Yize Li**, Rohit Gupta, Siming You. "Machine learning assisted prediction of biochar yield and composition via pyrolysis of biomass." Bioresource Technology 359 (2022): 127511.
2. **Yize Li**, Rohit Gupta, Qiaozhi Zhang, Siming You. "Review of biochar production via crop residue pyrolysis: Development and perspectives." Bioresource Technology (2022): 128423.
3. **Yize Li**, Siming You. "Biochar soil application: soil improvement and pollution remediation." Biochar in Agriculture for Achieving Sustainable Development Goals. Academic Press, 2022. 97-102.
4. **Yize Li**, Asam Ahmed, Ian Watson, Siming You. "Waste-to-biofuel and carbon footprints." Waste Biorefinery. Elsevier, 2020. 579-597 -95%
5. **Yize Li,** Rohit Gupta, Wangliang Li, Yi Fang, Jaime Toney, Siming You. “Machine learning-assisted life cycle assessment of biochar soil application.” (Under preparation).

Nomenclature

Definitions/Abbreviations

AC	Activated Carbon
AEC	Anion Exchange Capacity
AI	Artificial Intelligence
Al_2O_3	Aluminium Oxide
ANFIS	Artificial Neuro-Fuzzy Inference System
ANN	Artificial Neural Network
APBO	Aqueous Phase Bio-Oil
C	Carbon
CaO	Calcium Oxide
CBA	Cost Benefit Analysis
Cd	Cadmium
CEC	Cation Exchange Capacity
CO_2	Carbon Dioxide
CP	Conventional Pyrolysis
Cr	Chromium
Cu	Copper
EC	Electrical Conductivity
FAO	Food and Agriculture Organization
FC	Fixed Carbon
Fe_2O_3	Iron(III) Oxide
FU	Functional Unit

GA	Genetic Algorithm
Ga	Gallium
GBA	Gradient Boosting Algorithm
GHG	Greenhouse Gas
GPR	Gaussian Process Regression
GRA	Grey Relational Analysis
GWP	Global Warming Potential
H	Hydrogen
H_2S	Hydrogen Sulfide
Hg^0	Elemental Mercury
HHV	Higher Heating Value
HR	Heating Rate
IPCC	Intergovernmental Panel on Climate Change
K_2CO_3	Potassium Carbonate
KNN	K-Nearest Neighbors
KOH	Potassium Hydroxide
L-C-H	Lignin, Cellulose, and Hemicellulose
LB	Lower Bound
LCA	Life Cycle Assessment
LCI	Life Cycle Inventory
LCIA	Life Cycle Impact Assessment
LSBoost	Least Square Boost
MABAC	Multi-Attributive Border Approximation Area Comparison

MC	Moisture Content
MCCP	Microwave Pyrolysis Combined with Conventional Pyrolysis
MCDM	Multi-Criteria Decision Making
MF	Membership Function
MFC	Microbial Fuel Cell
ML	Machine Learning
MLP-NN	Multi-layer Perceptron Neural Network
MOO	Multi-Objective Optimization
MWP	Microwave Pyrolysis
N	Nitrogen
N_2O	Nitrogen Oxides
Na_2CO_3	Sodium Carbonate
NaOH	Sodium Hydroxide
NH_3	Ammonia
NN	Neural Network
NO_x	Nitrogen Oxides
NPK	Nitrogen-Phosphorous-Potassium
NSGA-II	Non-dominated Sorting Genetic Algorithm II
Obs	Number of observations per second
Pb	Lead
PCC	Pearson Correlation Coefficient
PEM	Proton Exchange Membranes
PROBID	Preference Ranking On the Basis of Ideal-average Distance

PSO	Particle Swarm Optimization
PT	Pyrolysis Temperature
PV	Pore Volume
R^2	Coefficients of Determination
RBF	Radial Basis Function
ReLU	Rectified Linear Unit
RF	Random Forest
RMSE	Root-Mean-Square Error
RT	Residence Time
S	Sulphur
SAW	Simple Additive Weighting
SD	Standard Deviation
SFG	Surface Functional Groups
SO_2	Sulphur Dioxide
Sr	Strontium
SR	Sensitivity Ratio
SVM	Support Vector Machine
Tanh	Hyperbolic Tangent
TiO_2	Titanium Dioxide
TOPSIS	Technique for Order of Preference by Similarity to Ideal Solution
UB	Upper Bound
UN	United Nation
VM	Volatile Matter

XGB	eXtreme Gradient Boosting
Zn	Zinc
ZnO	Zinc Oxide
Zr	Zirconium

Chapter 1 Introduction

1.1 Background

The Intergovernmental Panel on Climate Change (IPCC) has presented evidence indicating a significant rise in global temperatures over the past three decades, with an approximate increase of 0.78°C. This emphasises the urgent need to limit the temperature rise to mitigate the adverse impacts of global warming. Effective reduction in Greenhouse Gas (GHG) emissions is necessary to achieve the net-zero target established by the IPCC [1]. However, mitigating climate change requires not only reducing GHG but also the withdrawal of atmospheric Carbon Dioxide (CO_2). The utilisation of biomass waste is one of the feasible methods to facilitate the fulfilment of the net-zero target. Globally, about 140 Gt of biomass waste is generated annually, which poses a major management problem, as directly discharged biomass can negatively impact the environment [2]. Recently, agricultural waste has received significant attention, as the increasing demand for food and farmland resources by a growing population leads to the intensification of agricultural activities. Significant emissions from direct discharge and subsequent combustion of agricultural wastes deplete soil organic matter and micronutrients, leading to soil degradation and increasing GHG emissions, contributing to air pollution and climate change [3]. In numerous developing countries, most agricultural wastes are not utilised or disposed of but are left to decompose naturally in the field or openly combusted. This results in air pollutants such as Hydrogen Sulfide (H_2S), Sulphur Dioxide (SO_2) and Ammonia (NH_3) emissions and limited resource utilisation efficiency [4]. About 21 per cent of GHG emissions have been recorded as coming from agricultural activities, which negatively affects the environment and human health [5]. Subsequently, recent research has focused on developing new approaches for environment-friendly bioresource recovery from agricultural waste towards achieving global net-zero goals.

Agricultural waste can be converted to various value-added products via thermochemical or thermophysical treatments. Among them, pyrolysis is a thermochemical process that involves the heating of carbon-rich materials (*e.g.*, crop residues, animal manure, woody waste *etc.*) in an inert atmosphere to generate biochar, bio-oil, and gas as value-added products [6]. There are six major types of pyrolysis technologies: fast pyrolysis, flash pyrolysis, slow pyrolysis, vacuum pyrolysis, hydro-pyrolysis, and Microwave Pyrolysis (MWP). These technologies differ by their Heating Rate (HR), Pyrolysis Temperature (PT), Residence Time (RT), reaction environments, and heating methods. In general, different pyrolysis technologies produce varying proportions of value-added products [7]. For example, the fast, flash, and vacuum pyrolysis processes favour the production of bio-oil, while hydro-pyrolysis mainly produces gas under high pressure and in a hydrogen atmosphere [8,9]. Among these technologies, slow pyrolysis is promising for biochar production [10,11].

Biochar, being a carbon-rich material has been utilized in a wide variety of applications due to important characteristics such as high carbon (C) content, N content and structural stability [12]. It has the potential for carbon sequestration by effectively removing carbon from the atmospheric carbon cycle and transferring it to long-term storage in the soil [13]. The performance of biochar in these applications and associated environmental impacts is contingent upon the physicochemical properties of biochar that are closely related to pyrolysis process conditions and the composition of feedstocks [14,15]. The environmental benefits (or drawbacks) of a biochar production technology are strongly interlinked with the selection of feedstock, operating conditions, reactor

specifications, and targeted applications, which necessitates adopting a whole-system approach for rapid process design and optimization.

Over the past decades, the prediction of biochar pyrolysis processes has relied heavily on theoretical models. They are based on theoretical frameworks and principles derived from empirical observations, mathematical proofs, or logical reasoning. These models typically attempted to describe the underlying mechanisms of the biochar production process. Despite the value of these models in complex process design, their semi-empirical nature and computational complexity have limited their widespread use in biochar production prediction. Comparatively, empirical correlation methods are constrained by experimental conditions and biomass range, making it difficult to generalise their use [16]. However, with the large amount of pyrolysis experimental data and the development of Artificial Intelligence (AI) technology, data-driven modelling has become popular. Machine learning (ML) models are data-driven and they learn patterns from large datasets and use this learnt information to make predictions or decisions without explicit programming for the task. Major model types include Neural Network (NN), Support Vector Machine (SVM), Random Forest (RF), K-Nearest Neighbors (KNN), Gradient Boosting Algorithm (GBA), Tree regression, Ensembles, Artificial Neuro-Fuzzy Inference System (ANFIS), and Gaussian Process Regression (GPR) [17]. These models have data prediction ability and short computation time and can effectively handle complex data trends.

Data-driven ML model has become an advanced approach for processing complex data and building efficient predictive models. Meanwhile, Multi-Objective Optimization (MOO) method is widely used to solve complex problems that require simultaneous consideration of multiple

objectives or evaluation criteria. The core idea of MOO is to find trade-offs among different objectives to achieve optimal performance in each aspect [18]. To further guide and refine the decision-making process, Multi-Criteria Decision Making (MCDM) provides an integrated approach for evaluating and selecting the best solution (especially among multiple feasible solutions). Combining ML with MOO and MCDM offers a practical approach to extracting information from data, optimising multiple objectives, and incorporating multi-criteria evaluation to develop informed decisions [19]. However, this combination is not simply a stack of technologies. Thus, the effectiveness of the overall approach will be evaluated in conjunction with the biochar applications when integrating ML, MOO and MCDM.

Biochar soil applications in climate change mitigation strategies contribute to food security by effectively managing agricultural waste and using it as a soil amendment. The soil application of biochar combats climate change by directly increasing the soil carbon storage and reducing N_2O emissions, and indirectly by improving soil fertility and reducing the need for chemical fertilisers and promoting efficient N cycling in terms of its use as a N fertiliser substitute. Both reflect the important role of biochar in sustainable agriculture and environmental protection. Meanwhile, biochar promotes soil microbial diversity by improving soil quality, crop drought tolerance and nutrient utilisation, thereby supporting effective agricultural practices, increasing crop yields and contributing to food security. It is also key to maintaining healthy soil conditions for No Poverty and Zero Hunger as part of the United Nation (UN) Sustainable Development Goals [20]. Hence, there has been significant research on biochar production and soil application in the past decade. Two of the most promising advantages are its carbon sequestration potential and the ability to serve as a substitute for N fertiliser. It can remain in the soil environment for decades or longer and

significantly reduce/delay carbon emissions from biomass. From a carbon sequestration perspective, the application of biochar is a potential climate change mitigation strategy [21]. On the other hand, the application of biochar to soil can also reduce the need for N fertiliser. Biochar has been shown to have the ability to enhance soil nutrient retention, which can provide a source of slow-releasing N for crops to increase crop growth. In addition, GHG emissions associated with N fertiliser production and application can be indirectly reduced through the replacement of N fertiliser by biochar [22].

Life Cycle Assessment (LCA) is an essential tool in environmental management, providing a comprehensive approach to assessing the environmental impact of a product, process, or service from "cradle to grave". By providing a comprehensive plan for the entire life cycle, from raw material extraction to end-of-life disposal, LCA reveals the holistic and breakdown environmental impacts of processes and applications. It also can help identify the key "hotspots" to improve the environmental impacts of a product, process, or system. Since the late 1990s, ISO has been working to coordinate the LCA process and developed ISO 14040 series standards. Using LCA, it is possible to determine all energy requirements, material requirements, and environmental emissions related to the product's manufacturing, transportation, application, and disposal phases throughout its life cycle. LCA consists of four phases: goal and scope definition, Life Cycle Inventory (LCI), Life Cycle Impact Assessment (LCIA), and Life Cycle Interpretation [23,24]. LCA is increasingly used to assess the environmental footprint of biochar soil systems and to reveal their potential as sustainable soil amendments. It allows the overall environmental impact of biochar production to be measured, from the source of the biomass to pyrolysis and its subsequent

soil application. LCA approach is essential for identifying issues that need to be improved and ensuring that biochar applications are in line with sustainable development goals [25].

During the last decade, there has been an increasing amount of research on ML and LCA for biochar production and its application in soils. However, not just considering each method in isolation but integrating each method into a comprehensive framework has attracted significant interest and shows great potential for fulfilling the research gap. A more comprehensive and refined integrated framework is needed to understand biochar production and its applications. In this study, ML was integrated with MOO- MCDM, then subsequently with LCA. Developing this integrated framework provides an in-depth understanding of the process efficiency and environmental benefits of biochar systems.

1.2 Research Aim and Objectives

This study aims to provide a comprehensive assessment of the production process and properties of biochar, as well as its benefits and potential for soil applications. By analysing in depth how biochar improves soil quality and exploring its contribution to environmental sustainability, it aims to provide sustainable solutions for agricultural waste treatment, as well as assessment for biochar carbon sequestration potential and reduction of GHG emissions. To achieve the research aims and objectives, this study proposed a framework that integrates ML modelling, LCA and MOO-MCDM. The framework aims to assess the production and application processes of biochar and optimise their environmental benefits. Firstly, the high accuracy and comprehensive ML models were designed to predict the biochar yield and its properties. Then, through MOO-MCDM, the optimal process condition solutions were selected. Finally, LCA was utilised to quantify the Global

Warming Potential (GWP) of biochar in soil applications. Thus, the core objectives of this study can be summarised as follows:

- To identify and discuss the impact factors affecting biochar production and properties, which include PT, RT, HR, Fixed Carbon (FC), Volatile Matter (VM), ash.
- To build high accuracy ML models to predict biochar yield and properties, and to explore the importance level between different factors on biochar yield and properties.
- The ML model is to be combined with MOO-MCDM to explore the optimised pyrolysis conditions and the properties of the feedstock to achieve a relatively optimal solution of biochar yield and properties.
- The optimised solution of biochar yield and properties will be coupled with the LCA approach to assess the environmental impacts of biochar soil application to to assess the production and application processes of biochar to optimise its environmental benefits.

1.3 Thesis Outline

This thesis is constructed as an alternative format thesis. Chapters 2 to 5 are based on manuscripts that have been published or are intended for publication. Fig. 1-1. illustrates the components of this study, and the structure of the thesis.

In Chapter 2, The impact of biomass composition on biochar production is explored, and different pyrolysis reactions and their technical characteristics are reviewed in detail. Subsequently, the impact of pyrolysis parameters on biochar yield and properties is analysed. Furthermore, an in-depth review of advanced biochar applications, including biochar stability, LCA, ML modelling and other state-of-the-art applications, is provided. Also, it reveals the key challenges in biochar production and application.

In Chapter 3, two data-driven ML models based on Multi-layer Perceptron Neural Network (MLP-NN) and ANFIS are developed. The data-driven models predict biochar yield and compositions from a variety of input feedstock compositions and pyrolysis process conditions. Feature importance assessment of the input dataset revealed their competitive significance for predicting biochar yield and compositions.

In Chapter 4, a framework combining ML modelling and LCA is presented to assess the carbon footprint of biochar soil applications. Five ML models are developed to predict the yield and properties of biochar, and the performance of five different models is assessed. The optimised model prediction results are further applied to the LCA of biochar soil applications. An environmental impact analysis is conducted considering biochar produced at different PTs for two fertiliser substitution scenarios, as well as carbon sequestration potential.

In Chapter 5, an integrated ML-MOO-MCDM-LCA framework is developed. The optimization strategy is provided for pyrolysis-based biochar production and soil application with the consideration of environmental impacts and process efficiency. The ML models in Chapters 3 and 4 provide the necessary predictive data to support the LCA in the framework. The optimised biochar production parameters were applied in the LCA to analyse the GWP of the optimal scenario which was then compared with the baseline scenario shown in Chapter 4.

Chapter 6 summaries the outcomes of the research, makes recommendations based on the issues arising from the research and gives ideas for future work desired.

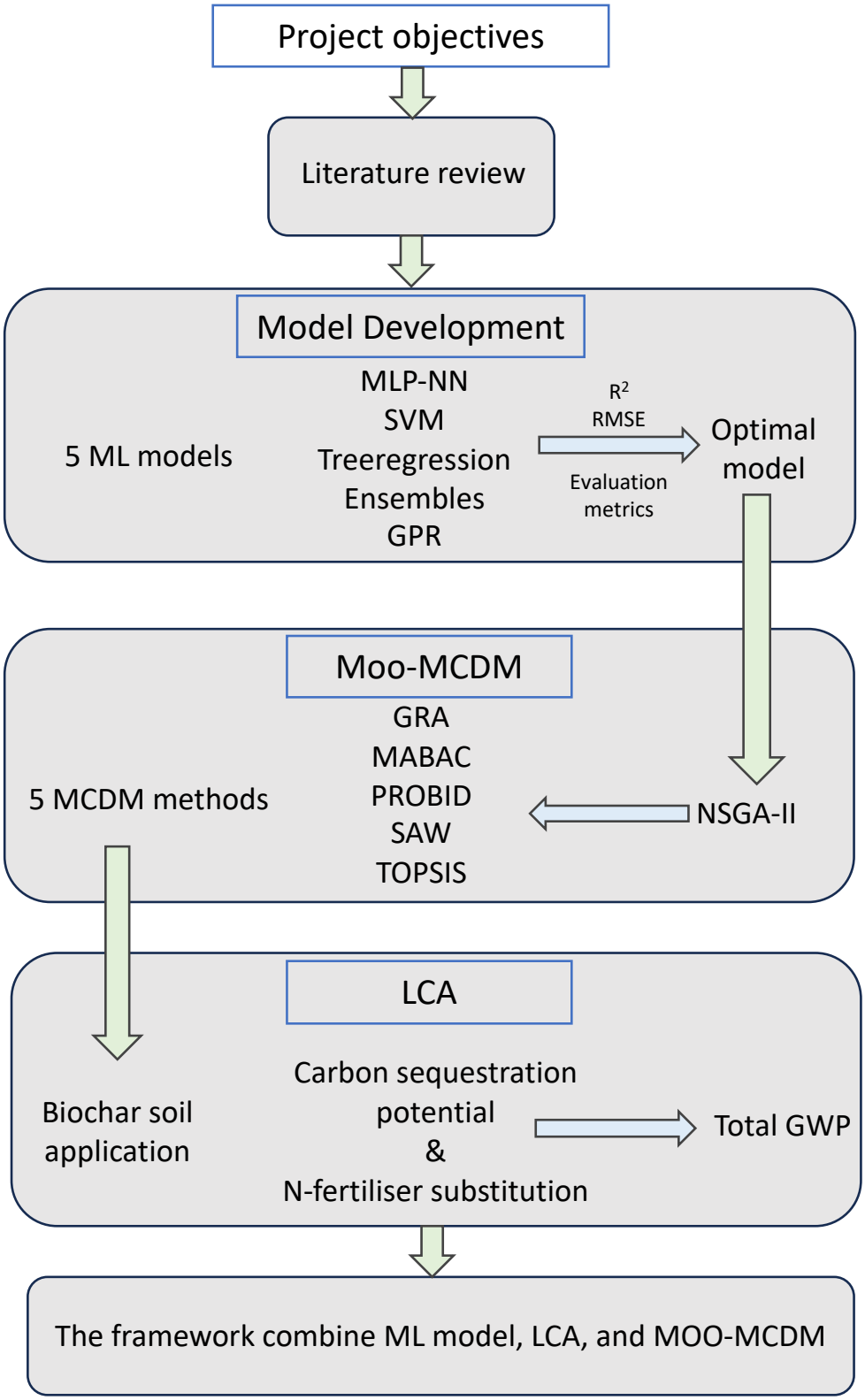

Fig. 1-1. Project flow chart, including the different stages of the study and the analytical methods used. The arrows indicate how the processes are interrelated.

Chapter 2 Literature Review

The Chapter is based on the publication "**Yize Li** *et al.* "Review of biochar production via crop residue pyrolysis: Development and perspectives." Bioresource Technology (2022): 128423".

2.1 Agricultural Waste

The composition of feedstocks plays a vital role in biochar production and determines the final product characteristics and quality [26]. Compared to woody biomass and organic waste (*e.g.*, manure, sewage sludge, and compost), agricultural wastes have low ash contents, high calorific values, and fewer voids [27]. A wide variety of agricultural wastes can be utilized as feedstock for pyrolysis-based biochar production (See Table 2-1). Proximate, ultimate, and lignocellulosic are the three main compositional metrics for agricultural wastes. The proximate composition of biomass includes FC, VM, ash, and MC. For most agricultural waste feedstocks, FC, VM, ash, and MC content are in the ranges of 3–26%, 65–90%, 1–15%, and 0–10%, respectively (see Table 2-1). FC, VM, ash content and MC are critical in affecting the pyrolysis process and the production biochar, and this section focuses on how agricultural waste composition affects biochar composition. How the composition of biochar affects its application will also be discussed. The feedstock type predominantly influences the FC and ash contents of biochar. Among these compositions, ash and VM contents are critical factors for biochar when utilized for soil amendment applications [28], whilst biochar with a high ash content shows great potential as a catalyst for thermal conversion technologies. Nevertheless, a high ash content of biochar may be undesirable for adsorption-related applications, since it can limit the accessibility of adsorption sites on biochar surface and a high ash content often reduces the micropore surface area. Generally, agricultural wastes have lower ash contents than organic waste, which leads to higher SSA and porosity in agricultural wastes-based biochar [29]. The FC content of biochar is a key parameter

in assessing its stability and potential for sequestering atmospheric carbon. Moreover, MC can significantly affect harvest, transport, storage, and biochar production [30]. Intuitively, a lower value of MC is favourable for transportation and storage purposes due to significant volume reduction and is generally good for achieving higher energy efficiency for pyrolysis.

Another important compositional aspect is the ultimate composition, which includes C, H, O, N, and S. Among all these elements, C has the highest proportion in most biomass followed by O and H, accounting for 40–65%, 25–50%, and 5–10%, respectively (See Table 2-1). Besides, the negligible amount of S and N in raw agricultural biomass indicates that limited toxic gases (H_2S and N_2O) are emitted during the pyrolysis process. The C content of biochar depends on the types of feedstocks, and agricultural wastes-based biochar generally has a higher C content than organic wastes such as manure and sewage sludge [27]. It was reported that higher C and O contents in feedstocks could result in higher yields and the net calorific value of biochar [31]. The H/C and O/C ratios in produced biochar determine its stability, aromaticity, and polarity. The decrease in H/C and O/C ratios corresponds to the high aromaticity and low polarity of biochar, suggesting that the biochar has excellent resistance to microbial decomposition, making it a strong contender in the MFC industry [32]. The N content of biochar is a critical factor for its fertiliser application. A high content of macromolecular amino acids and proteins in the feedstock will result in a high N content in biochar. Among agricultural waste, woody biomass and organic wastes, the N content of agricultural waste is normally higher than woody biomass and lower than organic wastes [33].

The structural composition of agricultural wastes is quantified by Lignin, Cellulose, and Hemicellulose (L-C-H) contents, which strongly regulate biochar yields and properties. The L-C-

H of agricultural biomass is in the range of 9–27%, 28–47%, and 11–39%, respectively [34,35]. They decompose in the temperature range of 200 to 500 °C, 300 to 380 °C, and 200 to 300 °C, respectively [34]. The degradation of L-C-H with increasing PT leads to an increase in gas yields (*e.g.*, CO, CO_2, CH_4, and H_2), indicating a decrease in biochar yields. Meanwhile, the pyrolysis rate increases when cellulose and hemicellulose contents are higher than lignin, which results in high bio-oil and low biochar yields [36]. However, The SSA and porosity of biochar are higher if there is a higher lignin content in feedstock [29].

Table 2-1. The proximate and ultimate analysis of various crop-based biomass (db: dry basis).

Feedstock	FC (% db.)	VM (% db.)	Ash (% db.)	MC (% db.)	C (% db.)	H (% db.)	O (% db.)	N (% db.)	S (% db.)	Refs
Corncob	12.45	82.38	5.04	0	47.4	5.8	50.1	0.6	0.1	[37]
Corn stalk	14.68	82.42	2.91	0	43.6	5.8	49.4	1.1	0.1	[37]
Corn stover	8.93	82.21	8.86	0	43.28	5.92	39.32	1.96	0.66	[38]
Sugarcane bagasse	8.87	81.23	2.51	7.39	49.26	5.26	44.95	0.43	0.1	[39]
Coconut shell	11.10	75.50	3.20	10.10	64.23	6.89	27.61	0.77	0.50	[40]
Coconut fiber	11.10	80.85	8.05	0	47.75	5.61	45.51	0.90	0.23	[40]
Wheat straw	9.93	80.7	9.37	0	42.95	5.64	40.51	0.76	0.78	[38]
Rice husk	11.44	73.41	15.14	0.01	41.92	6.34	-	1.85	0.47	[41]

Rice straw	10.06	76.87	13.07	0	40.06	5.47	40.23	0.69	0.48	[42]
Rape stalk	7.49	86.09	6.42	0	43.92	5.92	42.54	0.49	0.71	[38]
Cassava stem	16.07	81.51	2.42	0	44.47	5.82	48.88	0.01	0.83	[35]
Cassava rhizome	9.08	83.64	7.28	0	41.78	5.97	51.07	0.26	0.92	[35]
Cotton stalk	10.17	82.38	7.45	0	43.95	5.81	41.12	1.12	0.56	[42]
Banana leaves	16.92	84.82	6.72	0	43.50	6.20	42.30	0.80	0.90	[43]
Sugarcane straw	3.22	87.61	9.17	3.12	41.88	5.87	41.72	0.47	-	[44]
Barley straw	11.83	78.8	6.43	2.94	45.41	6.1	46.21	1.18	-	[45]
Flax straw	11.4	81.3	2.9	4.4	44.4	6.7	46.5	1.4	1.2	[46]
Maize cobs	25.51	72.95	1.54	0	46.92	6.08	44.86	0.61	-	[47]
Maize husk	22.79	74.24	2.97	0	44.96	6.02	45.57	0.48	-	[47]
Maize leaves	22.73	67.78	9.49	0	43.68	5.82	39.88	1.06	0.06	[47]

2.2 Pyrolysis Technologies

Based on the choice of agricultural wastes feedstock for pyrolysis, appropriate pyrolysis technology must be selected for optimal biochar production in terms of (*e.g.*, process efficiency, economics, environmental impacts, *etc*). This review focuses on six major types of pyrolysis technologies: fast, slow, flash, vacuum, MWP, and hydro pyrolysis depending on operation conditions (see Table 2-2).

Table 2-2. Different types of pyrolysis processes and associated reaction parameters.

Technology	Fast	Slow	MWP	Flash	Vacuum	Hydro
Pressure (Mpa)	0.1	0.1	0.1-0.3	0.1	0.01-0.10	10-17
RT (s)	0.5-10	300-7200	<30	<1	<1	60-120
HR (°C/s)	10-200	0.1-1	0.5-2	>1000	0.1-1	10-300
PT (°C)	500-1200	300-600	300-700	900-1300	300-700	350-600
Gaseous environment	Inert	Inert	Inert	Inert	Inert atmosphere under vacuum	Hydrogen
Refs	[8,48,49]	[13,36,49–51]	[11,52,53]	[49,54,55]	[9,56–58]	[59–62]

2.2.1 Slow Pyrolysis

Slow pyrolysis is operated at a relatively low HR (0.1 to 1 °C/s) and long RT (300 to 7200 s), while having PT in the range of 300 to 700 °C [13]. The low HR reduces secondary pyrolysis and thermal cracking of biomass, favouring biochar formation as the main product [50]. Biswas *et al.* [41] carried out slow pyrolysis experiments for four types of agricultural wastes that were converted to bio-products. In the experiments, the PT was within the range of 300–450 °C, while the RT and HR were kept constant (RT = 3600 s and HR = 0.33 °C/s). Among the four feedstocks (corn cob, rice straw, rice husk, and wheat straw), rice husk achieved the highest biochar yield (43.3%) at 300 °C. Furthermore, the biochar yield decreased from 43.3% to 35.0% when the PT increased

from 300 to 450 °C. Zhang *et al.* [51] utilized slow pyrolysis of agricultural wastes such as wheat, corn, rape, and rice straws to produce biochar. The associated PT was varied within the range of 300–600 °C, while the HR and RT were fixed at 0.17 °C/s and 3600 s. For the different types of feedstocks, the effects of PT on biochar yield were similar, and the biochar yield decreased for higher values of PT. For instance, the highest biochar yield was 51.4% from rice straw at 300 °C, while the lowest biochar was 27.32% at 600 °C from rape straw.

2.2.2 Microwave Pyrolysis

MWP is an emerging technology for efficient biomass conversion into value-added bio-products. Unlike Conventional Pyrolysis (CP), the heating energy is supplied via microwaves that penetrate the feedstocks, and cause their internal molecules to vibrate *i.e.*, phononic oscillations non-intrusively [63]. The MWP parameters that significantly influence product yields and characteristics include microwave power, amount and concentration of microwave absorber, initial MC, purge gas flow rate, and RT [64].

There have been several studies to assess the influences of parametric changes toward the efficacy of MWP-based processes. For instance, canola and wheat straws were pyrolysed under variable PTs (300, 400, and 500 °C) with a microwave frequency of 2.45 GHz [11]. As the PT increased, the biochar yield decreased while the thermal stability of the derived biochar increased. Besides, the biochar produced at 500 °C was more favourable for use as a soil conditioner with the highest carbon stability, while the biochar prepared at 300 °C showed the greatest affinity for inorganic and polar organic pollutants due to its highest polarity, which could be used as an adsorbent. This suggests that by tuning the MWP parameters, the resultant biochar can be tuned for a bespoke application. Li *et al.* [53] proposed a new approach by combining conventional pre-pyrolysis with

MWP to produce biochar from the cotton stalk. Experiments were conducted within a PT range of 250–450 °C while lowering the ramp-up time from 124 to 20 s (compared to MWP). This is synergetic to increase the HR in the case of CP processes. By adopting this strategy, the biochar yield was increased from 21% to 33% (compared to MWP) with a high C content (>70%). The biochar produced by MWP is also featured by a higher SSA and adsorption ability than those derived via CP. According to a latest study, where the corn stalk was irradiated for 600 s within a power range of 100–600 W, the maximum SSA of the produced biochar was 325.2 m^2g^{-1}, which could adsorb aromatic hydrocarbons (*e.g.*, 54.75 mg/g benzene and 48.73 mg/g o-xylene) [65].

2.2.3 Fast and Flash Pyrolysis

Fast pyrolysis is featured a high HR (10–200 °C/s), during which biomass is prone to be converted to liquid products over biochar formation [8]. The PT is within the range of 500–1200 °C, at which thermal cracking occurs, and the RT is controlled within the range of 0.5–10 s to reduce char formation [48,49]. Flash pyrolysis being a variation of fast pyrolysis has a higher HR (>1000 °C/s) and PT (>900 °C) [54]. The high HR combined with the high PT and short RT (<1 s) result in high bio-oil and low biochar yields. Both fast and flash pyrolysis are unfavourable for biochar production. Although fast and flash pyrolysis do not favour biochar formation, the biochar formed by these methods has higher SSA than that derived through slow pyrolysis. As the solid matrix of the biochar contracts at elevated temperatures, its initially larger pores diminish in size. This compaction effect consequently increases the SSA of biochar, as more SSA is encapsulated within smaller pores. Additionally, this enhances the accessibility of diffusion and reaction sites, as more reactive sites become readily exposed to the surrounding environment [66].

2.2.4 Vacuum Pyrolysis

Vacuum pyrolysis utilises a reactor operating in a sub-atmospheric pressure regime to thermally degrade the feedstock in the absence of O. The pressure, PT, and HR were reported to be in the ranges of 0.01–0.20 MPa, 300–700 °C, and 0.1–1 °C/s, respectively [56,67]. Due to the inhibition of secondary degradation, which is essential for biochar production, the vacuum pyrolysis reaction produces high yields of bio-oil [9]. This is attributed to the disproportionate removal of VM at a higher PT, generating higher levels of heating and thus higher levels of biomass decomposition. For vacuum pyrolysis, raising the PT lowers the biochar yield which is synergistic with other types of pyrolysis [58].

2.2.5 Hydro-Pyrolysis

Hydro-pyrolysis is with a high-pressure hydrogen atmospheric condition within the reactor for the process. The process parameters for hydro-pyrolysis are generally in the following ranges: pressure = 10–17 MPa, PT = 350–600 °C, HR = 10–300 °C/s, and RT > 60 s [60]. It was reported that the technology under a high-pressure hydrogen-based gaseous condition could increase the yields of gas and aromatic hydrocarbons by 19% and 57%, respectively, when compared with CP operating at an inert atmosphere condition [62]. High hydrogen pressure synergistically increases the biochar yield and reduces the yield of tar and light aromatics through secondary reactions. According to Wang and Song [61], the co-loading of Zinc (Zn) and Gallium (Ga) in hydro-pyrolysis significantly increased the aromatic hydrocarbon yield by 37.4%. However, due to the presence of oxygenated compounds (*e.g.*, acids and aldehydes), the produced bio-oil cannot be directly used as a transportation fuel. Therefore, it needs to be further upgraded by *e.g.*, hydrotreating, incurring additional process complexity and costs and making hydro-pyrolysis a less-popular standalone technology [59].

2.3 Effects of Pyrolysis Process Attributes

The prior discussion on various pyrolysis technologies indicated that the selection of optimal process parameters is required for application-specific biochar production. Essential parameters that dictate the yield and quality of biochar are PT, particle size of feedstock, RT, HR, gas flow rate, reactor pressure, reactor design, and catalyst usage. The quality of biochar is usually assessed in terms of the chemical (elemental composition) and physical properties (SSA and Pore Volume (PV)) of the biochar (see Table 2-3, Table 2-4).

2.3.1 Effects of Pyrolysis Temperature

2.3.1.1 Biochar Properties

The H/C and O/C ratios in produced biochar affect its stability and aromaticity. It was found that the C content in biochar increased when the PT increased. A further increase in PT resulted in fewer H- and O-containing functional groups due to dehydration and deoxygenation [68]. The increase in the C content and decrease in the H content resulted to a decrease of H/C, implying a more stable structure of biochar. In addition, the content of molten aromatic ring structures in biochar increased with PT, while that of unstable non-aromatic ring structures decreased [69].

The PV and SSA increased with increasing PT, especially when the PT was raised to above 550 °C. This is due to the release of VM from the feedstock. The biochar produced from *Symphytum officinale L* achieved the highest SSA and PV, being 273.8 m^2g^{-1} and 0.243 cm^3g^{-1}, respectively, when the PT was 750 °C. Higher PTs created more cracks on the surface of biochar, resulting in greater porosity [70].

2.3.1.2 Biochar Yield

PT largely dictates biochar yields which generally decrease at elevated temperatures due to an increase in the primary decomposition of organic matter present in agricultural wastes. Secondary decomposition of biochar residues (charring and shedding) can also contribute to lower biochar yields by producing bio-oil. It was observed that the biochar yield from straw and corn stalk pellets decreased significantly as temperature increased [71]. According to Zhang *et al*. [51], the yield of straw-based (*i.e.*, wheat, corn, rape, and rice straw) biochar decreased significantly with increasing the PT. A more stable downward trend in the biochar yield was observed when temperatures exceeded 400 °C. Another study showed the effect of PT on the yield of biochar produced from *Symphytum officinale L* For the PT range of 350–750 °C, the biochar yield gradually decreased with increasing PT [70].

2.3.2 Effects of Heating Rate

2.3.2.1 Biochar Properties

The HR also critically affects the PV and SSA of biochar. It was shown that the SSA of biochar prepared from rapeseed stem increased from 295.9 m^2g^{-1} to 384.1 m^2g^{-1} when the HR of the process increased from 1 °C/min to 20 °C/min [72]. It was due to that a higher HR condition caused a larger extent of thermal decomposition. Furthermore, low HR conditions can facilitate the retention of structural complexity and avoid thermal cracking of biomass [73].

The ultimate composition of biochar can be affected by the HR. Li *et al*. [6] analysed the ultimate composition of biochar prepared from a lignin-dominated feedstock. Under different pyrolytic HRs (5, 10, 15, 20 °C/min), the elemental contents of biochar varied, even though the PT was kept same. The HR was varied from 5 °C/min to 20 °C/min and the PT was fixed to 700 °C. The C

content of biochar decreased from 94% to 85.4%, while the H content varied from 1.2% to 1.5%. It indicated that the H/C ratio increased as the HR increased, which indicated a lower biochar stability.

2.3.2.2 Biochar Yield

Under low HR conditions, the secondary decomposition of biomass is minimised, ultimately increasing the biochar yield. In contrast, large amounts of liquid and VM are produced at high HR conditions, resulting in lower biochar yields [74]. Tripathi *et al.* [49] investigated the effects of HR on biochar production from safflower seeds, *Ferula orientalis L* and *Charthamus tinctorius L*. The biochar yield decreased when the HR was increased from 30 °C/min to 50 °C/min at different temperatures between 400 and 600 °C. Zhao *et al.* [72] analysed the effects of HR on biochar production from rapeseed. As the HR was increased from 1 °C/min to 5 °C/min, the yield first showed a positive correlation with the rate, and the highest yield (27%) was achieved at 5 °C/min. Increasing the HR to above 5 °C/min reduced the biochar production and resulted in high yields of by-products due to the enhanced decomposition of organic matter and the production and release of carbon-rich vapour.

2.3.3 Effect of Feedstock Particle Size

2.3.3.1 Biochar Properties

The particle size of feedstock usually affects biochar's physical properties rather than elemental properties and controls the heat and mass transfer rate during the process. For instance, the SSA area of biochar increased from 5.2 to 51.1 m^2g^{-1}, while the porosity of biochar marginally decreased when the feedstock particle size decreased from 1 to 0.053 mm [75]. Besides, it was also reported that the Cation Exchange Capacity (CEC) and Anion Exchange Capacity (AEC) of biochar increased when particle size decreased from 0.25 mm to 0.053 mm [75,76]. According to

Chen *et al.* [77], finer feedstock-derived biochar is suitable to be applied for soil amendment, due to the higher degree of particle destruction and subsequent release of nutrients into the soil.

2.3.3.2 Biochar Yield

The particle size of feedstock also influences biochar yield. Larger biomass particles can result in longer contact time between vapour phase species and char layer, leading to a higher probability of secondary reactions and subsequent formation of additional biochar through re-polymerization [49]. This hypothesis is supported by findings in the literature where the biochar yield increased from 31.2% to 38.6% when the particle size of rice husk increased from 0.07 mm to 2.00 mm with 500 °C PT [78]. Another study by Hong *et al*. [42] also showed a similar biochar yield trend regarding particle size: the biochar yield increased from 69.8% to 73.9% when the particle size of cotton stalk increased from 0.07 mm to 1.7 mm.

2.3.4 Effect of Residence Time

2.3.4.1 Biochar Properties

The RT could affect biochar's ultimate composition. Abbas *et al.* [78] analysed the effects of RT on the biochar produced from rice husk. The C content was increased from 63.28% to 70.89% and H content slightly decreased from 4.87% to 2.09% when the RT increased from 30 min to 90 min at 500 °C. Accordingly, the H/C ratio decreased from 0.924 to 0.354, indicating a more stable structure of biochar. The effects of RT on biochar properties have been determined alongside other influential parameters such as PT, feedstock type, and HR [26]. More research is needed to unveil the contribution of RT towards biochar characteristics independently.

2.3.4.2. Biochar Yield

The RT is recommended to be within the range of 5–90 min for biochar production via slow pyrolysis [51]. It was shown that increasing the RT from 10 to 100 min decreased the biochar yield

from 29.6% to 28.6% [72]. For a *what-if* scenario analysis on RT, Sun *et al.* [15] increased the RT from 0.5 h to 24 h with a constant PT of 300 °C and wheat straw as the feedstock. The study showed that the biochar yield drastically decreased from 58.2% (RT = 0.5 h) to 18.8% (RT = 24 h), while the FC and ash contents of biochar increased from 28.3% to 44.4%, and from 8.6% to 9.8%, respectively. This was because longer RT enabled further decomposition of feedstock that converted biochar into the two co-products (*i.e.,* bio-oil and gas).

2.3.5 Effect of Other Parameters

2.3.5.1. Gas Type and Flow Rate

The gas flow rate through the pyrolysis reactor affects the contact time between the primary vapour and biochar, therefore affecting the degree of secondary char formation. Moderate to high levels of vapours are formed during the pyrolysis of biomass. If not removed, the vapours will participate in secondary reactions, changing the composition and yield of biochar. Low gas flow rates favour higher biochar yields and are favourable on slow pyrolysis, while higher gas flow rates are used for fast pyrolysis to effectively strip out the vapour once it has been formed. For example, it was shown that biochar yield decreased from 24.4% to 22.6% when the nitrogen flow rate was increased from 1.2 L/min to 4.5 L/min [49].

Pathomrotsakun *et al.* [79] applied a low CO_2 flow (flow rate = 50 mL/min) in their process, where the corresponding optimal values of RT and PT were 30 min and 300 °C. The H/C and O/C ratios, Higher Heating Value (HHV), and energy yields of the resulting biochar were 0.94 and 0.14, 31.12 MJ/kg, and 48.04%, respectively. This work suggested that CO_2 can be used as a substitute for nitrogen, which has the potential to improve the environmental footprint of biochar production by integrating it with a CO_2 source. Sessa *et al.* [80] investigated the impacts of four different types

of inert gases (helium, nitrogen, argon, and CO_2) on biochar production. The scenario with CO_2 as the inert gas achieved the highest yield and best quality of biochar. When the flow rate was 0.1 L/min, the biochar yield reached 41.2% in a CO_2 environment, higher than the other types of inert gas (*i.e.*, helium, nitrogen, and argon).

2.3.5.2. Pressure

Except for hydro-pyrolysis, all other types of pyrolysis are carried out under an inert environment. High pressure can extend the RT of pyrolysis vapours, increasing the decomposition rate [73]. Also, it was reported that biochar yields decreased with increasing pressure. Melligan *et al.* [81] showed a slight decrease in the biochar yield obtained from Miscanthus giganteus, when the pressure increased from 0 to 12 bar with a temperature condition of below 800 °C. It should be noted that pyrolysis at high-pressure conditions requires more stringent reactor design and thus higher construction or capital costs. Also, high pressures conditions require high maintenance costs for the operation of pyrolysis reactors.

2.3.5.3 Reactor Selection

Large-scale biochar production has stringent requirements on continuous production and quality control, which is contingent upon pyrolysis reactor design and operation [82]. Fig. 2-1 shows six types of popularly used pyrolysis reactors: (a) fixed bed, (b) earthen kiln, (c) rotary kiln, (d) fluidised bed, (e) auger reactor, (f) spouted bed [83]. The fixed bed pyrolysis reactor typically consists of a fixed bed with heating, a gas collector, a liquid condenser, and a temperature controller. It has several typical features such as operation under batch regime, easy design, and high adaptability for various feedstock particle sizes. However, it also has some drawbacks, such as heat transfer limitations and challenges for continuous operation [84]. A fluidised bed reactor is typically suitable for the condition of high HR, short RT, and continuous operation. Nevertheless,

the drawbacks of this type of reactor include complex design and operation (high costs) and fine-sized feedstocks requirement (<0.08 mm) [85]. The earthen kiln is a traditional type of biochar production design, with difficult-to-control operating parameters, long RT, and a low production conversion efficiency [86]. The indirect-heating pyrolysis technology has been applied to a rotary kiln, which could perform in a continuous mode without a heat carrier. However, its poor heat transfer efficiency and gas–solid contact limit the catalyst application for higher process performance [87]. An auger reactor has similar advantages to a rotary kiln, but its mechanical drive often leads to high energy consumption [83,88]. The spouted bed reactor is characterised by high heat transfer rates and gas–solid contact. It does not have a strict requirement on particle size, thus reducing the requirement for feedstock grinding. The main product of spouted bed pyrolysis is bio-oil, and only produces a small amount of biochar [83].

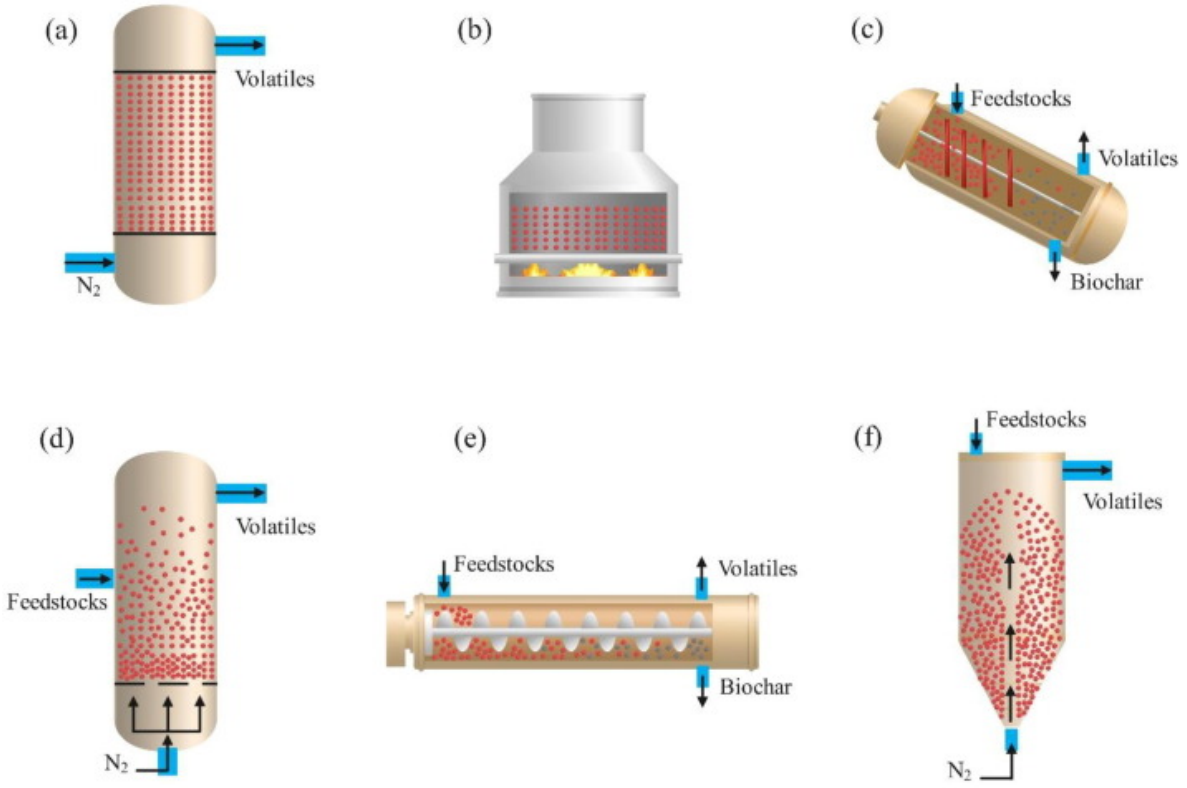

Fig. 2-1. Reactors for biochar production: (a) fixed bed, (b) earthen kiln, (c) rotary kiln, (d) fluidized bed, (e) auger reactor, and (f) spouted bed. Reproduced from the literature [83].

2.3.5.4. Catalyst

The use of catalyst can affect the relative distribution of the pyrolysis products. The catalysts used for pyrolysis can be divided into two types: primary and secondary. Primary catalysts are those that are mixed with biomass prior to pyrolysis, while secondary catalysts are not mixed with biomass but are kept in a secondary reactor downstream of the main pyrolysis reactor [49]. Typical catalysts that have been used in biomass pyrolysis processes include alkaline catalysts (*e.g.*, Potassium Hydroxide (KOH), Sodium Hydroxide (NaOH), Potassium Carbonate (K_2CO_3), and Sodium Carbonate (Na_2CO_3)), metal oxides (*e.g.*, Iron(III) Oxide (Fe_2O_3), Aluminium Oxide (Al_2O_3), Zinc Oxide (ZnO), Calcium Oxide (CaO) and Titanium Dioxide (TiO_2)) and Activated Carbon (AC) [89]. It was found that increasing the proportion of catalyst raised the temperature and reduced the time required to reach the desired PT. Moreover, the addition of catalyst increased the biochar yield. This may occur when the catalyst facilitates the polymerisation and carbonation reactions of a portion of the feedstock components, thereby increasing the production of solid residue (i.e. biochar). During the process, the catalyst promoted a stable C structure of biochar and prevented further char pyrolysis which would have otherwise been converted to bio-oil and gas [49].

Table 2-3. The properties and yields of biochar are influenced by PT.

Feedstocks	PT (°C)	Yield (wt.%)	C (wt.%)	H (wt.%)	O (wt.%)	N (wt.%)	SSA (m2g-1)	PV (cm3g-1)	Refs

	350-	8.8-	39.75-	1.73-	14.07-	0.71-	2.90-	0.024-	[71]
Rice straw	650	41.9	50.44	3.55	14.70	0.91	14.33	0.100	
	300-	32.8-	56.42-	0.12-	5.71-	1.90-			[51]
Rice straw	600	51.4	61.30	2.95	17.73	2.15	-	-	
	350-		41.66-	1.86-	35.41-	0.93-	1.15-	0.005-	[71]
Canola stalk	650	8.7-34	61.87	3.42	37.36	1.96	7.94	0.017	
	300-		61.48-	0.52-	7.35-	1.10-			[51]
Wheat straw	600	31.6-47	67.39	2.73	19.61	1.40	-	-	
	300-		58.04-	1.65-	9.33-	2.11-			[51]
Corn stalk	600	30-43.3	63.93	4.28	18.79	2.75	-	-	
	300-	30.9-	61.20-	0.18-	8.98-	2.12-			[51]
Corn straw	600	45.9	67.48	3.68	17.39	2.93	-	-	
	300-	29.3-	61.80-	0.18-	7.89-	0.90-			[51]
Rape straw	600	44.3	67.85	3.54	17.95	10.02	-	-	
Symphytum	350-		33.56-	0.93-	7.48-	1.52-	11.54-	0.021-	[70]
officinale L	750	37-48.4	41.08	2.73	10.72	1.87	273.8	0.243	

Table 2-4. Effects of pyrolysis process parameters on biochar yield for different crop-residues.

Feedstocks	Particle size (mm)	PT (°C)	RT (s)	HR (°C/s)	Reaction environment	Biochar yield (wt.%)	Refs
Rice husk	2.5-10	300-500	1800,3600,5400,7200	0.1,0.16, 0.33	Media: Nitrogen with synthetic air Flow rate: 0.1 L/min Reactor: Stainless steel bed	33.7-51.3	[75]

Rice straw	0.42-0.62	550	600	0.1	Media: Nitrogen Flow rate: 0.3 L/min Reactor: Stainless steel bed reactor	37.9	[90]
Palm kernel shell	0.5-2	500	3600	0.1	Media: Nitrogen Flow rate: 0.05 L/min Reactor: Stainless steel bed	37.7	[91]
Empty fruit bunch	0.5-2	500	3600	0.1	Media: Nitrogen, Flow rate: 0.05 L/min Reactor: Stainless steel bed	35.1	[92]
Symphytum officinale L	<0.15	350-750	3600	0.1	Media: Nitrogen Reactor: Stainless steel bed reactor	37-48.4	[70]
Rice straw	<0.84	300-600	3600	0.17	Media: Nitrogen Flow rate: 0.1 L/min Reactor: Stainless steel bed reactor	32.6-52	[51]
Wheat straw	<0.84	300-600	3600	0.1	Media: Nitrogen Flow rate: 0.1 L/min Reactor: Steel bed reactor with tube furnace	31.6-47	[51]
Corn straw	<0.84	300-600	3600	0.1	Media: Nitrogen Flow rate: 0.1 L/min Reactor: Steel bed reactor with tube furnace	30.9-45.8	[51]
Rape straw	<0.84	300-600	3600	0.1	Media: Nitrogen Flow rate: 0.1 L/min Reactor: Steel bed reactor with tube furnace	29.3-44.3	[51]
Corn stalk	5	300-800	3600	0.1	Media: Nitrogen Flow rate: 0.1 L/min Reactor: Steel bed reactor with tube furnace	30-43.3	[93]
Rapeseed stem	10-20	200-700	600, 1200, 2400, 3600, 4800	0.1,0.16,0.25, 0.33	Media: Nitrogen Flow rate: 0.3 L/min Reactor: Steel bed reactor with muffle furnace	18.3-80	[72]

Maize cobs	2	300-600	1800,3600,5400	0.1,0.16,0.25	Media: Nitrogen Reactor: Steel batch reactor	22-33.8	[47]
Maize husk	2	300-600	1800,3600,5400	0.1,0.16,0.25	Media: Nitrogen Reactor: Steel batch reactor	21.7-30.7	[47]
Maize leaves	2	300-600	1800,3600,5400	0.1,0.16,0.25	Media: Nitrogen Reactor: Steel batch reactor	25.7-38.3	[47]
Cotton stalk	0.62-0.82	250-450	7200	0.33	Media: Nitrogen, Flow rate: 0.1 L/min Reactor: Horizontal tubular furnace	20-26.5	[53]

2.4. Emerging Topics on Biochar Production

Various emerging aspects of biochar production are critically reviewed, including (a) biochar, bio-oil, and gas nexus, (b) balance between yield and stability, (c) climate change mitigation and LCA, (d) economics of pyrolysis and biochar data-driven modelling of biochar production via pyrolysis, and (f) emerging applications of biochar. A summary of these aspects and associated research works are provided in Table 2-5.

Table 2-5. Overview of state-of-art in biochar production studies with respect to Chapter 2.4.

Topic	Highlights	Refs
Biochar, bio-oil, and gas nexus	MWP coupled with conventional pre-pyrolysis for stalks treatment. Conventional pre-heating enhanced the MWP performance of stalks.	[53]
Biochar, bio-oil, and gas nexus	The most desirable process for biochar production was slow pyrolysis. MWP could offer a balance product distribution in biochar, oil and gas.	[94]
Biochar, bio-oil, and gas nexus	Two-step microwave-assisted processes were used to prepare magnetic porous biochar.	[95]

	MWP biochar had a higher surface area and PV than CP biochar.	
Biochar, bio-oil, and gas nexus	Effects of microwave power and Na_2CO_3 catalyst were investigated. The catalyst increased the bio-oil and gas yield.	[96]
Biochar, bio-oil, and gas nexus	APBO washing pre-treatment increased bio-oil yield. APBO washing has a better improvement effect on pyrolysis products than acid washing.	[90]
Balance between yield vs. stability	PT was the dominant processing parameter to biochar stability. Both biochar yield and stability were decisive to carbon sequestration potential. Elemental and proximate analysis, and biochar structure analysis were methods for measuring biochar stability.	[31,97]
Balance between yield vs. stability	Aromaticity determined thermal stability while surface area was critical for chemical stability.	[98]
Balance between yield vs. stability	Pyrolysis process parameters had an impact on the stability and yield of biochar. The unsaturation or aromaticity of biochar can be assessed by the H/C or O/C ratios.	[99]
Climate change mitigation and LCA	Average energy demands were 6.1 MJ/kg biochar and 97 MJ/kg AC. Biochar had lower environmental impacts than AC even after transportation stage.	[30]
Climate change mitigation and LCA	LCA of biochar application as carbonaceous water treatment adsorbents. Combining biochar and hydrochar with regeneration was desirable to replace AC.	[100]

Climate change mitigation and LCA	Most GHG was contributed by covering the energy deficit caused by pyrolysis.	[101]
Economics of pyrolysis and biochar	Biochar price was between US$454 and US$871 per tonne for CP. Biochar price was between US$588 and US$1020 per tonne for MWP.	[102]
Economics of pyrolysis and biochar	Compared to inorganic fertilisers, biochar had a long-term capacity for agricultural improvement. The grain yield and net benefit increased from 4.54-4.70 ton/ha and 293-438 US$/ha.	[103]
Data-driven modelling of pyrolysis-derived biochar	RF showed good prediction ability for biochar yield and carbon contents. The highest R^2 were 0.855 and 0.848 for biochar yield and C content prediction.	[104]
Data-driven modelling of pyrolysis-derived biochar	XGB model showed good prediction ability for biochar yield. The prediction accuracy achieved 0.844 as R^2.	[105]
Data-driven modelling of pyrolysis-derived biochar	MLP-NN and ANFIS were employed to predict biochar yield and composition. Statistical analysis of various feedstock and biochar properties is performed. The prediction accuracy achieved 0.964 for biochar yield.	[106]
Applications of biochar	Comprehensive description and analysis of different biochar applications in MFC.	[107]

	Biochar has the potential as an electrode material for MFC and as a cathode catalyst and contributes to PEM applications.	
Applications of biochar	Biochar is also used as a catalyst for biodiesel and hydrogen production. Biochar can be utilized for electrode preparation used in MFC.	[108]
Applications of biochar	The addition of biochar combined with gypsum shortened composting time. Applying biochar reduces the composting duration and nitrogen and carbon losses, and potential ecological hazards.	[109]
Applications of biochar	Waste sugarcane bagasse-based acidic catalyst was synthesized. Biochar produced from sugarcane bagasse archived optimal conditions when the PT is 400°C.	[110]
Applications of biochar	The suitability of biochar mixed with solid waste for agricultural soil applications was investigated. The application of biochar to the soil decreased the concentration of heavy metals in leachate by 40-95%.	[111]

2.4.1. Biochar, Bio-oil, and Gas nexus

There exists a trade-off between the three pyrolysis products: biochar, bio-oil and gas. Optimal pyrolysis production should match the relative yields of the products with the purpose of production with the consideration of economics and environmental footprints. For a system mainly configured for biochar production, appropriate production of bio-oil and/or gas has the potential to improve the economics of the system [112]. It is important to adopt a nexus perspective upon the design of pyrolysis production. As shown above, the relative yields of the products depend on the types of feedstocks and pyrolysis process conditions and design. Accordingly, a technology that favours the accurate control of the yields will be desirable for optimization. MWP serves as a candidate technology that has the potential to support technology innovation towards accurately

controlling the relative production of biochar, bio-oil, and gas. A large pool of literature has focused on analysing bio-oil and gas production from MWP. For example, Li *et al.* [53] studied the production of combined MWP and CP processing (as known as MWP) Combined with Conventional Pyrolysis (MCCP)) of cotton stalk under 11 different PTs. Fig. 2-2a shows the yield distribution of the three products under the different temperature scenarios. M−1 referred to MWP with 1 g microwave absorbent (biochar) under 600 W without pre-heating. For A-(250–450) and A-(250–450)-1, 250–450 referred to preheat temperatures and A-(250–450)-1 referred to MWP under the preheat condition. M−1 had the lowest biochar yield and achieved the most gas production. A-250–1 had the highest biochar yield among all scenarios. The MCCP technology was most favourable for biochar production, while the MWP technology had the highest gas yield. Preheating has played a significant role in biochar production. The highest biochar yield of 34.1% was achieved at 250 °C and the highest bio-oil yield was 50.2% when it was at the first stage of 450 °C.

Mahmoud Fodah *et al*. [96] studied biochar and bio-oil production from corn stover via MWP cooperated with catalysis. Fig. 2-2c compared product distribution from catalytic MWP and non-catalytic MWP in the power range of 500–700 W. In the non-catalytic case, a significant decrease in biochar yield and an increase in gas yield were observed when the power increased from 500 W to 900 W. The addition of Na_2CO_3 catalyst improved the bio-oil and gas yield, reducing the biochar yield. It was shown that in the case where Na_2CO_3 was used as a catalyst, the catalyst promoted pyrolysis reactions towards bio-oil and gaseous production, which usually means that more organic components were converted to volatiles, thus reducing the yield of solid residues. Specifically, alkaline catalysts such as Na_2CO_3 promote reactions such as dehydration and decarboxylation,

increasing the yield of gas and bio-oil products. Cen *et al.* [90] investigated the influences of wash pre-treatment on biomass pyrolysis polygeneration. The pyrolysis experiment was carried out at PT = 550 °C and HR = 10 °C/min. The rice straw showed the highest biochar yield (38%). The Aqueous Phase Bio-Oil (APBO) washing rice straw showed the highest yield (35%) as shown in Fig. 2-2d. The bio-oil shows decrease trend under different wash pre-treatment conditions (from Raw-RS to Bio-RS).

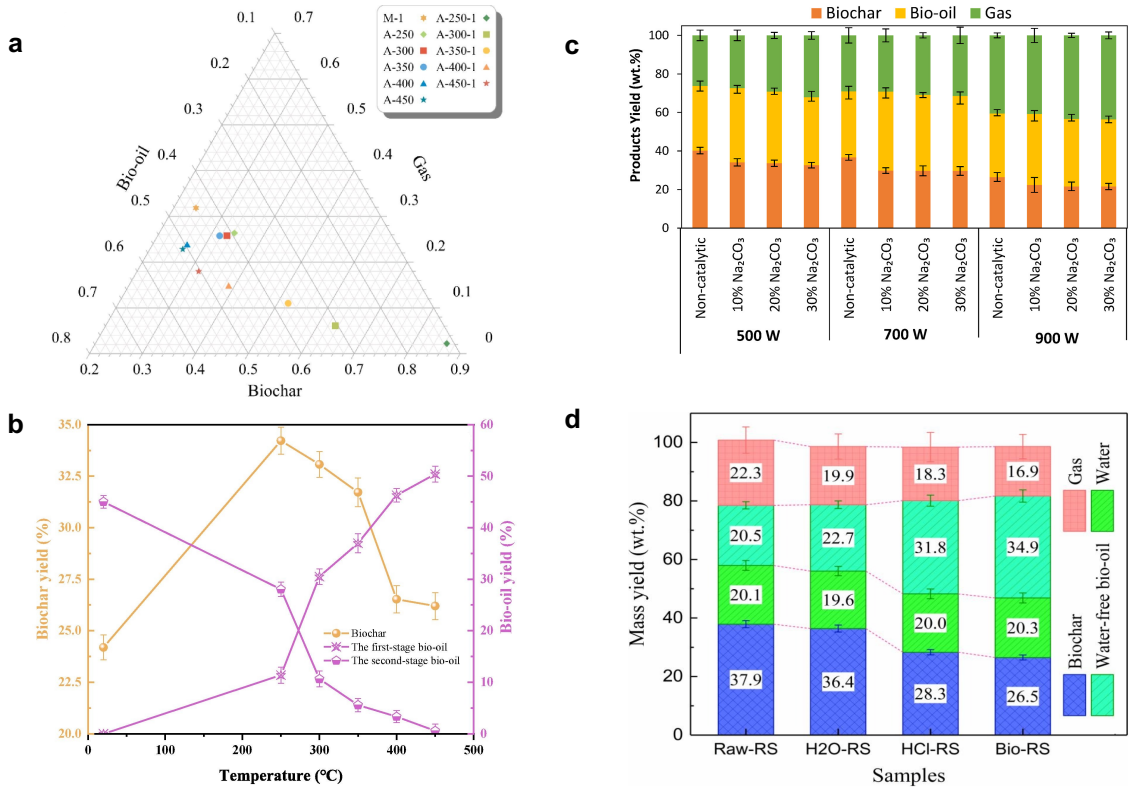

Fig. 2-2. (a) The product distributions of different scenarios [53]. (b) The trend of biochar and bio-oil yields with respect to PT [53]. (c) The product distribution from catalytic and non-catalytic MWP: the yield of biochar, bio-oil, and gas [96]. (d) The product distribution from the processes with different pre-treatment methods [90].

2.4.2 Balance Between Biochar Yield and Stability

Biochar C content recalcitrance and biochar stability have played a critical role in carbon sequestration. Biochar stability can be considered by the proportion of initial C remaining after oxidation treatment and can be determined by the mass of stable C remaining in the biochar residue after oxidation. Numerous challenges exist to reconciling the trade-offs between biochar stability and yield [97].

The degree of aromaticity and aromatic condensation are two essential evaluation metrics that dictate the stability of biochar [98]. The unsaturation or aromaticity of biochar can be assessed according to biochar elemental ratios (H/C and O/C) [99]. Han *et al.* [113] conducted pyrolysis of rice straw at 250-600°C. H/C and O/C ratios were employed to analyse the biochar stability. The H/C and O/C ratios of biochar decreased from 0.87 to 0.34 and 0.36 to 0.13 with the increasing PT. The increase in PT led to a trend towards greater carbonisation with more poly-aromatic content, which promoted biochar stability. Vendra Singh *et al.* [114] studied the trade-offs between yield and stability of biochar derived from rice straw pyrolysis with PT between 300-600°C. The H/C and O/C ratios increased from 0.52 to 0.23 and from 0.15 to 0.07, indicating an improvement in biochar stability. On the other hand, the biochar yield decreased from 38.23% to 27.14%, with PT increasing from 300-600°C. Leng and Huang [31] summarised that long residence time, slow HR, high pressures, biomass feedstocks with high lignin contents, and large particle size would be preferred for biochar yield and stability, and it would also contribute to improved carbon sequestration ability by biochar.

2.4.3 Climate Change Mitigation and Life Cycle Assessment

LCA is a tool routinely used to assess the environmental impacts of biochar production via pyrolysis processes. It adopts a whole lifecycle perspective and typically includes processes

ranging from raw material extraction and pyrolysis production to waste disposal and recycling. Fig. 2-3 illustrates the typical elements considered during the LCA of pyrolysis and biochar production processes.

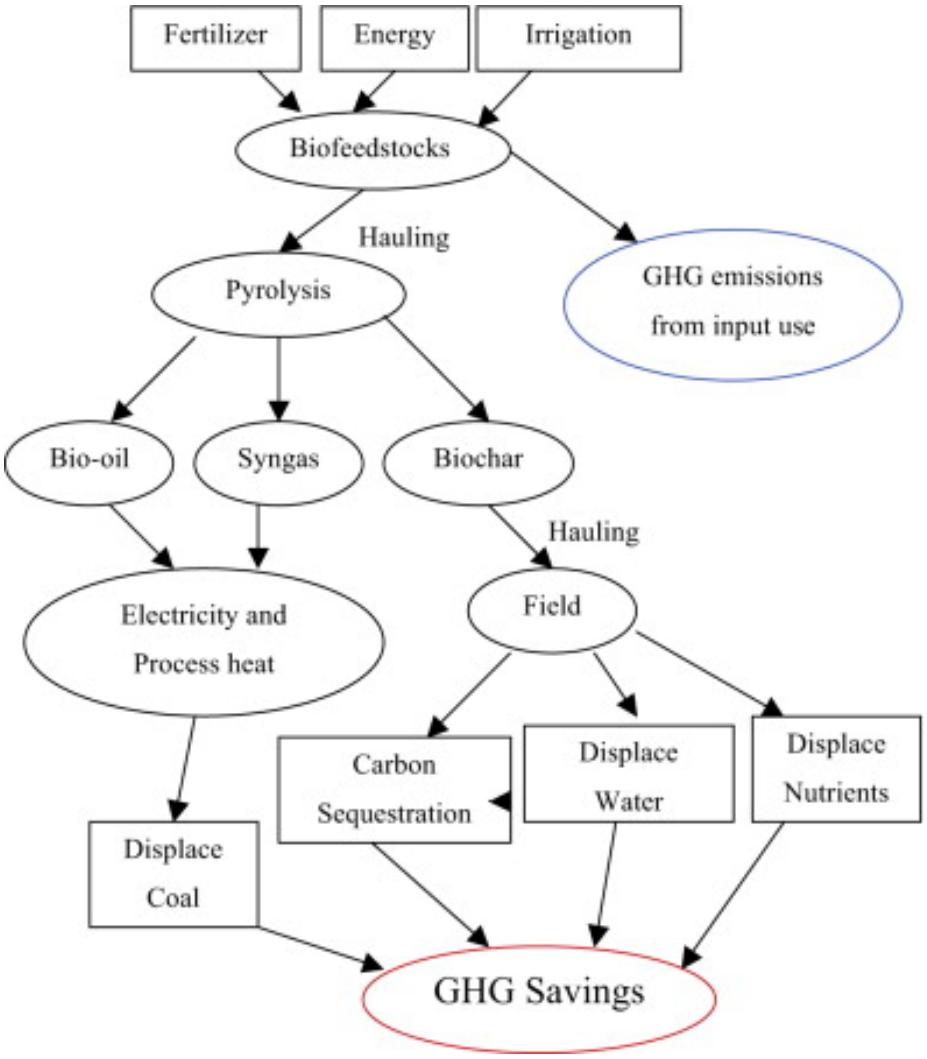

Fig. 2-3. A whole system example of biochar production [115].

Alhashimi and Aktas [30] applied LCA to compare the environmental impacts of biochar and AC. Especially, long-distance transportation (*i.e.*, nation to nation) was included as part of the biochar/AC developments analysed. The GWP for biochar and AC were −0.9 kg CO_2-eq/kg and 6.6 kg CO_2-eq/kg, respectively. This work revealed cumulative energy demands for biochar and

AC production processes were 6.1 MJ/kg and 97 MJ/kg, respectively. Kozyatnyk *et al.* [100] evaluated the environmental footprints of biochar application as a carbonaceous water treatment adsorbent using the approach of LCA. The end-of-life stages were considered in this study including incineration, landfill, and regeneration, and biochar, hydrochar, and AC were the three primary materials assessed. It was shown that combining biochar and hydrochar with regeneration could be an environmentally feasible option to replace AC. The production of sorbents was the most significant GWP contributor within the framework of the LCA study. Therefore, increasing the sorption capacity of sorbents would offer economic and environmental benefits since higher sorption capacities reduced the use of sorbents.

Lefebvre *et al.* [101] evaluated GHG emissions of two agricultural wastes utilisation scenarios which are sugarcane residue combustion for heat and power generation and pyrolysis for biochar production. It was shown that sugarcane residue biochar could sequester 36 mega tonnes CO_2-eq/year. Most of the GHG emission was contributed by compensating for the energy deficit caused by pyrolysis. This biochar scenario led to a 23% reduction in the total amount of GHG. Azzi *et al.* [116] carried out an LCA study for large-scale biochar production for negative emission. This work compared the climate impact of biomass pyrolysis with biomass combustion. The main applications were energy and power applications, and the potential as a fertiliser additive was also explored. In total, five scenarios were explored, including agricultural application, carbon sequestration, electricity substitution, heat substitution, and transport fuel substitution which had a GWP were -1300 kg CO_2-eq/ton, -1100 kg CO_2-eq/ton, -335 kg CO_2-eq/ton, -60 kg CO_2-eq/ton and 240 kg CO_2-eq/ton in 2040, respectively. This study suggested that LCA helps to design

biochar systems with the comparison of the GHG emission trade-offs among various possible applications.

2.4.4 Economics of Pyrolysis and Biochar

Despite significant environmental benefits, the current market scenario suggests that biochar applications are prohibitively expensive and economically inviable. This is associated with the high capital costs of pyrolysis plants and low incentives offered by government bodies for achieving carbon-negativity [117]. Techno-economic analysis (or Cost Benefit Analysis (CBA)) has commonly been used to explore various *what-if* scenarios from improved economics. For example, Haeldermans *et al.* [102] compared biochar production from CP and MWP through techno-economic assessment. Minimum prices ranged from US$454/ton to US$871/ton for CP-biochar and US$588/ton to US$1020/ton for MWP-biochar (Exchanged the EUR to US$ via currency rate 1.04). CP is a simplified and developed technology that makes it more affordable. However, it was mentioned that MWP-biochar had greater quality and better technical feasibility than CP-based biochar. Moreover, biochar price per ton was a critical evaluation criterion for biochar production plants and strongly depended on the government carbon tax.

The economics of biochar production systems has been assessed with respect to raw material or feedstock used, the conversion technology employed, carbon sequestration subsidies and carbon credits reflecting the social value of GHG emission reductions. Implementing smart farming practices could increase crop yields and improve the economic situation of farmers while reducing the adverse effects of climate change [102]. Compared to inorganic fertilisers, biochar has a long-term capacity for agricultural improvement in the economic aspect. When biochar was used in combination with plant growth-promoting rhizobacteria and Nitrogen-Phosphorous-Potassium (N-

P-K) fertiliser, the wheat crop's grain yield and economic results were significantly increased. An increase in grain yield from 4.54 ton/ha to 4.70 ton/ha resulted to a rise of net benefit from 293 US$/ha to 438 US$/ha (*i.e.*, 50% relative increment), respectively [103]. This indicated the potential opportunistic benefit from the use of biochar could be an important contributor to the profitability of biochar production.

2.3.5 Data-Driven Modelling of Pyrolysis-Derived Biochar

Over the past decades, theoretical models have been widely used for predicting the yields of pyrolysis processes [118]. However, these models are often complex, time-consuming, and of semi-empirical nature (depending on the use of experimental data), which limits their use for biochar yield prediction towards more sophisticated process design and optimization. Researchers have also developed empirical correlations based on the predictions from the theoretical models or experiments [119]. However, these empirical correlations are constricted to a limited range of experimental conditions and biomass feedstocks, and they are normally not suitable for extrapolative scenarios.

With the advent of AI and an abundance of pyrolysis experimental data, data-driven modelling has become a popular method for predicting biochar production. These methods have superior prediction accuracy, shorter computation time, and complex data trend-reproducing capabilities [119]. In particular, the method could effectively predict biochar production through limited experimental and system data. It finds the relationship between input and output variables through training and produces results without any a priori assumptions. To ensure an accurate whole-system analysis of biochar production from agricultural wastes, generalizable modelling of pyrolysis processes is essential. ML-assisted prediction of biochar yield and composition has

gradually become an important tool in recent years. Popular ML approaches evidenced in the biochar modelling literature include RF, SVM, eXtreme Gradient Boosting (XGB), ANFIS, and MLP-NN *etc.*

Zhu *et al.* [104] developed an RF-based model to predict biochar yield and C content. 245 datasets of biochar yield and 128 datasets of C content were collected in this study. The highest Coefficients of Determination (R^2) were 0.855 and 0.848 for biochar yield and C content prediction. In an effort by Pathy *et al*. [105], an XGB model was developed based on 91 datasets considering ultimate composition and elemental composition ratios as input data. However, only one output (biochar yield) was included in this study. The model performance was only evaluated by R^2, which was 0.844. the MLP-NN prediction model was employed by Khan *et al.* [120] for biochar yield production, where NNs were coupled with metaheuristic models. R^2 and Root-Mean-Square Error (*RMSE*) of biochar yield prediction were 0.93 and 1.74. Recently, Li *et al.* [106] developed a comprehensive ML-assisted predictive model for biochar yield and composition (FC, VM, ash, C, H, O, N). This study applied MLP-NN and ANFIS, which predicted biochar production from pyrolysis based on 226 datasets. The R^2 values for each of the output variable was biochar yield = 0.96, FC = 0.9, VM = 0.9, ash = 0.94, C = 0.92, H = 0.86, O = 0.88 and N = 0.88. Additionally, feature importance analysis revealed a high dependence of biochar yield and composition on PT, ash content, and N content. Overall, the data-driven models for biochar production can be used in parallel with LCA model to develop a better understanding from a whole-system perspective.

2.3.6 Machine Learning aided Multi-Objective Optimization and Multi-Criteria Decision Making

MOO algorithms incorporating MCDM are becoming increasingly popular for optimization problems with three or more objectives, often referred to as MOO Problems. MOO focuses on finding the optimal solution between multiple competing objectives, while MCDM focuses on making the best choice among a range of alternatives based on multiple evaluation criteria. These algorithms elicit, a priori or interactively, the preferences of a single or multiple decision makers to guide the search to the decision maker's most preferred solution, rather than the entire Pareto optimal frontier [121]. ML technologies can play a crucial role in this process by providing new solutions for a variety of engineering fields. They can analyse complex datasets and identify hidden patterns and trends, thus assisting decision makers in understanding and resolving potential conflicts between goals or criteria. For example, with ML algorithms, it is possible to predict the potential outcomes of different decision-making scenarios or identify which factors have the greatest impact on the decision-making process. This combination allows decision makers to consider a wider range of variables and scenarios in a broader data-driven environment, increasing the accuracy and efficiency of decision making [122].

Lu *et al.* (2021) [123] presented an approach to incorporate ML modelling into MOO. A Radial Basis Function (RBF) NN was used to construct models for functional evaluation. A central combinatorial design was used as a sampling strategy to construct models individually for different optimization objectives to improve prediction accuracy and address the high computational demand in MOO of complex nonlinear distillation processes. This study ultimately succeeded in obtaining a design that achieves a trade-off between capital and operating costs. However,

optimization objectives should be extended to include environmental impact, safety, *etc*. Furthermore, Wang *et al.* (2023) [121] introduced a novel framework that employs ML to enhance MOO and MCDM in chemical engineering. The approach started with the selection of ML models, followed by model training and tuning of algorithms using Particle Swarm Optimization (PSO) as well as the formulation of the MOO problem to be solved. Finally, a systematic MCDM analysis was carried out to recommend an optimal solution to implementation. The proposed framework was effective for chemical and related process design. It proved to be beneficial for the optimization of complex chemical processes for supercritical water gasification processes aiming to produce hydrogen-rich syngas with low GHG emissions. The goal is to increase energy output and reduce environmental pollution.

The integration of ML with MOO and MCDM has been successfully applied in various chemical processes and engineering designs. However, to the authors' knowledge, this framework has not been used for biochar production and application analysis. There is a opportunity to develop and apply the ML-MOO-MCDM framework specifically for biochar production and soil application. By doing so it will be possible to explore and optimise the environmental benefits of biochar production and soil application, potentially leading to more sustainable and efficient agricultural practices. It can also create new avenues for enhancing the production and utilisation of biochar, thereby contributing to environmental sustainability.

2.4.7 Applications of Biochar

Process operating conditions and reactor designs are required to be manipulated to meet the specific requirements of biochar applications with the consideration of economics and environmental implications. An overview of different application areas (*e.g.*, energy, agriculture,

and chemical) of agricultural waste-derived biochar is given and Fig. 2-4 presents the conversion pathway from agricultural waste into various biochar applications.

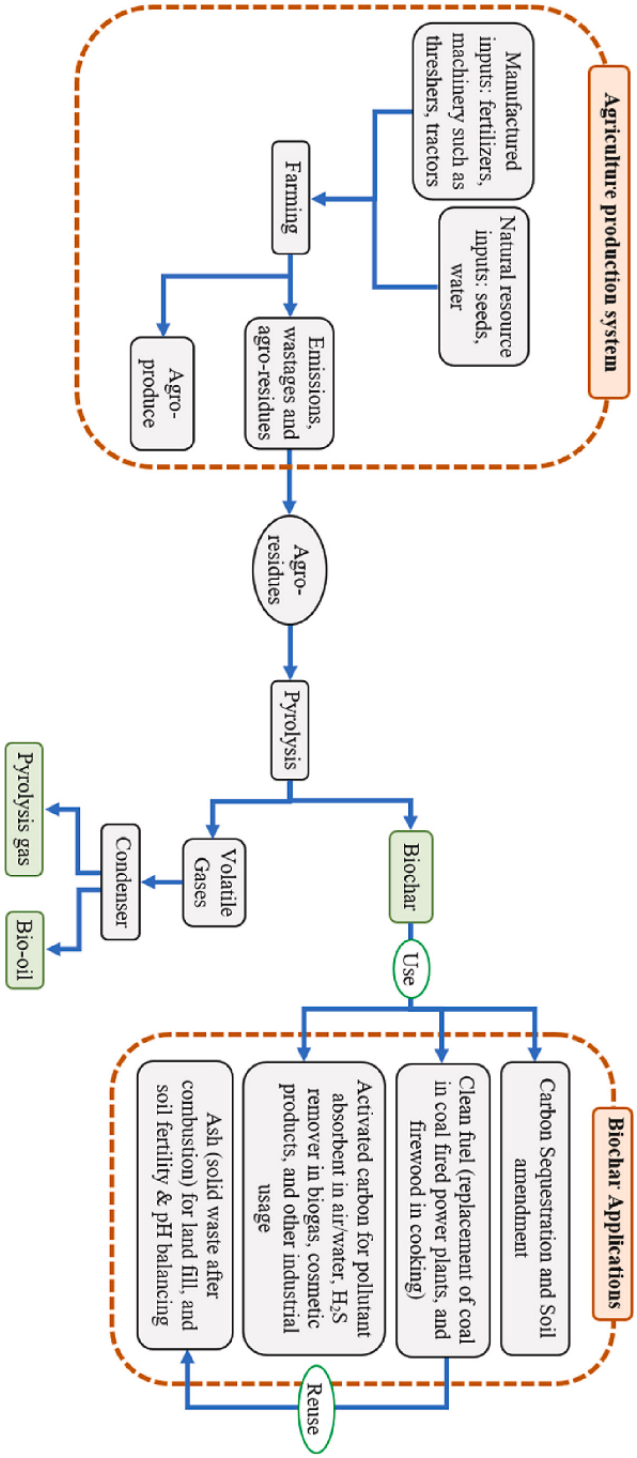

Fig. 2-4. Conversion pathway from agricultural waste to various applications of biochar [124].

Chakraborty *et al.* [107] suggested that biochar could be an alternative material to substitute electrodes, cathode catalysts, and Proton Exchange Membranes (PEM) in MFC applications. MFC can convert the energy captured in the chemical bonds of organic compounds into electrical energy while using wastewater as a substrate. Biochar has the potential to be used as an electrode material for MFC and a cathode catalyst. According to Cao *et al.* [125], the biochar-based electrode was low-priced compared to commercial electrodes. The material cost of N/Fe-C was about $0.03-0.08/g, which is a thousand times lower than a commercial platinum electrode. However, several issues remain to be tackled prior to practical deployments, such as process efficiency improvement, biochar quality control, and effective biochar applications.

Kant Bhatia *et al.* [108] reported that biochar can be used as a catalyst for the transesterification of oils for biodiesel production. Biodiesel is considered as a favourable fuel because of its high energy density and presence of C14-C20 long C chain fatty acids. The porous structure of biochar allows easy access of reactants to the active site to facilitate the transesterification process, and biochar's hydrophobic surface helps remove unwanted products generated during catalytic reactions. Behera *et al.* [126] analysed the efficiency of acidified biochar catalysts for transesterification. The peanut shell was pyrolyzed under three PTs (300, 400, and 600°C), among which biochar produced at PT = 400 °C had the highest catalytic efficiency. The optimal values of biochar's SSA and pore size were 6.61 m^2g^{-1} and 2.98 nm, at which the highest biodiesel yield was achieved (94.94%). Akinfalabi *et al.* [110] applied biochar as a catalyst for biodiesel production. The biochar produced from sugarcane bagasse achieved optimal properties when the PT was 300 °C: the SSA was 310 m^2g^{-1}, and the pore size was 3.92 nm. The conditions for the highest biodiesel production (98.6%) were 1.5 h reaction time, 60 °C, and 2 wt.% catalyst loading.

Acidified biochar catalysts can reduce processing costs and the environmental impact of corrosive chemicals.

Biochar also has great potential for environmental management in various applications. For example, Qu *et al.* [109] analysed the effect of agricultural composting using biochar combined with gypsum. The results showed that the application reduced composting duration, N and C losses, and potential ecological hazards. Biochar mixed with gypsum improved compost quality and nutrient retention. In another study, Vamvuka *et al.* [111] investigated the suitability of mixing biochar with solid waste for agricultural soil applications. The following physicochemical properties were obtained from the biochar produced from grape husks at 500 °C: pH = 9.7, Electrical Conductivity (EC) = 15.3 mS/cm, CEC = 205.2 mmol/kg, PV = 0.12 cm^3g^{-1}, average pore size = 4.53 nm and SSA = 0.9 m^2g^{-1}. For all combinations of composts biochar and soil, alkali and alkaline earth metals showed the greatest solubility. Consequently, it increased the pH of the extracts and thus reduced the leachability of heavy metals Chromium (Cr), Copper (Cu), Zirconium (Zr) and Strontium (Sr). In this study, heavy metals concentrations were reduced by 40%-95%.

2.5 Summary

The critical review of biochar production from agricultural waste pyrolysis revealed extensive developmental efforts during the past decade focusing on biochar yield and property optimization, modelling, and applications. Nevertheless, significant future efforts are necessary for application-specific system efficiency improvement. Specifically, existing research for agricultural waste-biochar systems is mainly conducted at the laboratory or pilot scale. This apparent lack of ML modelling in agro-waste biochar systems research may limit the understanding, optimisation and

scale-up of the production process. Although the influences of process parameters on biochar yield and stability have been extensively researched, the environmental impacts of whole production and applications have not been quantified, indicating an opportunity for holistic LCA framework development. Furthermore, the LCA and process optimization frameworks require rapid prediction models, where ML-assisted predictive modelling for a wide range of biochar constituents can offer significant reduction in computational complexity. In the future, ML models should include chemical and proximate composition as input features. Although biochar has the potential to displace several chemicals in agricultural and industrial sectors, the current business models do not offer significant government incentives to support the high capital expenditure needs for setting up production plants. Therefore, application-specific techno-economic analysis must be extensively conducted in the future, while assessing various business models to support policymaking decisions.

This literature review investigated the influences of different agricultural waste and pyrolysis reaction conditions on the properties and yield of biochar. Moreover, state-of-art biochar production and application were summarised including advanced approaches associated with the trade-off of the different products of pyrolysis processes. Meantime, the use of LCA and economic analysis for evaluating the environmental benefit and economic feasibility of biochar applications was also analysed. ML-assisted modelling and MOO-MCDM are becoming the effective approaches supporting biochar production prediction which is important for the optimal design and deployment of biochar systems.

key knowledge gaps:

- ML Model Development: There is a need to develop more accurate ML-assisted predictive modelling techniques to predict biochar compositions. Specifically, there is a need to incorporate parameters such as proximate and ultimate composition into ML models and to develop efficient models to improve prediction accuracy and comprehensiveness.
- Lack of a comprehensive LCA framework: There is a need to develop a comprehensive LCA framework that accurately incorporates the influences of process and feedstock conditions towards biochar production to assess the environmental footprint of biochar production and application.
- Need for MOO-MCDM integrated with ML modelling: MOO and MCDM techniques are considered to be effective methods to support biochar production forecasting. However, there is a lack of integration of these methods in the biochar production process. Incorporating MOO-MCDM into the research framework could enhance the potential for optimal design and deployment.

Chapter 3 Machine Learning Assisted Prediction of Biochar Yield and Composition via Pyrolysis of Biomass

The Chapter is based on the publication "**Yize Li**, Rohit Gupta, Siming You. "Machine learning assisted prediction of biochar yield and composition via pyrolysis of biomass." Bioresource Technology 359 (2022): 127511".

3.1 Introduction

With the advent of AI and an abundance of pyrolysis experimental data, data-driven modelling has become a popular method for predicting biochar production. These methods have superior prediction accuracy, shorter computation time, and complex data trend-reproducing capabilities [119]. In particular, the method could effectively predict biochar production through limited experimental and system data. It finds the relationship between input and output variables through training and produces results without any a priori assumptions. However, the accuracy of existing ML-based biochar prediction models is limited especially when a small pool of datasets was used for the model development. For example, prior work has developed a RF regression-based biochar yield and C content prediction model based on 245 datasets covering various biomass feedstocks and process operating conditions. The work achieved a R^2 value of 0.855 and 0.848 for predicting biochar yield and C content [104]. Another work explored the accuracy of the XGB ML model for predicting, which had an R^2 value of 0.84 based on 91 training datasets [105]. A recent work achieved an improved $R^2 = 0.92$ for predicting biochar yield using an Artificial Neural Network (ANN) coupled with metaheuristic algorithms [120]. However, there have been no prior efforts for developing a comprehensive data-driven model that can simultaneously predict biochar yield and compositions (proximate and ultimate). As evidenced in the literature, the yield and compositions of biochar can have significant trade-offs based on the choice of pyrolysis conditions and biomass

feedstock compositions. Therefore, it is of significant scientific interest to develop a comprehensive ML model that can predict both biochar yield and composition, which serves as the purpose of the present research work.

MLP-NN and ANFIS are two popular prediction methods. MLP-NN is a widely used data-driven modelling method in pattern recognition, signal processing, function approximation, and process simulation. They are often used to model complex relationships between inputs and outputs parameter spaces, explore patterns in data, or capture statistical structure in unknown joint probability distributions between observed variables [127]. In contrast, ANFIS is a combination of adaptive control techniques, ANN, and fuzzy inference systems. As a deep learning algorithm, fuzzy logic allows the ambiguity of human perception or decision-making to be represented as a mathematical model [128]. The application of the models toward biochar production prediction is still limited.

This study envisions the significance of developing data-driven models to predict biochar yield, proximate composition, and ultimate composition prediction. To the best of the author's knowledge, this is the first work that develops a comprehensive model to predict biochar yield and composition, simultaneously, given the pyrolysis conditions and biomass feedstock compositions. The work also highlights a comparison of the predictive performances of two different data-driven models: MLP-NN and ANFIS. During the data assimilation stage, feedstock compositions of various types of organic waste, related pyrolysis process parameters, biochar yields, and biochar composition have been considered. The influences of various model parameters and training-

testing dataset split are investigated through the metrics the *RMSE* and R^2. Finally, the findings are discussed and concluded, while indicating areas for future improvements.

3.2 Methods

3.2.1 Data Collection and Pre-processing

In total, 226 dataset points were collected from the literature (19 studies) to develop the data-driven models, summarised in Table 3-1. The dataset includes a wide range of feedstocks such as Corncob, Corn stover, Bagasse, Cocopeat, Coconut shell, Coconut fibre, Wheat straw, Rice husk, Rice straw, Pine, Pine sawdust, Pine wood, Bamboo, Orange bagasse, Orange pomace, Rape stalk, Cassava stem, Cassava rhizome, Cotton stalk, Palm kernel shell, Wood stem, Wood bark, Agro-food waste, Canola hull, Oat hull, Vine pruning, Poultry litter, and Hinoki cypress [34–36,38,40–42,129–140]. To ensure generalizability, various attributes were considered during the data collection stage, which included (1) proximate composition of biomass feedstock (2) ultimate composition of biomass feedstock, (3) L-C-H composition of biomass feedstock, (4) major pyrolysis conditions, (5) biochar yield, (6) proximate composition of biochar, (7) ultimate composition of biochar, (8) HHV of biochar, and (9) energy yield of biochar (amount of energy that are obtained in the biochar produced during the pyrolysis process. This energy yield can be measured by various metrics, such as the calorific value of the biochar, which indicates the amount of heat energy released per unit mass of biochar when it is burned). Although particle size of feedstock has been considered in prior works [104,120], it was not included the present work due to significant methodological inconsistencies and uncertainties associated to the data collection.

Table 3-1. Statistical summary of input and output variables for the raw dataset.

I/O	Type of variable	Variable	Min	Max	Mean	SD	No. of samples (% of total dataset)
Input	Feedstock proximate composition	FC (% db.)	4.33	27.80	13.84	5.36	226 (100%)
		VM (% db.)	68.20	91.16	79.83	4.91	226 (100%)
		ash (% db.)	0.16	15.14	6.33	3.94	226 (100%)
	Feedstock ultimate composition	C (% db.)	35.70	64.23	44.19	5.44	226 (100%)
		H (% db.)	4.10	10.18	5.94	0.99	226 (100%)
		O (% db.)	27.61	53.10	42.44	5.20	210 (92.9%)
		N (% db.)	0.00	9.61	1.29	1.66	226 (100%)
		S (% db.)	0.09	0.92	0.48	0.24	152 (67.3%)
	Feedstock lignocellulosic composition	Cel (% db.)	17.89	47.67	37.52	8.24	122 (53.9%)
		Hem (% db.)	11.48	56.29	24.97	13.30	117 (51.7%)
		Lig (% db.)	4.99	32.26	22.56	6.54	122 (53.9%)
	Pyrolysis condition	RT (min)	1.00	90.00	38.08	18.76	226 (100%)
		PT (°C)	200	800	460.7	124.8	226 (100%)
		HR (°C/min)	5.00	25.00	11.37	5.69	226 (100%)
Output	Process Efficiency	Biochar yield (%)	17.68	95.89	39.53	15.10	226 (100%)
		Energy yield (%)	38.40	99.80	60.07	14.66	87 (38.5%)

	HHV (MJ/kg)	3.6	37.66	23.28	5.50	105 (46.5%)
Biochar proximate composition	FC (% db.)	15.04	94.11	53.57	19.77	159 (70.4%)
	VM (% db.)	0.49	82.72	32.37	20.00	159 (70.4%)
	ash (% db.)	0.32	37.91	14.05	9.02	159 (70.4%)
Biochar ultimate composition	C (% db.)	44.12	94.61	64.57	12.07	162 (71.7%)
	H (% db.)	1.26	8.72	3.69	1.50	150 (66.3%)
	O (% db.)	0.00	45.17	17.39	10.27	150 (66.3%)
	N (% db.)	0.00	9.05	1.48	1.38	162 (71.7%)
	S (% db.)	0.00	1.29	0.53	0.31	115 (50.9%)

The proximate compositions for both the biomass feedstocks and biochar were expressed in dry basis having the following components: FC, VM, and ash. It is important to note that the scope of the present dataset is limited to the feedstock ash content range 0-15%. To develop data-driven models for higher ash content input data, further expansion of the dataset is required in the future. The ultimate (or elemental) composition for the feedstocks and biochar is expressed in terms of C, H, O, N, and Sulphur (S). It is important to note that the literature contained a mix of wet-basis and dry-basis data for both feedstocks and biochar, which was converted on a dry-basis in the work using Eq. (3.1). The lignocellulosic composition of the feedstock contained three components such as lignin, cellulose, and hemicellulose (L-C-H). Essential pyrolysis process parameters found in the literature were PT, HR, and RT.

$$\mathrm{FC_{dry}} = \frac{\mathrm{FC_{wet}}}{1-\mathrm{MC}},\ \mathrm{VM_{dry}} = \frac{\mathrm{VM_{wet}}}{1-\mathrm{MC}},\ \mathrm{Ash_{dry}} = \frac{\mathrm{ash_{wet}}}{1-\mathrm{MC}} \quad (3.1)$$

Since the data collection was performed based on a wide range of literature, there were inevitably inconsistencies in the datasets, leading to missing values (see Table 3-1). For the input parametric space, several attributes were dropped if less than 70% of the data was available. Based on this, the S content and L-C-H composition of feedstock were excluded from model development. For the output dataset, the cut-off criteria were set to 65%, leading to exclusion of S content in biochar, HHV, and energy yield of biochar. Consequently, the modified dataset used for developing the model contained 10 input variables related to feedstock and pyrolysis conditions ($\mathrm{FC_{FS}}, \mathrm{VM_{FS}}, \mathrm{ash_{FS}}, \mathrm{C_{FS}}, \mathrm{H_{FS}}, \mathrm{O_{FS}}, \mathrm{N_{FS}}$, PT, HR, and RT) , and 8 output variables ($\mathrm{Yield_{BC}}, \mathrm{FC_{BC}}, \mathrm{VM_{BC}}, \mathrm{ash_{BC}}, \mathrm{C_{BC}}, \mathrm{H_{BC}}, \mathrm{O_{BC}}$, and $\mathrm{N_{BC}}$) quantifying biochar production.

The modified dataset still contained several missing values, which may lead to erroneous model training. To circumvent this problem, the missing values corresponding to an attribute were substituted by the mean of the attribute [141], which further ensured a continuous dataset. This process was only done during model training and therefore would not affect the performance of model testing. Model training is the process of using a dataset to teach a machine learning model to make predictions or classifications based on input data. During training, the model learns patterns and associations between samples by observing the samples and labels in the dataset. The goal of model training is to enable the model to accurately predict or classify new, unseen data. Data pre-processing steps such as dealing with missing values are critical in this process to ensure that the patterns the model learns from the data are accurate and meaningful. On other hand, model testing is the process of evaluating the performance of an already trained model on new, unseen

data. The test dataset is usually separated from the original dataset in order to evaluate the model's ability to generalise in real situations. During model testing, the test dataset is used to evaluate the model's ability to predict or classify unknown data. Through model testing, the performance of the model can be evaluated and any possible problems or room for improvement can be identified. Thus, model training and model testing are two very important phases in ML that work together to ensure that the model can learn valid patterns from the data and performs well on new data.

Since the dataset contained variables of different ranges, mean, and SD as shown in Table 3-1, data normalization was performed as an essential pre-processing step. Following conventional practices in ML, the standard normal variate Z_i was used, expressed as follows.

$$Z_i = \frac{X_i - \rho}{\sigma} \tag{3.2}$$

where X_i is the raw data, ρ is the mean, and σ is the SD of a variable.

To assess the relationship among any two variables (either between two different inputs or between inputs and outputs) Pearson Correlation Coefficient (*PCC*) was used, which quantify the degree of linear dependence (see Eq. 3.3) [104]. A *PCC* = 1 or *PCC* = -1 suggests that the variables are highly correlated, while a *PCC* = 0 means that the two variables are not correlated. This absolute value of *PCC* also revealed the relative importance of feature that impacts the output variables such as biochar yield, proximate composition (FC-VM-ash), and ultimate composition (C-H-O-N). Results obtained from the *PCC* and relative importance of various features are discussed in Chapter 3.3.1.

$$PCC = \frac{\sum_{i=1}^{n}(x_i - \bar{x})\sum_{i=1}^{n}(y_i - \bar{y})}{\sqrt{\sum_{i=1}^{n}(x_i - \bar{x})^2}\sqrt{\sum_{i=1}^{n}(y_i - \bar{y})^2}} \tag{3.3}$$

Here, $\bar{x}$ and $\bar{y}$ are the two variables of interest among which *PCC* is to be determined and *n* is the number of datapoints.

3.2.2 Artificial Neuro-Fuzzy Inference System

ANFIS is based on the Takagi-Sugeno inference method, which creates a nonlinear mapping from the input space to the output space using IF-THEN rules. The IF-THEN rules represent the form of "if A and B, then C" as presented in Table 3-2. The ANFIS model combines the characteristics of ANN and the fuzzy inference system [142].

Table 3-2. Simplified formulation of the ANFIS framework implemented in MATLAB.

Attribute	Mathematical structure
General rule	Rule 1: IF X is $A1$ AND Y is $B1$, THEN $f_1 = p_1X + q_1Y + r_1$
	Rule 2: IF X is $A2$ AND Y is $B2$, THEN $f_2 = p_2X + q_2Y + r_2$
First layer	$O_{1,i} = \mu_{Ai}(X)$, $i = 1,2$
	Gaussian Membership Function (MF): $\mu_{Ai}(X) = e^{\frac{-(X-\rho)^2}{2\sigma^2}}$, $i = 1,2$
Second layer	$O_{2,i} = W_i = \mu_{Ai}(X) \times \mu_{Bi}(Y)$, $i = 1,2$
Third layer	$O_{3,i} = \overline{W_i} = \frac{W_i}{\sum_{i=1}^{2} W_i}$
Fourth layer	$O_{4,i} = \overline{W_i} f_i = \overline{W_i} (p_iX + q_iY + r_i)$, $i = 1,2$
Fifth layer	$O_5 = \sum_i \overline{W_i} f_{i_i} =$ final output

The ANFIS model has five layers. The interactions between the different layers of the ANFIS model are shown in Fig. 3-1. The first layer nodes represent the input variables (*i.e.*, proximate composition of feedstock, ultimate composition of feedstock, HR, PT, and RT) and fuzzification. Each node in this layer is a fuzzy set and any output from it is the membership degree given from

the MF of the fuzzy set. The node of layer 2 is the rule node. This layer calculates the degree of MF by activating the AND operator of IF-THEN rules. Each output node in this layer represents the trigger strength of each rule. The third layer is responsible for determining the relative value of each rule in relation to the firing strength. The result of this layer is called the normalised firing strength. Nodes of layer 4 uses the consequent part of the Takagi-Sugeno approach, where subsequent parameter values and normalised firing strengths from the third layer of the rule base are calculated. The layer 5 is the output node, which corresponds to biochar yield, proximate composition, and ultimate composition. A simplified mathematical formulation of ANFIS is shown in Table 3-2. Here $A1$, $A2$ and $B1$, $B2$ are MFs of inputs X and Y, which are used to manipulate variables (or known as fuzzification). p_1, q_1, r_1 and p_2, q_2, r_2 are the relevant parameters of the output function determined during the model training. $O_{1,i}$ represents the output of the i^{th} node, and μ_{Ai} is the MF of Ai. Based on the literature the ANFIS developed here utilizes Gaussian MF due to its superior performance [128]. For the generalized Gaussian MF, ρ and σ are the mean and SD of the dataset, respectively. The ANFIS used seven MFs and 500 training epochs to give the optimal results, which is implemented in MATLAB R2021b.

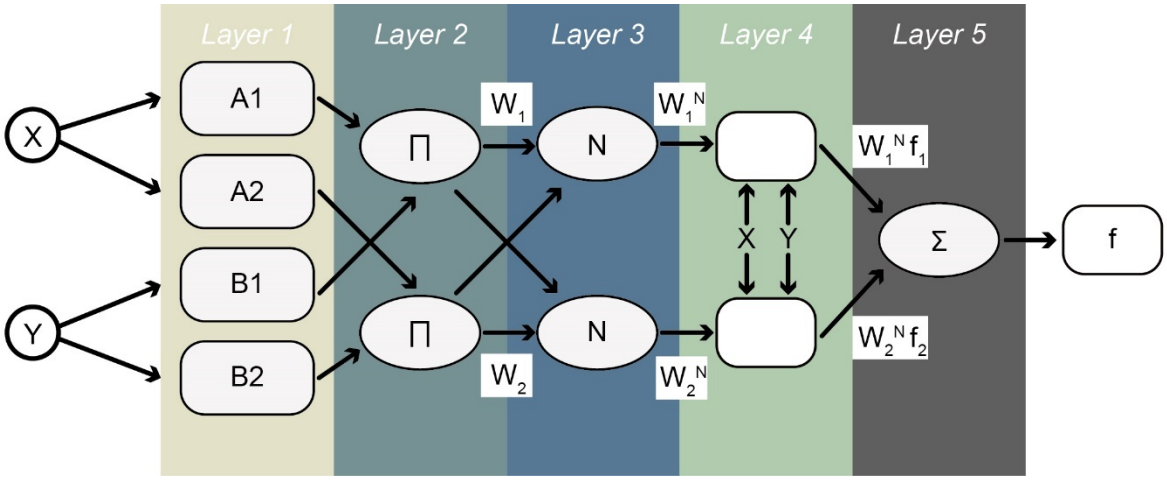

Fig. 3-1. Schematic representation of the ANFIS model.

3.2.3 Multi-layer Perceptron Neural Network

MLPs are fully connected feedforward NN used in supervised regression problems and utilize Levenberg-Marquardt back-propagation algorithm for training. The input data was applied to the MLP-NN in this training process, and the network's output was calculated employing randomly chosen initial weights. The output was then compared with the target and a weight correction process was performed in the opposite direction of the mean square error gradient. As a result, the difference between the network output and the desired output could be reduced.

MLP-NN usually has three layers: input layer, hidden layer, and output layer. Typically, it consists of small processing units called neurons. Each neuron composes of five components: input layer, basis and bias, summation function, activation function, and target. In this work the MLP-NN architecture has an input, an output layer, and the number of hidden layers varies between one, two, and three [141]. Previously, researchers have shown that this architecture can capture complex non-linear characteristic [127,143]. A representative schematic of the MLP-NN is shown in Fig. 3-2.

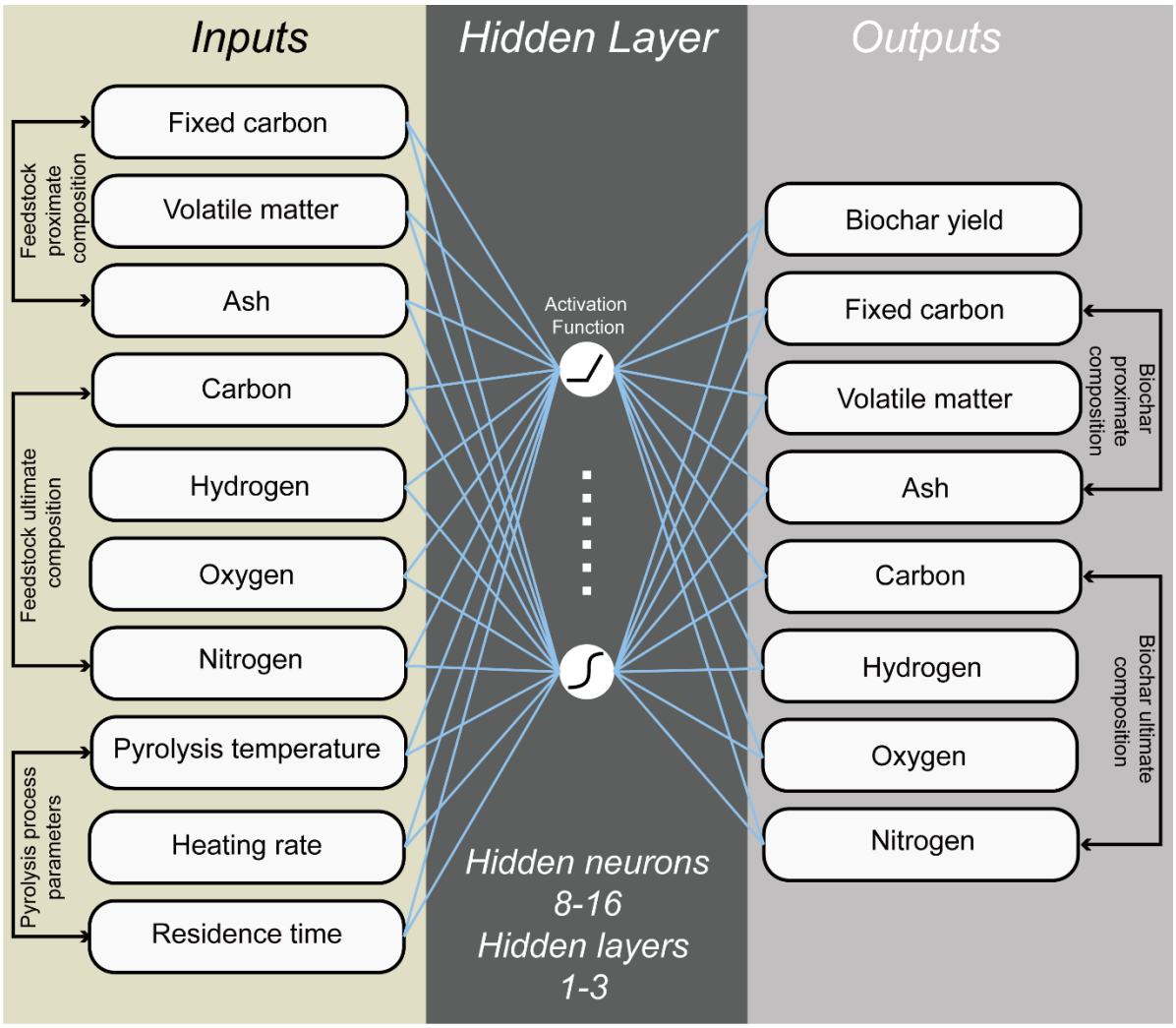

Fig. 3-2. Schematic representation of the MLP-NN architecture showing input variables, hidden layers, and output variables.

The activation function, also known as the transfer function, is either a linear or non-linear function that converts the weighted sum of the inputs (internally generated sum) into an output value. Here, three different activation functions such as (a) Rectified Linear Unit (ReLU), (b) Hyperbolic Tangent (Tanh), and (c) Sigmoid (see Eqs. 3.4-3.6) were considered. Different hyperparameters for the MLP-NN were also explored where the number of neurons varied from 8 to 16 and number of hidden layers were varied from 1 to 3. Three different combinations of data splitting for model training and testing were also evaluated *i.e.*, 80%/20%, 70%/30% and 60%/40%. Other fixed

parameters for the MLP-NN are maximum epoch = 300 and learning rate = 0.01. The entire model was implemented in Anaconda (a Python environment) with aid of the Sklearn library.

$$\text{ReLU} = \max(0, x) \tag{3.4}$$

$$\text{Tanh} = \frac{e^{x}-e^{-x}}{e^{x}+e^{-x}} \tag{3.5}$$

$$\text{Sigmoid} = \frac{1}{1+e^{-x}} \tag{3.6}$$

where x in Equations 3.4, 3.5, and 3.6 serves as the input to the respective activation functions, where it can vary over the entire real number domain.

3.2.4 Model Accuracy Evaluation Metrics

The performance of two data-driven models is examined and evaluated using different training-testing split on the dataset containing 226 datapoints. Two different metrics are considered, which are popular for ML regression problems such as *RMSE* and R^2, calculated as,

$$RMSE=\sqrt{\frac{1}{N}\sum_{i=1}^{N}\left(Y_i^{exp}-Y_i^{pred}\right)^2} \tag{3.7}$$

$$R^2= 1-\left[\frac{\sum_{i=1}^{N}\left(Y_i^{exp}-Y_i^{pred}\right)^2}{\sum_{i=1}^{N}\left(Y_i^{exp}-Y_{ave}^{exp}\right)^2}\right] \tag{3.8}$$

Here Y_i^{exp} and Y_i^{pred} are the experimental and model predicted biochar yields, Y_{ave}^{exp} is the average of all the experimental biochar yields, and N is the total number of datapoints which is 226 in this work.

3.3 Results and Discussion

3.3.1 Exploration of Dataset

The statistical characteristics for input (FC_{FS}, VM_{FS}, ash_{FS}, C_{FS}, H_{FS}, O_{FS}, N_{FS}, PT, HR, and RT) and output (Yield_{BC}, FC_{BC}, FC_{BC}, ash_{BC}, C_{BC}, H_{BC}, O_{BC}, and N_{BC}) variables were quantified via the

means and SDs of the input variables as shown in Table 3-1. Furthermore, the linear correlation among any two variables was assessed by *PCC* (see Eq. 3.3) and presented in form of a heatmap (Fig. 3-3a). Here, $PCC \approx 0$ signifies that the variables are weakly correlated, whereas $PCC \approx \pm 1$ suggests the highest correlation strength. Among the input parameters, strong correlations (with $PCC \geq 0.4$) were observed between several components of proximate and ultimate composition of biomass feedstock (PCC = 0.71 FC_{FS} vs. VM_{FS}, PCC = -0.54 for C_{FS} vs. ash_{FS}, PCC = 0.48 for FC_{FS} vs. ash_{FS}, PCC = 0.41 for H_{FS} vs. O_{FS}). Similar works in the literature reported the existence of a correlation between the proximate and ultimate compositions of biomass feedstock [104,120].

Subsequently, the $|PCC|$ values among inputs and outputs were visualized in Fig. 3-3b to 3-3d, which signify the relative importance of an input feature in predicting outputs. Fig. 3-3b revealed that the $Yield_{BC}$ is strongly affected by the input variable PT ($|PCC|$ = 0.76). The negative symbol of *PCC* for PT in Fig. 3-3a signified that increasing PT will reduce biochar yield. However, increasing PT could improve the C content in the biochar by reducing volatile components such as H, O, and N in biochar, which indicated the existence of a trade-off [144]. Fig. 3-3c showed the dependence of biochar proximate compositions ($FC_{BC}, FC_{BC}, \text{and } ash_{BC}$) on input variables. Strong correlations were observed between the following output vs. input pairs (in decreasing order): $|PCC|$ = 0.78 for FC_{BC} vs. PT, $|PCC|$ = 0.65 for ash_{BC} vs. ash_{FS}, $|PCC|$ = 0.65 for FC_{BC} vs. PT, and $|PCC|$ = 0.41 for FC_{BC} vs. ash_{FS}. Similarly, Fig. 3-3d revealed the significant dependence of biochar ultimate composition ($C_{BC}, H_{BC}, O_{BC}, N_{BC}$) on input variables as follows (in decreasing order): $|PCC|$ = 0.79 for O_{BC} vs. PT, $|PCC|$ = 0.74 for N_{BC} vs. N_{FS}, $|PCC|$ = 0.65 for H_{BC} vs. PT, $|PCC|$ = 0.53 for C_{BC} vs. PT, and $|PCC|$ = 0.5 for C_{BC} vs. ash_{FS}. Exploration of the feature importance demonstrated the strong influence of PT, affecting 6 out of 8 output variables

including $Yield_{BC}$. The remaining two variables ash_{BC} and N_{BC} were affected by ash_{FS} and N_{FS}, respectively. Therefore, any uncertainties associated with these variables would strongly affect the predictive performance of the data-driven models.

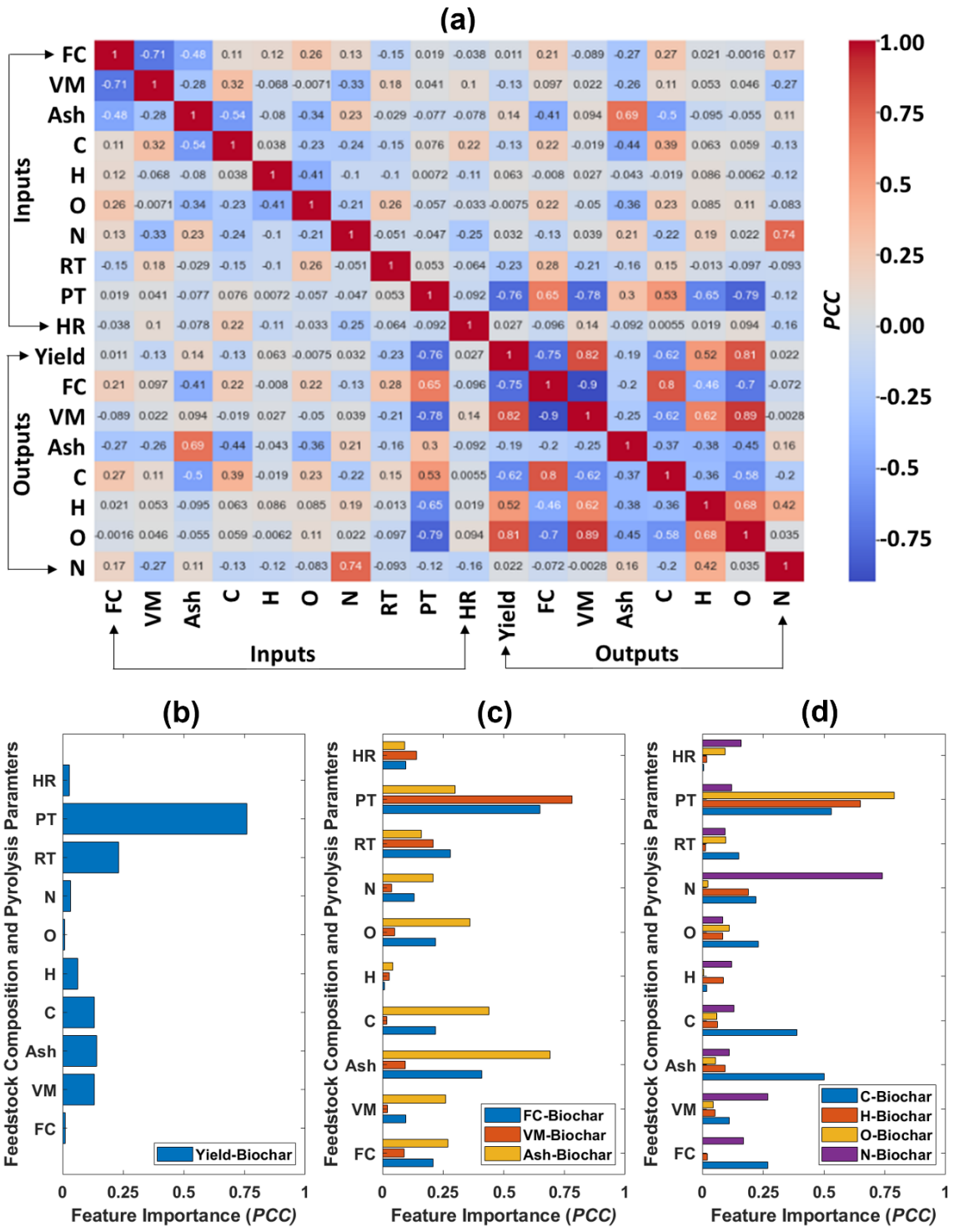

Fig. 3-3. (a) PCC between any two variables of interest. Relative importance of input features for predicting outputs: (b) biochar yield, (c) proximate composition of biochar (FC-VM-ash) and (d) ultimate composition of biochar (C-H-O-N).

3.3.2 Predictive Performance of Multi-layer Perceptron Neural Network

The predictive accuracy of an MLP-NN model depends on the hyperparameters selection, which includes choices for (1) the number of neurons within a hidden layer, (2) the number of hidden layers, and (3) the type of activation function. Table 3-3 lists various scenarios selected for determining the optimal hyperparameters. Cases 1A to 1E shows the influence of varying the number of neurons from 8 to 16 in an interval of 2. The fixed parameters for Cases 1A to 1E are 1 hidden layer, ReLU as the activation function, 80% training data, and 20% testing data. The choice of training-testing split is consistent with a prior work related to data-driven biochar yield prediction [104]. It is observed that as the number of neurons increases, the model accuracy improves at first. Beyond a certain value of neurons, *i.e.*, 14 in this case, the model accuracy degrades. When the MLP-NN consists of a lower number of neurons under a critical value (14 neurons), the model underfits the data and therefore results in higher *RMSE* and poor R^2. However, when the number of neurons is increased beyond a critical value, the MLP-NN model overfits and fails to achieve a higher accuracy in predicting the testing dataset [127,145]. This applied to all parameters. Overall, the optimal outcome of Cases 1A to 1E has the following accuracies for predicting biochar yield (R^2 = 0.964, *RMSE* = 3.4), proximate composition (average R^2 = 0.914, average *RMSE* = 4.4), and ultimate composition (average R^2 = 0.887, average *RMSE* = 1.8).

Table 3-3. Predictive performance of MLP-NN for variations in number of neurons, number hidden layers, and types of activation function for 80% training data and 20% testing data. R^2 and *RMSE* values for biochar yield, proximate composition (FC-VM-ash), and ultimate composition (C-H-O-N) are shown. Descriptions of various cases are described the text.

Case	Attribute	$Yield_{BC}$	FC_{BC}	VM_{BC}	ash_{BC}	C_{BC}	H_{BC}	O_{BC}	N_{BC}
1A	R^2	0.861	0.859	0.835	0.853	0.885	0.795	0.813	0.858
	RMSE	6.5	6.7	7.7	3.4	3.7	0.9	4.1	0.5
1B	R^2	0.892	0.880	0.861	0.874	0.893	0.823	0.846	0.876
	RMSE	5.1	6.2	6.9	2.9	3.6	0.7	3.8	0.4
1C	R^2	0.927	0.891	0.881	0.934	0.909	0.849	0.880	0.872
	RMSE	4.0	5.8	6.4	2.1	3.3	0.5	3.4	0.4
1D	R^2	0.964	0.903	0.899	0.940	0.918	0.855	0.887	0.888
	RMSE	3.4	5.1	6.1	2.0	3.1	0.5	3.3	0.4
1E	R^2	0.940	0.883	0.879	0.921	0.911	0.839	0.884	0.865
	RMSE	3.8	6.1	6.5	2.4	3.2	0.6	3.3	0.5
2A	R^2	0.964	0.903	0.899	0.940	0.918	0.855	0.887	0.888
	RMSE	3.4	5.1	6.1	2.0	3.1	0.5	3.3	0.4
2B	R^2	0.943	0.896	0.882	0.927	0.910	0.848	0.872	0.874
	RMSE	3.7	5.3	6.4	2.4	3.3	0.5	3.5	0.4
2C	R^2	0.917	0.879	0.865	0.918	0.901	0.839	0.853	0.871
	RMSE	4.2	6.2	6.8	2.5	3.5	0.6	3.7	0.4
3A	R^2	0.964	0.903	0.899	0.940	0.918	0.855	0.887	0.888
	RMSE	3.4	5.1	6.1	2.0	3.1	0.5	3.3	0.4
3B	R^2	0.918	0.888	0.891	0.929	0.901	0.846	0.869	0.876
	RMSE	4.2	5.8	6.1	2.3	3.3	0.5	3.6	0.4
3C	R^2	0.871	0.846	0.862	0.889	0.874	0.821	0.836	0.851
	RMSE	5.9	6.9	6.9	2.6	3.9	0.7	3.9	0.6

Once the number of neurons is fixed to 14 for the MLP-NN model, it is essential to further explore if increasing the number of hidden layers can improve the model predictions. Cases 2A to 2C in Table 3-3 correspond to increasing the hidden layer from 1 to 3. The fixed parameters for these cases are 14 neurons within a layer, ReLU as the activation function, 80% training data, and 20% testing data. Comparing the cases with the different number of hidden layers reveals that increasing the number of hidden layers to 2 and 3 diminishes the model prediction accuracy by up to 2.2% and 4.9% (with respect to Case 2A), respectively. Hence, using a single hidden layer in this case will not cause model overfitting and lead to better accuracy than a denser MLP-NN [127].

Subsequently, different activation functions such as ReLU (Case 3A), Tanh (Case 3B), and Sigmoid (Case 3C) were tested by fixing the number of neurons to 14 and number of hidden layers to 1. Utilizing the Tanh and Sigmoid activation functions degrade the model performance by up to 4.8% and 9.6%, respectively, when compared to the ReLU activation function. The nature of the ReLU activation function (see Eq. 3.4) avoids the vanishing gradient while training the MLP-NN model, since the function does not have any hard-bound upper limit. The Tanh activation function has a range of -1 to 1 (Eq. 3.5), while the range for the Sigmoid activation function is from 0 to 1 (Eq. 3.6). Therefore, the Sigmoid activation function is the most vulnerable to the vanishing gradient problem due to its shortest range, decreasing the accuracy of the model. It is essential to note that the MLP-NN model with both ReLU and Tanh activation functions significantly outperforms the existing works on biochar yield prediction which reports R^2 values 0.84 [105] and 0.85 [104] using the XGB and RF models, respectively. Moreover, the model developed had 3.7% better predictive accuracy, when compared to the best model reported (R^2 = 0.93) in the biochar yield prediction literature [120]. The parity plots shown in Fig. 3-4 to Fig. 3-11 compared the

predicted and actual values for 8 different outputs for the optimal scenario of MLP-NN. Actual values were from literature and prediction values were ML model outputs.

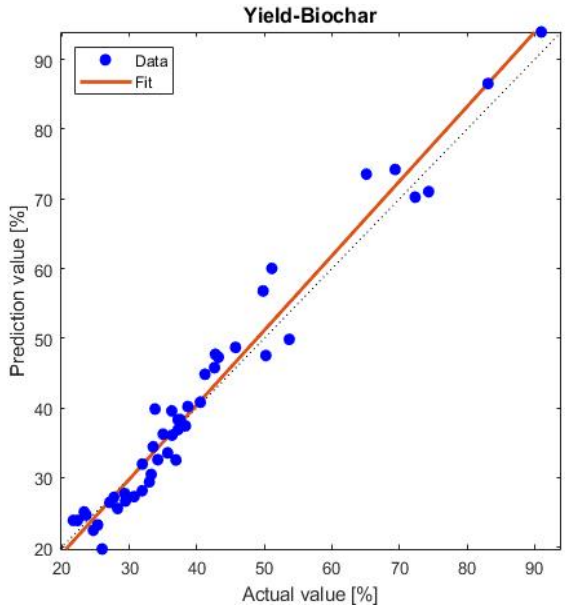

Fig. 3-4. Parity plots for MLP-NN comparing the actual and predicted values of biochar yield. The parity plots correspond to the optimal model training scenario with 14 neurons, 1 hidden layer, ReLU activation function, 80%/20% training–testing data split.

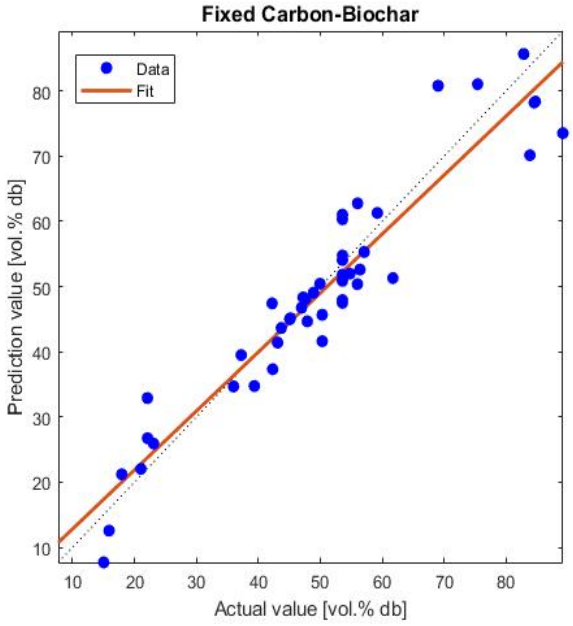

Fig. 3-5. Parity plots for MLP-NN comparing the actual and predicted values of FC in biochar. The parity plots correspond to the optimal model training scenario with 14 neurons, 1 hidden layer, ReLU activation function, 80%/20% training–testing data split.

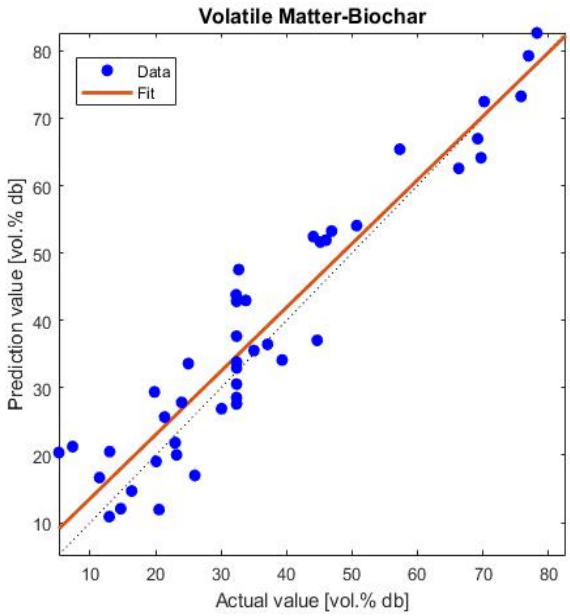

Fig. 3-6. Parity plots for MLP-NN comparing the actual and predicted values of VM in biochar. The parity plots correspond to the optimal model training scenario with 14 neurons, 1 hidden layer, ReLU activation function, 80%/20% training–testing data split.

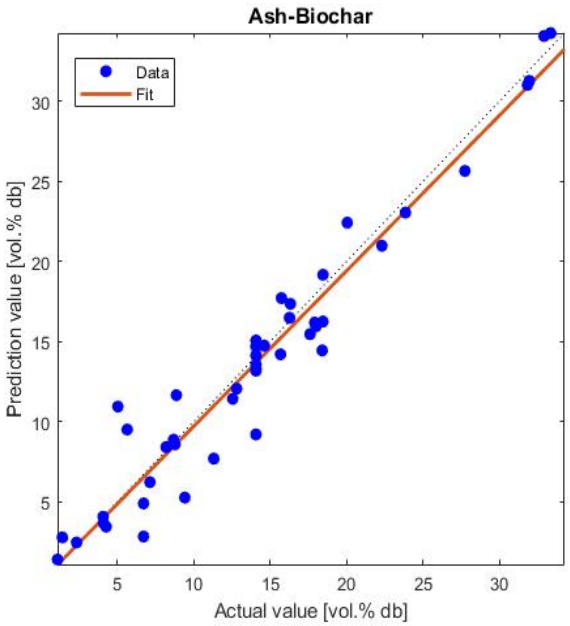

Fig. 3-7. Parity plots for MLP-NN comparing the actual and predicted values of ash in biochar. The parity plots correspond to the optimal model training scenario with 14 neurons, 1 hidden layer, ReLU activation function, 80%/20% training–testing data split.

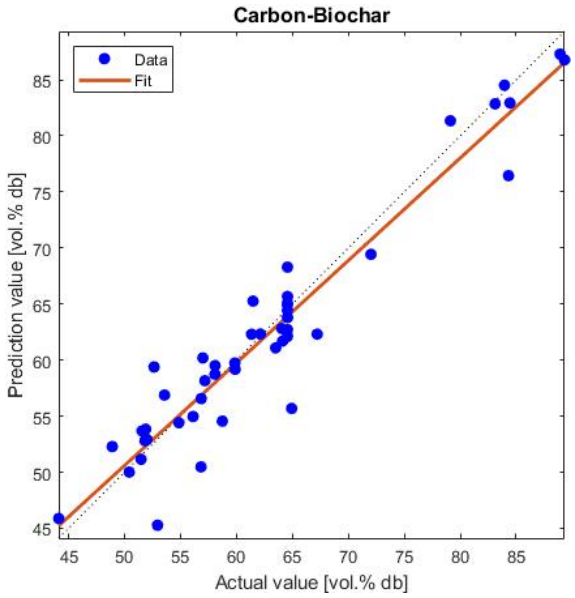

Fig. 3-8. Parity plots for MLP-NN comparing the actual and predicted values of C in biochar. The parity plots correspond to the optimal model training scenario with 14 neurons, 1 hidden layer, ReLU activation function, 80%/20% training–testing data split.

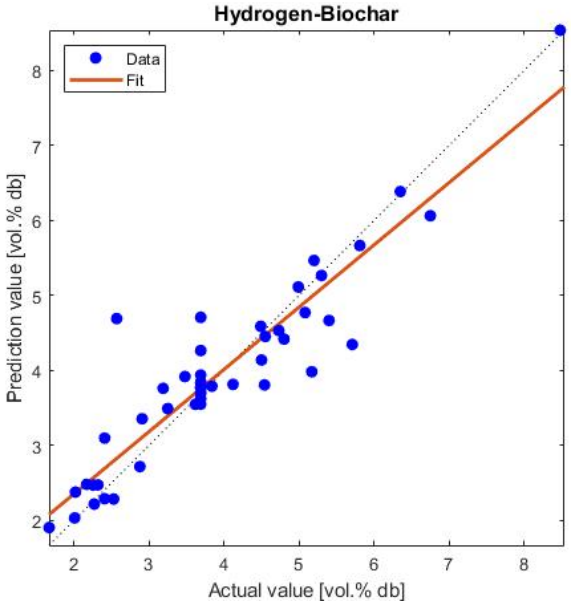

Fig. 3-9. Parity plots for MLP-NN comparing the actual and predicted values of H in biochar. The parity plots correspond to the optimal model training scenario with 14 neurons, 1 hidden layer, ReLU activation function, 80%/20% training–testing data split.

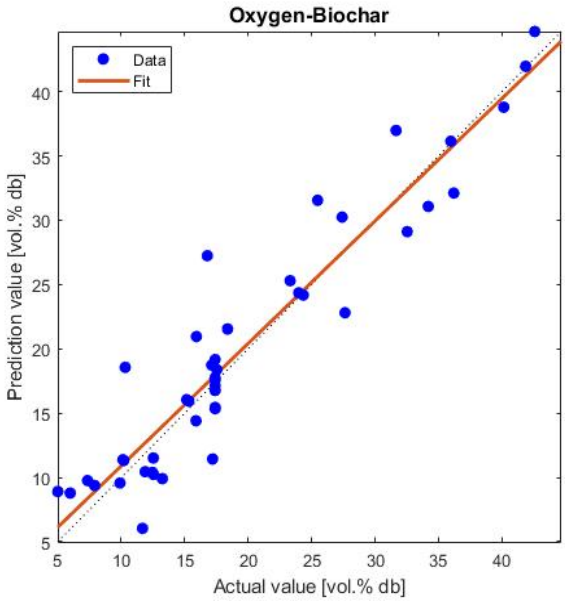

Fig. 3-10. Parity plots for MLP-NN comparing the actual and predicted values of O in biochar. The parity plots correspond to the optimal model training scenario with 14 neurons, 1 hidden layer, ReLU activation function, 80%/20% training–testing data split.

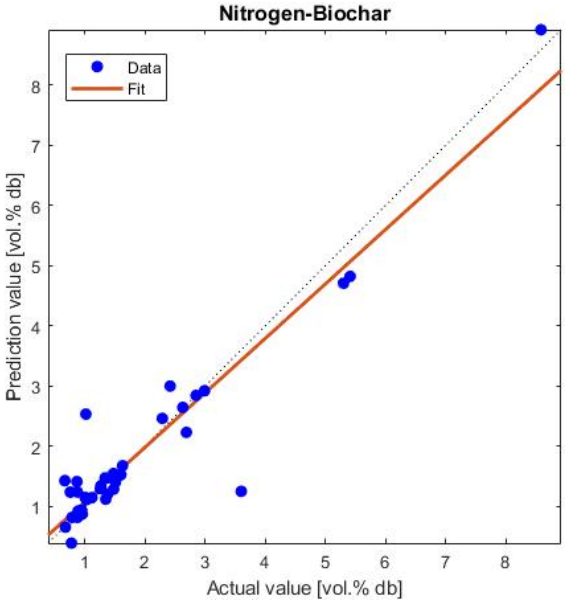

Fig. 3-11. Parity plots for MLP-NN comparing the actual and predicted values of N in biochar. The parity plots correspond to the optimal model training scenario with 14 neurons, 1 hidden layer, ReLU activation function, 80%/20% training–testing data split.

3.3.3 Predictive Performance of Artificial Neuro-Fuzzy Inference System

The predictive accuracy of ANFIS developed in this work was shown via the parity plots in Fig. 3-12 to Fig. 3-19. Overall, the ANFIS model had the following prediction accuracies for biochar yield (R^2 = 0.877, *RMSE* = 4.9), proximate composition (average R^2 = 0.838, average *RMSE* = 5.9), and ultimate composition (average R^2 = 0.855, average *RMSE* = 2.2). The ANFIS model with Gaussian MF, 7 MFs per input, 80% training data, and 20% testing data provided the optimal results. It was also found that the predictive accuracy of ANFIS for biochar yield, proximate composition, and ultimate composition were 9%, 8.3%, and 3.6% lower than those for MLP-NN. Nevertheless, the model provided a competitive R^2 value for predicting biochar yield compared to those reported in the literature [104,105].

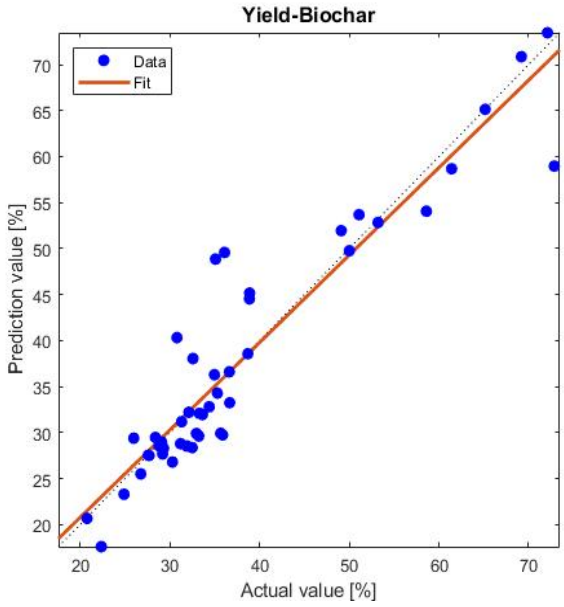

Fig. 3-12. Parity plots for ANFIS comparing the actual and predicted values of biochar yield. The parity plots correspond to the Gaussian MF, 7 MFs per unit, and 80%/20% training-testing data split.

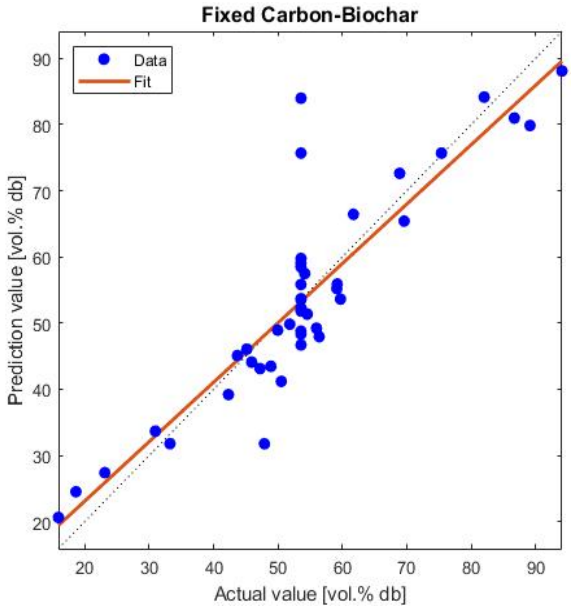

Fig. 3-13. Parity plots for ANFIS comparing the actual and predicted values of FC in biochar. The parity plots correspond to the Gaussian MF, 7 MFs per unit, and 80%/20% training-testing data split.

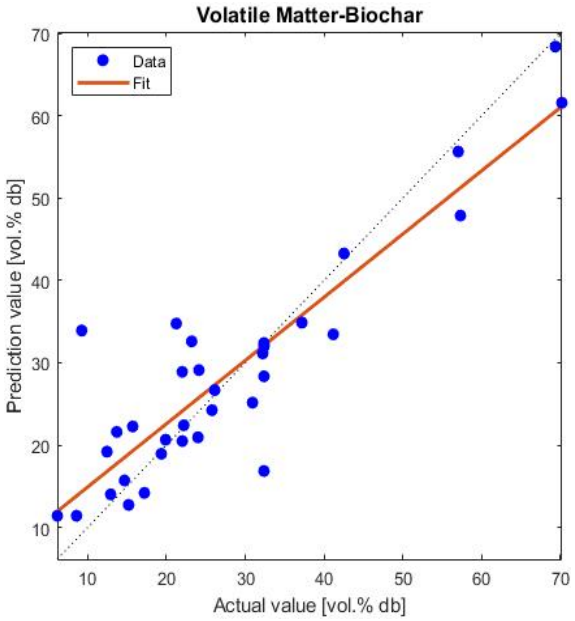

Fig. 3-14. Parity plots for ANFIS comparing the actual and predicted values of VM in biochar. The parity plots correspond to the Gaussian MF, 7 MFs per unit, and 80%/20% training-testing data split.

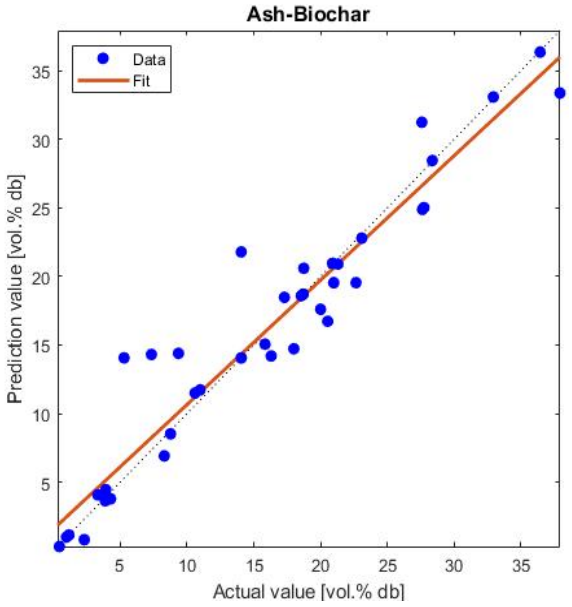

Fig. 3-15. Parity plots for ANFIS comparing the actual and predicted values of ash in biochar. The parity plots correspond to the Gaussian MF, 7 MFs per unit, and 80%/20% training-testing data split.

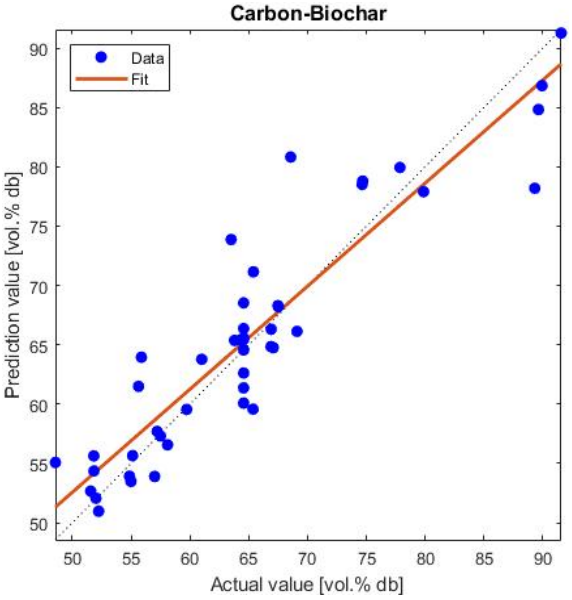

Fig. 3-16. Parity plots for ANFIS comparing the actual and predicted values of C in biochar. The parity plots correspond to the Gaussian MF, 7 MFs per unit, and 80%/20% training-testing data split.

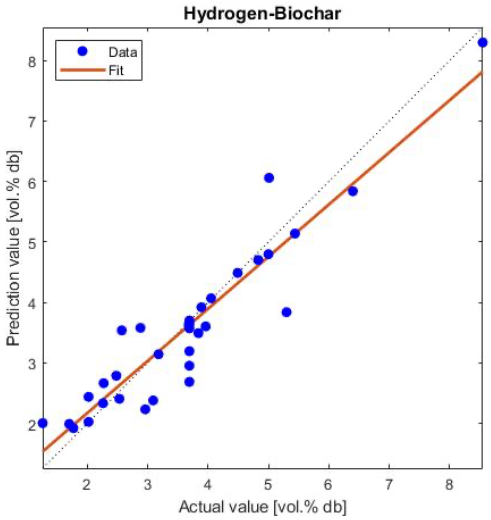

Fig. 3-17. Parity plots for ANFIS comparing the actual and predicted values of H in biochar. The parity plots correspond to the Gaussian MF, 7 MFs per unit, and 80%/20% training-testing data split.

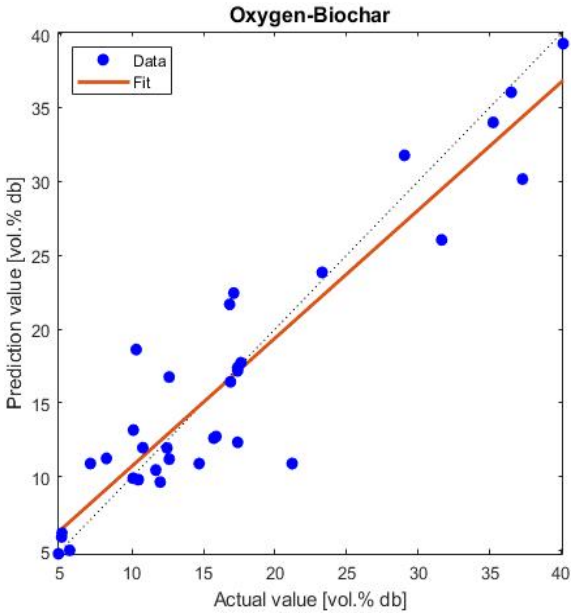

Fig. 3-18. Parity plots for ANFIS comparing the actual and predicted values of O in biochar. The parity plots correspond to the Gaussian MF, 7 MFs per unit, and 80%/20% training-testing data split.

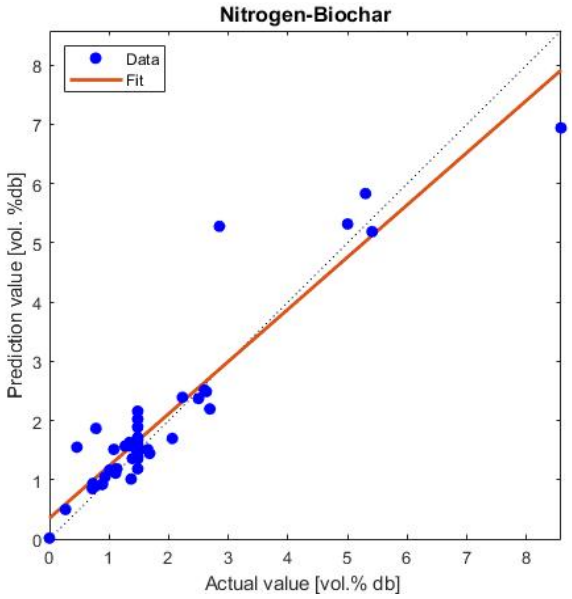

Fig. 3-19. Parity plots for ANFIS comparing the actual and predicted values of N in biochar. The parity plots correspond to the Gaussian MF, 7 MFs per unit, and 80%/20% training-testing data split.

3.3.4 Comparison of MLP-NN, ANFIS, and Existing Works

The generalizability of the MLP-NN and ANFIS model for predicting biochar yield, proximate composition, and ultimate composition was further investigated by varying the percentage of training testing dataset split. Three different training/testing percentage splits were considered for the overall database (226 datasets): 80%/20%, 70%/30%, and 60%/40%. Table 3-4 compares (1) MLP-NN with ReLu (Cases A-C), (2) MLP-NN with Tanh (Cases D-F), and (3) ANFIS (cases G-I) for different training/testing dataset split percentages. These results were further compared to relevant works from the data-driven biochar yield prediction literature [104,105,120,146].

Table 3-4. R^2 and *RMSE* values for biochar yield, proximate composition (FC-VM-ash), and ultimate composition (C-H-O-N) prediction using different proportions of training and testing data. The results are also compared to those reported in the biochar yield prediction literature. Descriptions of cases A to I are described the text.

Case	Attribute	$Yield_{BC}$	FC_{BC}	VM_{BC}	ash_{BC}	C_{BC}	H_{BC}	O_{BC}	N_{BC}
A	R^2	0.964	0.903	0.899	0.940	0.918	0.855	0.887	0.888
	RMSE	3.4	5.1	6.1	2.0	3.1	0.5	3.3	0.4
B	R^2	0.930	0.876	0.871	0.926	0.896	0.841	0.863	0.871
	RMSE	3.9	6.1	6.6	2.4	3.6	0.6	3.6	0.4
C	R^2	0.891	0.827	0.820	0.886	0.851	0.826	0.829	0.856
	RMSE	5.1	7.5	8.1	2.9	4.4	0.7	5.4	0.5
D	R^2	0.918	0.888	0.891	0.929	0.901	0.846	0.869	0.876
	RMSE	4.2	5.8	6.1	2.3	3.3	0.5	3.6	0.4
E	R^2	0.883	0.861	0.862	0.911	0.878	0.832	0.841	0.860
	RMSE	5.2	6.6	6.8	2.5	3.9	0.6	4.2	0.5
F	R^2	0.851	0.821	0.811	0.879	0.829	0.815	0.819	0.848
	RMSE	6.6	7.6	8.3	3.1	5.0	0.8	5.9	0.6
G	R^2	0.877	0.785	0.811	0.917	0.847	0.837	0.860	0.874
	RMSE	4.9	7.4	7.7	2.6	4.1	0.6	3.6	0.5
H	R^2	0.871	0.777	0.798	0.909	0.821	0.826	0.839	0.859
	RMSE	4.9	7.5	7.9	2.7	4.8	0.6	4.3	0.6
I	R^2	0.862	0.756	0.773	0.887	0.802	0.809	0.796	0.839
	RMSE	5.6	7.7	8.1	3.1	5.2	0.8	6.1	0.7
	R^2	0.855	---	---	---	0.848	---	---	---

RF model [104]	*RMSE*	3.4	---	---	---	5.8	---	---	---
SVM model [105]	R^2	0.804	---	---	---	---	---	---	---
	RMSE	6.4	---	---	---	---	---	---	---
XGB model [105]	R^2	0.844	---	---	---	---	---	---	---
	RMSE	---	---	---	---	---	---	---	---
ANN model [120]	R^2	0.93	---	---	---	---	---	---	---
	RMSE	1.74	---	---	---	---	---	---	---

Examining cases 1-3 revealed that changing the training-testing split from 80%/20% to 70%/30% decreases the predictive accuracy for biochar yield by 3.5%, proximate composition by 2.5%, and ultimate composition 2.2%. This suggested that with a 10% smaller training dataset, the performance of MLP-NN with ReLU was not significantly affected. Similar assessment was done for MLP-NN with Tanh activation function by comparing Cases 4-6. In this scenario, changing the training-testing split proportions from 80%/20% to 70%/30% degraded the predictive accuracy for biochar yield by 3.8%, proximate composition by 2.7%, and ultimate composition by 2.3%. For ANFIS (Cases 7-9), similar analysis reveals a performance degradation of 0.7% for biochar yield, 1.1% for proximate composition, and 2.1% for ultimate composition. Overall, the predictive accuracy of the MLP-NN with ReLU is up to 9.9% time better than that for ANFIS. An additional incentive offered by the MLP-NN model is that its computation time is 8 minutes for the present

work, which is approximately 3 times faster than the ANFIS model. All the model trainings were run on a desktop with 11th Gen Intel Core i5-11400F @ 2.50GHz processor with 8 GB RAM.

Further, the MLP-NN with ReLU activation function was compared to relevant works in the biochar prediction literature. It is important to note that relevant work in the biochar prediction literature is mostly limited to biochar yield prediction [105,120,146], except one where the carbon content of biochar was predicted in parallel to yield [104]. The MLP-NN with ReLU model has 4.8% better prediction accuracy than the best possible (R^2 = 0.92) biochar yield prediction model [120]. Simultaneously, the MLP-NN model has 8.2% better predictive accuracy for predicting C contents in biochar when compared to the RF model [104]. In addition, the present work predicts other elemental compositions (H-O-N) and proximate compositions (FC-VM-ash) of biochar produced via pyrolysis. These additional advantages proved the superiority of the present work, where a comprehensive model was developed for the biochar production process. Future research efforts are recommended to study the comparison of various data-driven models such as RF, XGB, SVM, and MLP-NN subjected to the same input dataset for simultaneous prediction of biochar yield and compositions.

3.4 Summary

Comprehensive data-driven models were developed to predict biochar yield and compositions based on pyrolysis conditions and biomass feedstock compositions. Feature importance analysis revealed high dependence of biochar yield and composition on PT, C content, and amount of N. The MLP-NN had predictive accuracies for biochar yield (R^2 = 0.964, *RMSE* = 3.4), proximate composition (R^2 = 0.914, *RMSE* = 4.4), and ultimate composition (R^2 = 0.887, *RMSE* = 1.8). The MLP-NN showed 9.9% and 12.7% performance improvement than ANFIS and existing works in

the literature, respectively. This opens avenues for future research in data-driven biochar process modelling and optimization.

Chapter 4 Machine Learning-assisted Life Cycle Assessment of Biochar Soil Application

In the previous chapter, the focus was on developing ML models and improving biochar predictive capabilities. Towards biochar production and application, it is key to know the the environmental impacts and LCA can play an important role. Combining ML with LCA can provide a more holistic view that utilises ML models to increase input data relevance and accuracy. Chapter 4 will cover a comprehensive assessment of different ML models with the aim of identifying and comparing their efficacy and applicability in LCA approach. Through comparative analyses, it will not only be able to validate the potential of the ML models developed in this Chapter, but also determine which model is best suited to deal with specific challenges in LCA. Such comparisons not only help to deepen the understanding of ML approaches in environmental assessment, but also provide a basis for selecting the most appropriate model to drive more accurate and reliable LCA results.

4.1 Introduction

Low quality soil is typically featured by high pH, high erosion rate and high nutrient leaching, adversely affecting the growth of agricultural products. Soil nutrient depletion is directly linked to food insecurity and is often caused by due to unsustainable intensified land use. Maintaining an appropriate level of soil organic matter and ensuring an effective nutrient biological cycle is essential for soil management [27]. Organic, inorganic, and chemical fertilisers have been developed as soil amendments to improve soil quality. However, there are various resource and environmental concerns about their applications. For example, rapid mineralization of soil organic matter is often encountered as a limitation upon the practical application of organic fertilisers in tropical areas. The production of fertilisers involves substantial inputs of non-renewable resources, including fossil fuels, which could emit large amounts of CO_2. The long-term use of chemical

fertilisers can cause various side effects such as soil pH value changes and damage to beneficial microbial ecosystems [13]. Overall, commercial N-fertilisers are widely used in agriculture but commonly have significant GHG impacts. In addition, soil microbial activity releases Nitrogen Oxides (N_2O) when applied to the soil. It has 265 times more potential environmental impact than CO_2 over 100 years [147]. In contrast, biochar as a soil amendment has great potential to mitigate the environmental issues and improve agricultural sustainability [148].

The core concept of biochar carbon sequestration is about fixing atmospheric CO_2 into biomass through photosynthesis and then pyrolyzing it into a stabilized solid product in the form of biochar, followed by soil applications for long-term carbon storage. The actual carbon sequestration capacity of biochar upon soil application, however, depends on various factors such as biochar yield and stable C content [149]. Hence, the capability of understanding and predicting the yield and properties of biochar is critical to designing optimal and efficient biochar systems for sustainable soil application. In particular, the environmental benefits of biochar production systems are contingent upon the efficiency of biochar production systems and need to be maximized to support the effective implementation of the systems [83].

Recently, ML-based models have been used to effectively estimate the yield and properties of biochar derived from a wide range of biomass. Typical ML models developed to predict biochar production include RF, XGBoost, ANN, and SVM [106]. ML modelling requires the preparation of a prior database based on which model training and testing are carried out. Generally, the database is split into a training dataset and a test dataset at a certain ratio. After the training process, the models are fed with testing data to assess their accuracy. In this study, five different ML models

were applied to predict the yield and properties of biochar produced from the pyrolysis of waste biomass.

It is important to understand the carbon-saving potential of biochar production and soil application to support widespread implementation of relevant technologies, for which the approach of LCA has been extensively applied. LCA is a standard protocol for quantifying the environmental impacts and resource use of processes and systems from a whole life-cycle perspective [150]. For example, Thers *et al.* [151] investigated the carbon sequestration potential of biochar produced from the pyrolysis of Danish oilseed rape. The carbon sequestration potentials were −392 and −429 kg CO_2-eq Mg^{-1} dry seed for 400°C and 800°C PT scenarios. Mohammadi *et al.* [152] evaluated the climate change impacts of biochar production system based on rice straw and husk in northern Vietnam. Compared to the direct rice straw open combustion scenario, the production of biochar from spring and summer rice straw reduced carbon footprint by 49% and 38%, respectively. However, for most of the existing LCA studies, nominal average parameters regarding biochar yields and properties were considered. There was limited capability to evaluate the carbon-saving potential of biochar soil applications with the accurate consideration of the influences of biochar production process conditions.

This work fills the knowledge gap by combining ML-based models with LCA for assessing the environmental impacts of biochar production and soil application under various process conditions. The optimal ML model informs the LCA model of the yield and properties of biochar, which systematically assesses the carbon saving potential of biochar production and soil application under different N fertiliser substitution scenarios. Feature importance analysis for ML modelling

and parameter sensitivity analysis for the overall LCA were also carried out. To the best knowledge of the authors, this is a maiden attempt to fulfil the comparison of a wide range of ML models for predicting pyrolysis-based biochar production and to apply ML modelling to assist LCA for biochar production and soil application.

4.2 Methods

The framework is based on the combination of ML modelling and LCA where data-driven ML models provided input parameters (biochar yield and properties) for the LCA to quantify the environmental impacts of biochar production and its soil application.

4.2.1 Machine Learning for Pyrolysis-based Biochar Production

4.2.1.1 Data Pre-processing

The work entailed deploying ML models to predict biochar yield and proximate and ultimate compositions of the biochar derived from biomass waste pyrolysis. The data-driven ML models were developed based on the data obtained from the literature which covered various feedstock properties and pyrolysis reaction conditions. The methodology of data pre-processing was summarised in section 3.2.1.

4.2.1.2 Machine Learning Model Development

Five types of ML methods were implemented in this work, which include MLP-NN, Tree, SVM, Tree Ensembles, and GPR. The ML modelling considers ten input features (*i.e.,* FC, VM, ash, C, H, O, and N contents of feedstock, PT, RT, and HR) and eight output features (*i.e.*, biochar yield, and FC, VM, ash, C, H, O, and N contents of biochar). Evaluating multiple methods on the identical dataset not only ensures that the robustness of modelling is not affected by the characteristics of a particular method, but also helps to identify a method for optimal prediction and application. MLP-NN was implemented in Anaconda (a Python environment) with the

assistance of the Scikit-learn library. Other four methods were tested based on the Regression Learner toolbox in the MATLAB R2023a software. The MATLAB toolbox delivers rapid training, validation, and selection of models using graphical interface, allowing fast exploration and comparison of different methods. The dataset was split into 80%/20% for model training and testing, respectively. The cross-validation folds number was set as 5. Meanwhile, the Bayesian Hyperparameter Optimization method was applied to optimize the hyperparameters for each ML model, with the number of iterations set to be 50.

The MLP-NN is a fully connected feedforward NN for supervised regression problems and can be trained using the Levenberg-Marquardt backpropagation algorithm. It generally has three layers: input, hidden, and output. Each layer has neurons which are small processing units consisting of five components: input variable, basis and bias, summation function, activation function, and target variable. Activation functions, also referred to as transfer functions, can be linear or nonlinear functions that convert a weighted sum (internally generated sum) of inputs to an output value. According to our previous work [106], the optimal hyperparameters for MLP-NN of biochar production are 3 layers, 14 neurons in one hidden layer, and ReLU for the activation function.

GPR is a kernel-based non-parametric, non-linear, and Bayesian probabilistic model. It has the advantage of performing well with small datasets. It can directly measure the model uncertainty and provide a distribution for the predicted value. The hyperparameters in the MATLAB toolbox allow the following options/ranges, respectively: Basis function (Constant, Zero, Linear); Kernel function *Rational quadratic, Matern 5/2, Squared Exponential, and Exponential); Sigma (0.0001–1.9087); Kernel scale (0.096–96).

The tree model, known as the regression tree, is constructed through an iterative process called binary recursive partitioning. It can be applied to both regression and classification problems. At each leaf, the regression tree produces a predicted value that is the average of all observation values in that leaf. The number of leaves were considered ranging from 1 to 83. The regression tree ensemble is a predictive model consisting of a weighted combination of multiple regression trees to improve the prediction accuracy of learning problems. In terms of performance, the ensemble often makes better predictions and achieves better performance than any single contributing model. Regarding robustness, the ensemble reduces the spread or dispersion of predictions and model performance. The process of ensemble learning can be divided into three phases: the prediction phase (train multiple individual tree models), the pruning phase (simplify and optimise the ensemble by pruning certain models or parts of models that may be overfitting), and the integration phase (combine the predictions from all models in the ensemble to produce a single final output). Essential hyperparameters considered included the ensembling method (Bagged and Least Square Boost (LSBoost)), the number of learners (10–500), learning rate (0.001–1), minimum leaf size (1–83), and the number of predictors to sample (1–10).

SVM constructs a model by training labelled datasets and then determines the hyperplane and decision boundary of the SVM model and uses a kernel function to separate unlabelled datasets of different classes. It aims to fit the data in a manner that errors do not exceed a certain threshold. The role of the kernel function is to improve the efficiency of determining the hyperplane and decision boundary. It is particularly effective for non-linear relationships between variables. By choosing appropriate parameters and kernels, it can capture complex relationships between input

and target variables. The optimisable hyperparameters (ranges or options) for the SVM model were kernel scale (0.001–1000), Epsilon (0.00021868–21.8681), Box constraints (0.001–1000), and kernel functions (Gaussian, linear, quadratic and cubic).

4.2.1.3 Model Performance Metrics

The performance of the data-driven models was examined and evaluated using *RMSE* and R^2. They are common metrics used for checking the accuracy and fit of regression-based problems as calculated by the following equations:

$$RMSE=\sqrt{\frac{1}{N}\sum_{i=1}^{N}\left(Y_i^{exp}-Y_i^{pred}\right)^2} \tag{4.6}$$

$$R^2=1-\left[\frac{\sum_{i=1}^{N}\left(Y_i^{exp}-Y_i^{pred}\right)^2}{\sum_{i=1}^{N}\left(Y_i^{exp}-Y_{ave}^{exp}\right)^2}\right] \tag{4.7}$$

where Y_i^{exp} and Y_i^{pred} are the experimental and model predicted outputs, Y_{ave}^{exp} is the average of all experimental outputs, and N is the total number of data points, which is 226 in this work.

4.2.2 Life Cycle Assessment

LCA can be applied to identify the "hotspots" of the environmental impacts of a product, process, or system. It consists of four phases: goal and scope definition, LCI, LCIA, and data interpretation. The LCA was carried out in Gabi software following the standard of ISO 14040:2006 and the details of the analysis are presented below.

4.2.2.1 Goal and Scope Definition

The objective of this study is to evaluate the environmental impact GWP of biochar production from pyrolysis and soil application. In this study, the GWP was measured in terms of carbon dioxide equivalent per tonne of feedstock ($kgCO_2$-eq/t feedstock). It allows the greenhouse effect of different GHGs to be expressed based on their equivalence to CO_2. The system boundary is shown in Fig. 4-1. The value shown in Fig.1 all reference in life cycle inventory (Table 4-1) The

Functional Unit (FU) is set to be the treatment of 1 tonne of feedstock. The system boundary covers biochar production and soil applications, including feedstock transportation, feedstock conditioning (grinding and drying), and pyrolysis plant operation, carbon sequestration potential, and fertiliser substitutions (urea ammonium nitrate and calcium ammonium nitrate). The system boundary excludes the application of bio-oil and syngas as pyrolysis co-products, as the focus of the study is on the application and production of biochar. The GWPs were investigated considering 3 PT conditions: 300°C, 400°C and 500°C, by which the influences of process temperature (a key influential factor for pyrolysis production) towards biochar properties and yields were incorporated into LCA.

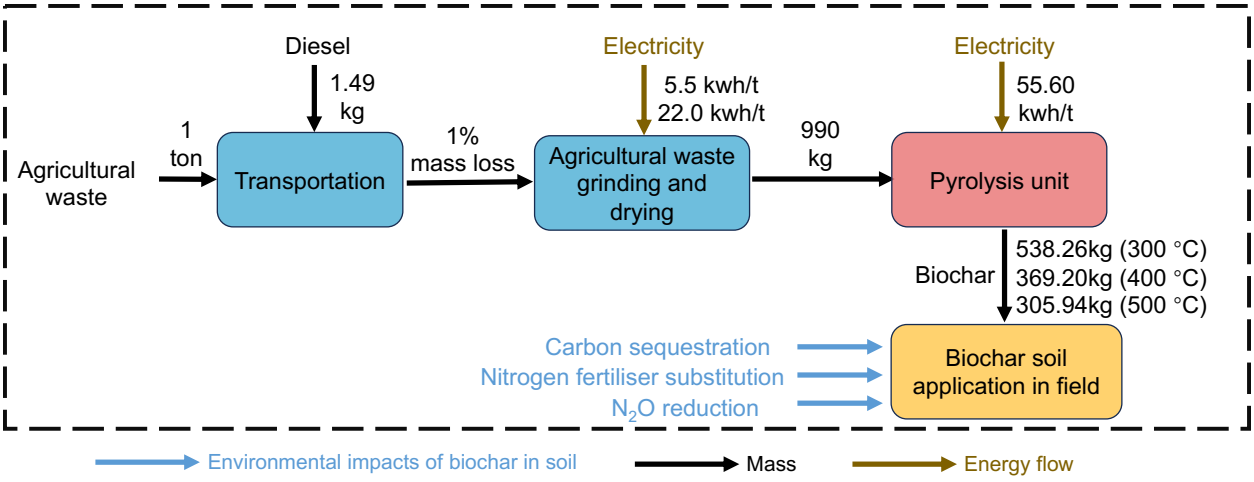

Fig. 4-1. The system boundary for the LCA of a biochar-soil system.

4.2.2.2 Life Cycle Inventory

Inventory data were collected from literature, laboratory data, commercial databases, and equipment operation manuals. Table 4-2 shows the inventory of input and output based on 1 tonne of feedstock. All data available from Gabi software database, the associated GWP calculated based on Gabi software. Gabi LCA software is a powerful software used to evaluate the environmental

impacts of various products, technologies, services, and systems. The electricity supplied by GB electricity grid (available in Gabi software) was used. The feedstock transport to the pre-processing and pyrolysis facility and road transport of biochar to the field by a truck (US: Truck - Dump Truck/52000 lb payload), the diesel consumption was 1.49 kg [153]. The related GWP was 4.790 $kgCO_2$-eq/t feedstock. The diesel mixed at refinery (GB: Diesel mix at refinery Sphera) associated GWP was 0.077 $kgCO_2$-eq/t feedstock. The feedstock was assumed to have a 1% mass loss after the transportation [153].

Prior to the pyrolysis processing of the feedstock, the raw material was ground using Cone Mill Machine CFZ-1000 with an electricity consumption of 5.5 kWh/t electricity [154]. The feedstock was then dried in the rotary disc dryer (TG-machines RDD-30), with pressure ranges up to 10 bar, temperatures from 158°C to 180°C, and an electricity consumption of 22.00 kWh/t [155]. The main components of the machine are the stator and the rotor.

Pyrolysis was carried out in a batch pyrolysis plant (Beston pyrolysis plant BLJ-16) with an electricity consumption of 55.60 kWh/t [156]. The biochar yields for 300°C, 400°C, and 500°C were predicted by the optimal ML model, which were outputs of ML model. The biochar mass can be calculated by the following equation:

$$M_B = B_y \times M_f \quad (4.8)$$

where M_B is mass of biochar (kg); $B_y$is the biochar yield (%); M_f is mass of feedstock (kg).

Table 4-1. The inventory of input based on 1t feedstock.

Processes	Value	Unit	Reference

Pre-processing			
Feedstock diesel consumption	1.49	kg	[153]
Feedstock grinding (electricity use)	5.50	kWh/t feedstock	[154]
Feedstock drying (electricity use)	22.00	kWh/t feedstock	[155]
Pyrolysis unit			
Pyrolysis electricity unit	55.60	kWh/t feedstock	[156]
Biochar production			
Biochar mass (300 °C)	54.36	wt.%	Model prediction
Biochar mass (400 °C)	37.29	wt.%	Model prediction
Biochar mass (500 °C)	30.90	wt.%	Model prediction
Biochar application			
Fraction of C contains in soil after 100 years (300 °C)	50%		[157]
Fraction of C contains in soil after 100 years (400 °C)	65%		[157]
Fraction of C contains in soil after 100 years (500 °C)	75%		[157]
Urea ammonium nitrate carbon footprint	2.37	$kgCO_2$-eq/kg product	[158]
Calcium ammonium nitrate carbon footprint	2.86	$kgCO_2$-eq/kg product	[158]

4.2.2.3 Biochar Soil Application

Biochar was applied to the field for carbon sequestration and N fertiliser displacement. Biochar has the potential to be used as an alternative to commercial fertilisers due to its nitrogenous nature [159]. The optimal ML model was used to predict the C and N contents of the biochar, which were then applied to estimate relevant GHG emissions. It is assumed that the N in biochar can be used

for a 1:1 substitute to N fertiliser. The urea ammonium nitrate and calcium ammonium nitrate have 30% and 27% N contents, and their carbon footprints are 2.37 $kgCO_2$-eq/kg product and 2.86 $kgCO_2$-eq/kg product, respectively [158]. Two fertiliser displacement scenarios were analysed corresponding to the two types of fertilisers. Also, the C stability (fraction of biochar C remaining in soil for durations after 100 years) of biochar produced at 300°C, 400°C and 500°C was assumed to be 0.50, 0.65 and 0.75 over 100 years, respectively [157]. The carbon sequestration potential and N fertiliser displacement were estimated as follows:

$$C_{CS} = -M_B \times C_{SC} \times C_B \times 3.67 \quad (4.9)$$

$$M_F = \frac{M_B \times N_C}{N_F} \quad (4.10)$$

where C_{CS} is carbon sequestration in soil ($kgCO_2$-eq); M_B is the biochar mass (kg); C_{SC} is the stable C content in biochar (%); C_B is the C content in biochar (%) predicted by the ML model; 3.67 is C-CO_2 conversion coefficient; M_F is the replacement fertiliser mass (kg); N_C is the N content in biochar (%); N_F is the N content in the fertiliser displaced by biochar (%).

Meanwhile, the application of biochar to soil also has the potential to reduce N_2O emissions. A meta-analysis by Kaur *et al.* [160] found that biochar significantly reduced soil N_2O emissions by 38.8%. According to Equation 4.10, the masses of the two N fertilisers (urea ammonium nitrate and calcium ammonium nitrate) replaced by biochar were 21.05 kg, 12.03 kg, 9.98 kg, 35.87 kg, 20.50 kg, and 17.00 kg for three different temperatures ranging from 300°C to 500°C, respectively. The biochar mass was 538.26 kg, 369.29 kg, and 305.93 kg, respectively. The Food and Agriculture Organization (FAO) illustrated that for a crop field per hectare, considering a correction factor, 52 kg of nitrogen fertiliser is required per hectare. This demonstrates the FAO's approach to optimizing nitrogen fertiliser use on farms, considering factors like crop yield and specific fertiliser

requirements [161]. According to Equation 4.11, the applied field area for the corresponding fertiliser weight can be calculated. In the context of wheat cropping, the maximum N_2O emission per hectare was 3.5 kg N_2O/ha at a rate of 100 kg N/ha [162]. Based on Equation 4.12, the N_2O emissions corresponding to the fertiliser applied to the field can be calculated. Equation 4.13 refers to the reduction in N_2O emissions following biochar application to the field.

$$A_a = \frac{M_F}{52} \tag{4.11}$$

$$E_{N_2O} = 3.5 \times \frac{M_F}{100} \tag{4.12}$$

$$E_R = A_a \times E_{N_2O} \times 38.8\% \tag{4.13}$$

Where A_a is fertiliser applied area (ha); E_{N_2O} is applied fertiliser N_2O emission per hectare (kg N_2O/ha); E_R is the reduction in N_2O emissions for the biochar applied to field (%).

4.2.2.4 Life Cycle Impact Assessment

LCA was implemented through the software GaBi for backend data support and calculation of impact categories. The GWP of the system over 100 years is considered as the environmental impact metric with a unit of kgCO_2-eq/t feedstock. GaBi provides several impact assessment quantification methods such as CML 2001–2016, EDIP 2003, ReCiPE 1.08, *etc*. CML 2001–2016 was applied as it is relatively transparent and has less uncertainty in its calculation [163].

4.2.2.5 Sensitivity Analysis

Sensitivity analysis was conducted to quantify the influences of major parameters (*e.g.,* biochar yield, stable C content in biochar, pyrolysis power consumption, N content in biochar) towards the results of LCA. Each parameter was varied by 10% while the other parameters remained unchanged for the sensitivity analysis. The individual effects of parameters on GWP were expressed in terms of a Sensitivity Ratio (SR) defined as:

$$SR = \frac{\left|\frac{GWP_i^{baseline} - GWP_i^{modified}}{GWP_i^{baseline}}\right|}{\left|\frac{\Phi_i^{baseline} - \Phi_i^{modified}}{\Phi_i^{baseline}}\right|} \quad (4.14)$$

where Φ_i and GWP_i are the values of the i^{th} parameter and the corresponding GWP.

4.3 Results and Discussion

4.3.1 Exploration of Data

The *PCC* values between the variables in the dataset were calculated to assess the correlation between them, which is presented as the heatmap in Fig. 4-2. The *PCC* values range from –1 to 1. Fig. 4-3 visualises the $|PCC|$ by the bar chart, revealing the relationship between the input variable (FC_{input}, VM_{input}, Ash_{input}, C_{input}, H_{input}, O_{input}, N_{input}, PT_{input}, RT_{input}, and HR_{input}) and output variable (Biochar yield, $C_{biochar}$, and $N_{biochar}$). For biochar yield, PT was the dominant parameter with a $|PCC|$ value of 0.76, which is also consistent with that reported by Zhu *et al.* [104]. This supports the consideration of the impacts of different temperature conditions in the LCA. Increasing PT reduces biochar yield but increases its C content by reducing volatile components like H, O, and N, highlighting a trade-off between yield and C content in biochar. In addition, the C content of the feedstock had second important effect on the C content of biochar ($|PCC|$ = 0.39). The most influential variable for the N content in biochar is the N content in the feedstock ($|PCC|$ = 0.74), which means that higher N content in the feedstock produces a consequential higher N content in the biochar. Research in the literature reported a similar correlation between the compositions of feedstock and biochar [120].

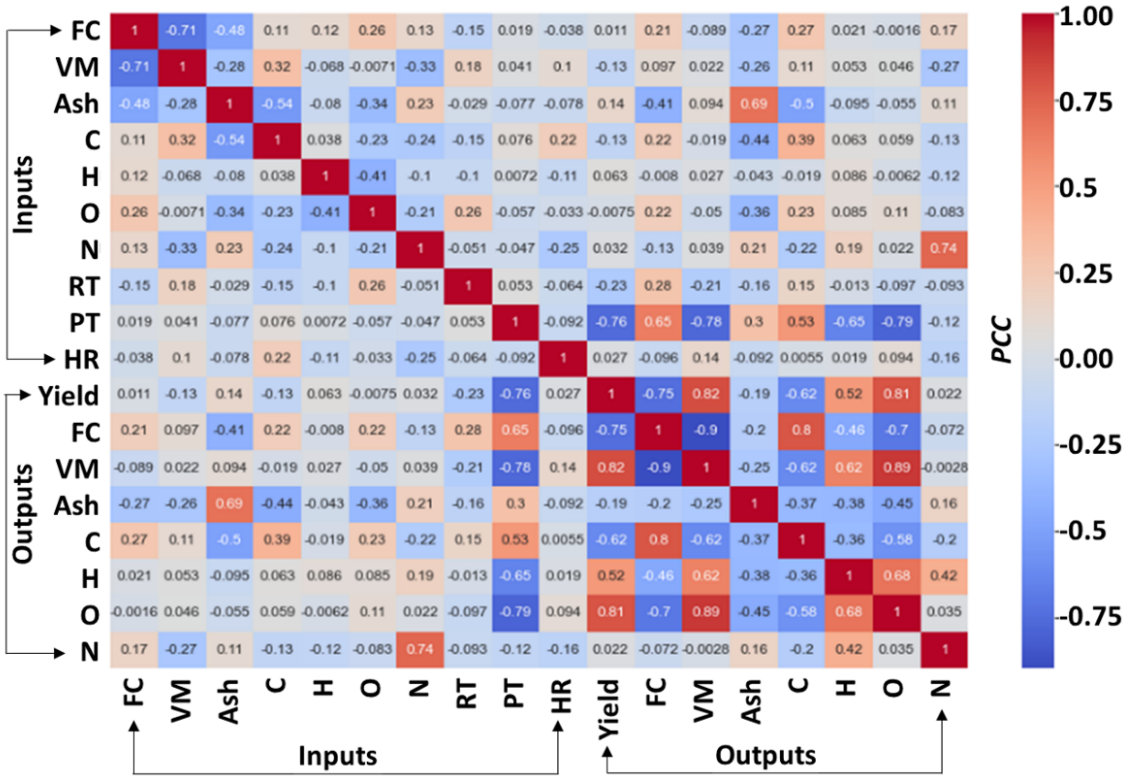

Fig. 4-2. Heatmap: PCC between any two variables of interest.

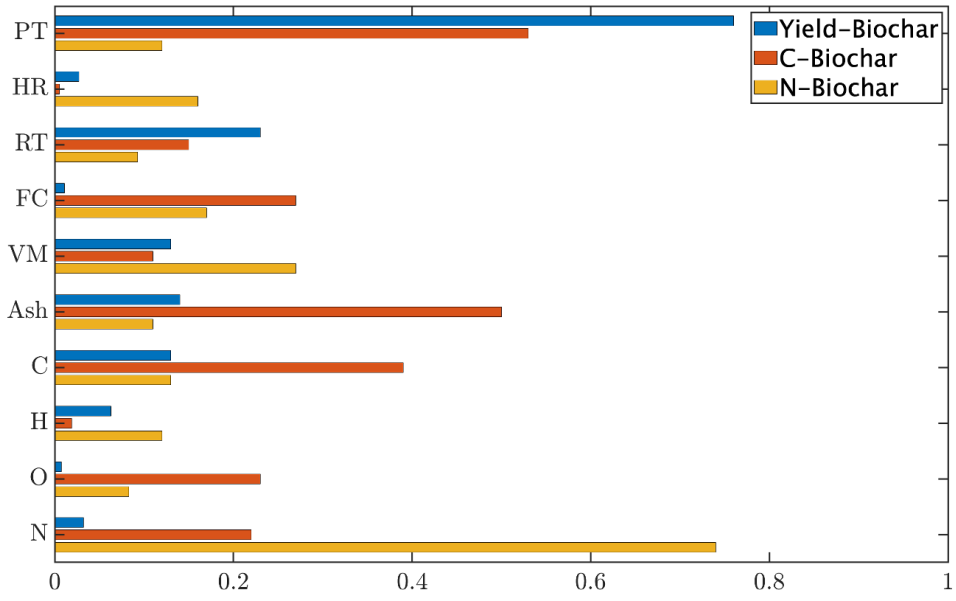

Fig. 4-3. The relative importance of input features to predicted outputs which are used in the LCA, *i.e.*, biochar yield, and C and N contents in biochar.

4.3.2 Machine Learning Model

A comprehensive comparison of the 5 data-driven models (MLP-NN, SVM and GPR, tree and ensembles) used to construct predictive models for biochar yield, C content and N content was presented in Table 4-3. In addition to the performance metrics, R^2 and *RMSE*, the information about the prediction speed (Obs/s) and training time (in seconds) was also presented.

Table 4-2. Comparison of the 5 data-driven models used to construct predictive models for biochar yield, and the C and N contents of biochar.

Output Attribute	Model type	Optimal Hyperparameters	R^2	*RMSE*	Prediction speed (Obs/s)	Training time (s)
Biochar yield (%)	MLP-NN	Hidden layer: 1, Activation: ReLU, Iteration limit: 395, Learning rate: 0.033, Momentum=0.364, Standardize data: Yes, MLP Regrressor: Early stopping	0.964	3.51	1123.8	3.213
	Ensembles	Ensemble method: Bagged tree, minimum leaf size: 8, number of learners: 30, number of predictors to sample: 10	0.891	5.29	1029.8	3.615
	SVM	Kernel function: Quadratic, Kernel scale: Automatic,	0.874	5.67	1181.7	3.185

		Box constraint: Automatic, Epsilon: Auto, Standardize data: Yes				
	Tree	Minimum leaf size: 4, Surrogate decision splits: Off	0.867	5.84	4655.5	6.429
	GPR	Basis function: Constant, Kernel function: Rational Quadratic, Use isotropic kernel: Yes, Kernel scale: Automatic, Signal SD: Automatic, Sigma: Automatic, Standardize data: Yes, Optimize numeric parameters: Yes	0.866	5.86	1045.1	2.119
Biochar C (%)	MLP-NN	Hidden layer: 1, Activation: ReLU, Iteration limit: 635, Learning rate: 0.085, Momentum=0.715, Standardize data: Yes, MLPRegrressor: Early stopping	0.918	3.20	2986.3	4.129
	Tree	Minimum leaf size: 4, Surrogate decision splits: Off	0.847	4.36	417.1	10.933

	SVM	Kernel function: Cubic, Kernel scale: Automatic, Box constraint: Automatic Epsilon: Auto, Standardize data: Yes"	0.845	4.39	2561.5	8.938
	GPR	Basis function: Constant Kernel function: Exponential, Use isotropic kernel: Yes, Kernel scale: Automatic, Signal SD: Automatic, Sigma: Automatic, Standardize data: Yes, Optimize numeric parameters: Yes	0.836	4.53	1179.8	18.416
	Ensembles	Minimum leaf size: 8, Number of learners: 30, Number of predictors to sample: 10	0.801	4.99	887.8	19.326
Biochar N (%)	GPR	Basis function: Constant, Kernel function: Exponential, Use isotropic kernel: Yes, Kernel scale: Automatic, Signal SD: Automatic, Sigma:	0.937	0.36	726.7	2.833

	Automatic, Standardize data: Yes, Optimize numeric parameters: Yes				
SVM	Kernel function: Quadratic Kernel scale: Automatic Box constraint: Automatic Epsilon: Auto, Standardize data: Yes	0.935	0.37	708.0	3.128
MLP-NN	Hidden layer: 1, Activation: ReLU, Iteration limit: 395, Learning rate: 0.029, Momentum=0.364, Standardize data: Yes, MLPRegrressor: Early stopping	0.933	0.37	3101.9	3.239
Tree	Minimum leaf size: 4, Surrogate decision splits: Off	0.850	0.56	5450.3	4.654
Ensembles	Minimum leaf size: 8, Number of learners: 30, Learning rate: 0.1, Number of predictors to sample: 10	0.758	0.72	684.3	3.462

For the prediction of biochar yield, the MLP-NN model with one hidden layer, ReLU activation function and optimised hyperparameters showed exceptional performance with an R^2 of 0.964 and

an *RMSE* of 3.51. It achieved a prediction speed of 1,123.8 obs/s and a short training time of 3.213s. In terms of biochar C prediction, the MLP-NN model (R^2 = 0.918, *RMSE* = 3.20) also exhibited the best performance, with the hyperparameters one hidden layer: and activation function ReLU. The nature of the ReLU activation function avoids the occurrence of gradient vanishing during the training of the MLP-NN model as it does not have any hard constrained upper bound. Furthermore, the MLP-NN model utilises the early stopping technique, which is an overfitting prevention technique by stopping the training process before the model completes its training. Regarding biochar N prediction, the GPR model with the Exponential kernel function exhibited remarkable accuracy (R^2 = 0.937, *RMSE* = 0.36), which was slightly better than the MLP model (R^2 = 0.933, *RMSE* = 0.37). Notably, the superior performance of the GPR model is attributed to the ability of the probabilistic Gaussian process to handle datasets with a high degree of variance. Overall, MLP-NN and GPR, as two different types of ML models, each have different advantages and applicable scenarios. For complex nonlinear relationships and data with more features, MLP-NN may be more applicable. GPR may be more advantageous for data with high stochasticity and noise, and where a good estimate of the uncertainty of the prediction is required. Such discrepant results provide more options for scientific research and emphasise the importance of the need to consider data characteristics and task requirements when selecting a model.

The parity plots shown in Fig. 4-4 to Fig.4-6 for the optimal model showed the comparison between the actual and predicted values of biochar (a) yield, (b) C, and (c) N. The parity plots (a) and (b) correspond to the MLP-NN model, and (c) to the GPR model.

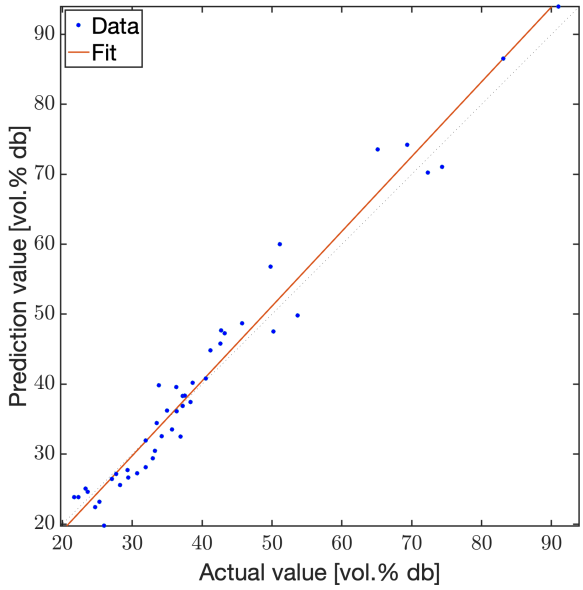

Fig. 4-4. Parity plots for optimal model comparing the actual and predicted values of biochar yield correspond to the MLP-NN model.

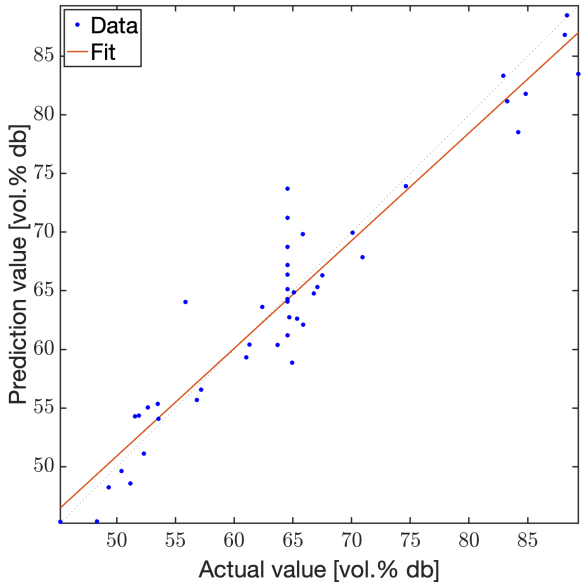

Fig. 4-5. Parity plots for optimal model comparing the actual and predicted values of C content in biochar correspond to the MLP-NN model.

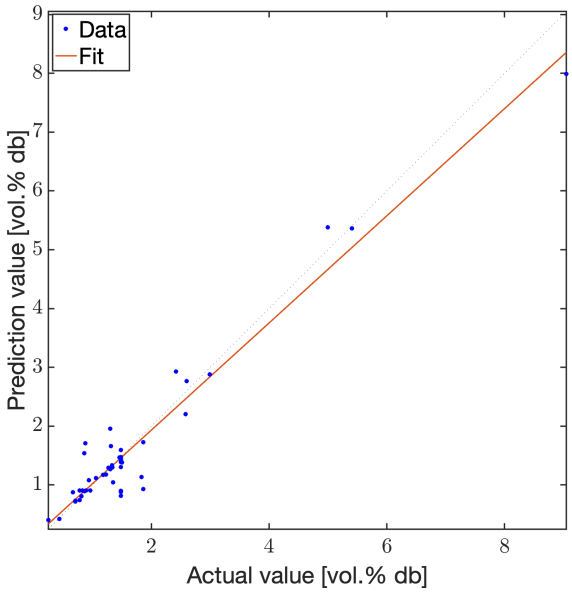

Fig. 4-6. Parity plots for optimal model comparing the actual and predicted values of N content in biochar correspond to the GPR model.

Fig. 4-7 provides showed the yield, and the C and N contents in biochar produced at three distinct PTs: 300°C, 400°C, and 500°C, as predicted by the optimal ML models. The centre line of each box represents the median of the data, while the upper and lower boundaries of the boxes represent the upper and lower quartiles. The whiskers show the maximum and minimum values of the data. In order to more clearly represent the differences in data distribution, Fig. 4-7(a) to Fig. 4-7(c) show the distribution of data within the domains of different predicted values for biochar yield, C content in biochar, and N content in biochar, respectively. This provides a comprehensive view of the data variation at different treatment temperatures. It is worth noting that all 5 ML models developed are able to predict biochar yields as well as proximate properties (FC-VM-Ash) and ultimate properties (C-H-O-N) of biochar, which creates a prospective path for future work to extend the application of biochar to the scenarios the properties are relevant.

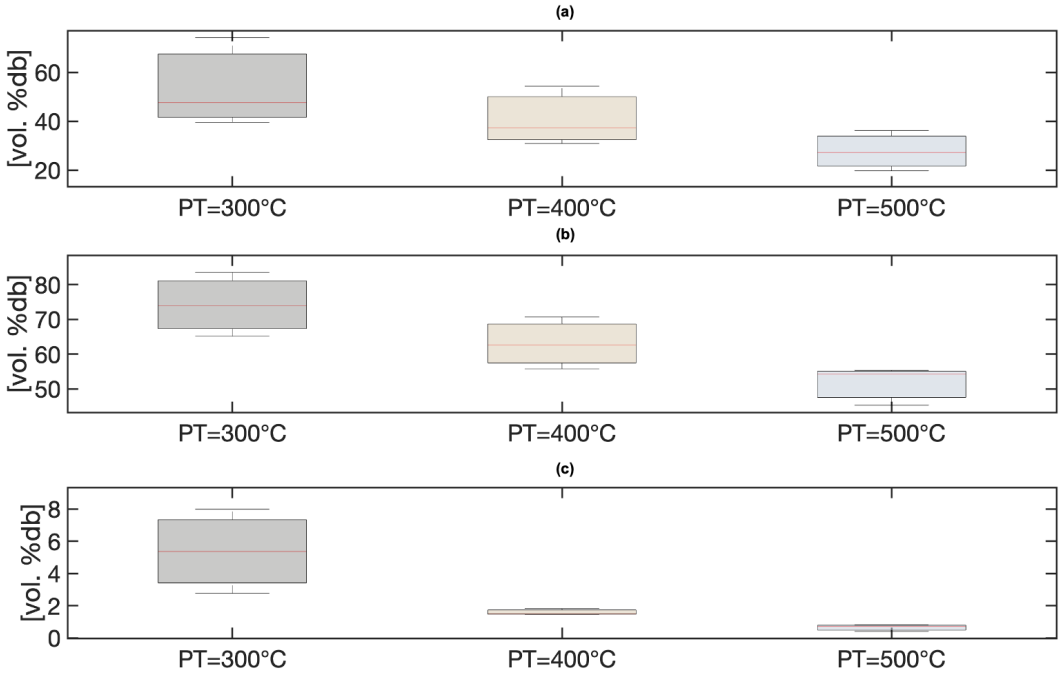

Fig. 4-7. Box and whisker chart for predicted values of (a) biochar yield, (b) biochar C content, and (c) biochar N content corresponding to PT at 300°C, 400°C and 500°C.

4.3.3 Life Cycle Assessment

Fig. 4-8 and 4-9 showed the GWP (measure in $kgCO_2$-eq/t feedstock) breakdown of biochar production and soil application. The scenarios are differentiated according to the two types of fertiliser displacement: urea ammonium nitrate and calcium ammonium nitrate and three PT conditions: PT=300°C, PT=400°C and PT=500°C. Significantly, the carbon sequestration by biochar carbon storage in soil showed a dominant negative impact (The meaning of environmental benefits) on GWP, while transportation, pyrolysis unit and preprocessing have consistently shown a minor, positive contribution to GWP. Especially due to the very short distances, transportation is very minor influencing factors. The influence of biochar carbon storage in soil on carbon sequestration increased with increasing PT, from -550.38 to -555.54 $kgCO_2$-eq/t feedstock. As per Chapter 4.3.1, the biochar C content increased with increasing PT, but the biochar yield decreased,

which caused an offset in the overall carbon sequestration as shown by Eq. (4.9). The biochar sequestration by biochar carbon storage in soil is not significantly affected by PT due to the compromise between the biochar yield and C content. In addition, the GWP of the transportation, pre-processing and pyrolysis unit were mainly affected by the type of truck (diesel consumption), the transport distance, and the power consumption of the type of pyrolysis equipment used.

The carbon saving by urea ammonium nitrate fertiliser substitution decreased with increasing pyrolysis temperature: For PT=300°C, the GWP by urea ammonium nitrate fertiliser was –76.5 $kgCO_2$-eq/t feedstock, which was increased by 40.24 $kgCO_2$-eq/t feedstock to –36.26 $kgCO_2$-eq/t feedstock for PT=500°C. Comparatively, the GWP of the calcium ammonium nitrate fertiliser substitution was –102.58 $kgCO_2$-eq/t feedstock for PT=300°C and was increased to –48.62 $kgCO_2$-eq/t feedstock for PT=500°C. Fig. 4-10 highlighted the GWP percentage difference between the two fertiliser substitution scenarios under the three PT conditions. The net GWPs of calcium ammonium nitrate displacement were smaller than that of urea ammonium nitrate displacement, for which the difference is consistently around 34%. This suggests that there are potentially great variations in the GWP of biochar soil applications depending on the type of fertiliser it displaces. With a limited variation in the N content of biochar, the amount of N fertiliser displaced by biochar decreases as the biochar yield decreases with increasing.

Substitution of urea ammonium nitrate and calcium ammonium nitrate by biochar reduced N_2O emissions. The reduction of N_2O emissions for the replacement of urea ammonium nitrate and calcium ammonium nitrate applied in the field was 11.5%, 3.7%, 2.6%, 33.7%, 10.9%, and 7.5%, respectively, for PT variations of 300°C-500°C. It was found that as PT increased, the ability of

biochar to reduce N_2O decreased because the mass of biochar became lower for N fertiliser substitution, which meant that the area of application became lower. At the same time, N_2O emissions increased. Considering these two factors, it is recommended that the PT be controlled below 400°C to obtain the ideal N_2O reduction effect.

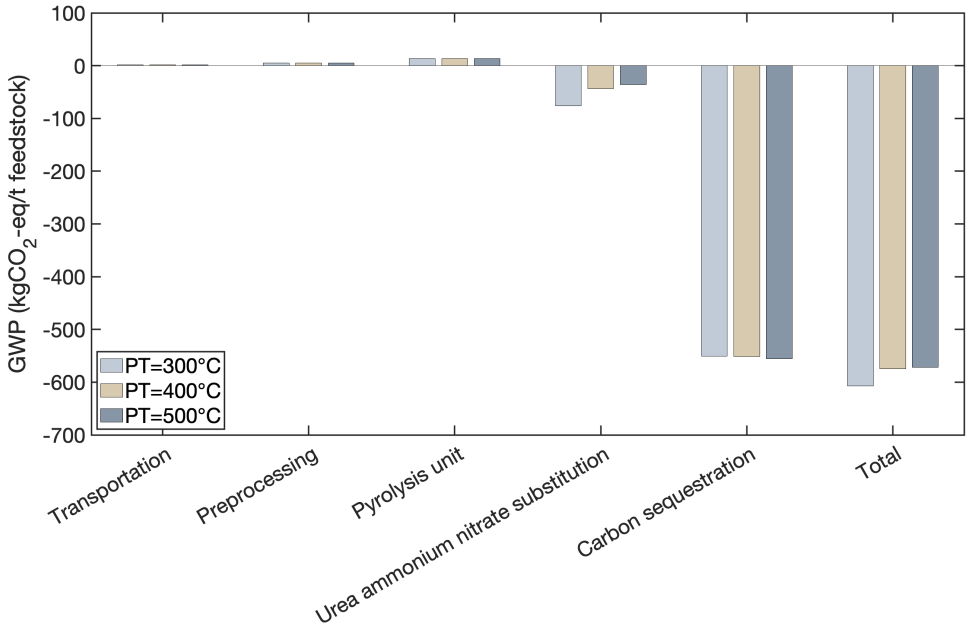

Fig. 4-8. Phase breakdown of GWP of biochar systems under different PTs for urea ammonium nitrate fertiliser substitution scenario.

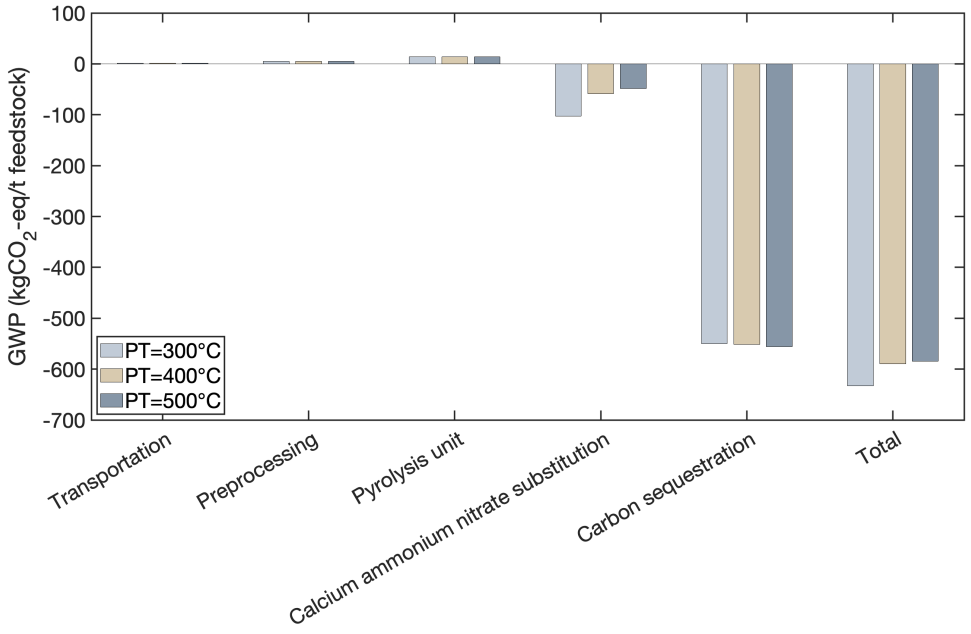

Fig. 4-9. Phase breakdown of GWP of biochar systems under different PTs for calcium ammonium nitrate substitution scenario.

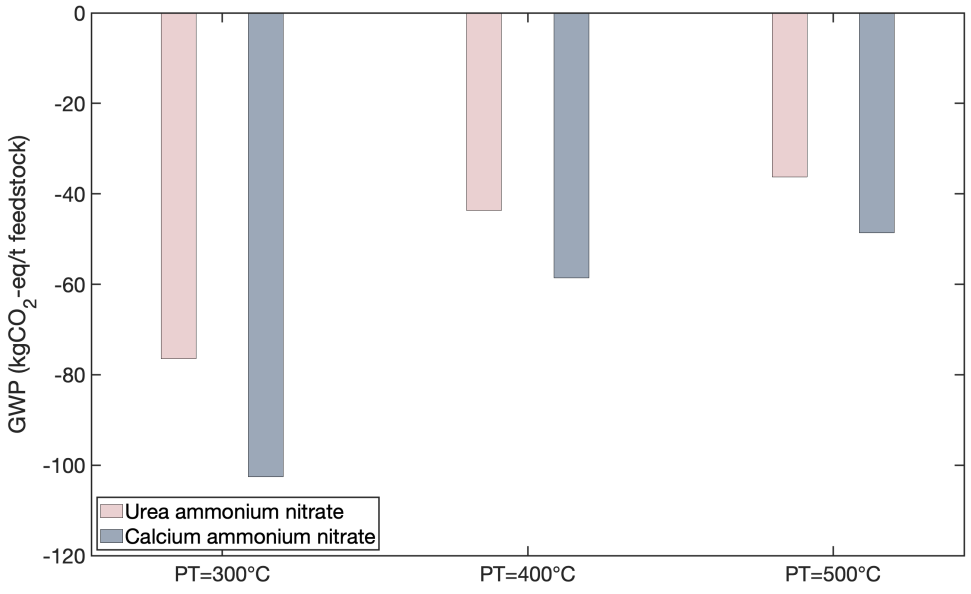

Fig. 4-10. Comparison of GWP savings between two N-fertiliser substitution under different PTs.

4.3.4 Data Interpretation

Fig. 4-11 illustrates the results of a one-way sensitivity analysis for the six conditions varied. The red dashed line corresponds to SR = 0.2, and it is considered that the conditions with SR values below 0.2 have a non-significant effect on GWP and vice versa. Fig. 4-11 showed that the GWP of biochar production and soil application is more sensitive to the stable C content and N content in biochar in the urea ammonium nitrate fertiliser substitution scenario as compared to the calcium ammonium nitrate fertiliser substitution scenario. The sensitivity of GWP to the biochar yield was the other way around. Meanwhile, the pyrolysis power consumption parameter had similar effects across the scenarios. The SRs for the biochar yield and stable C content in biochar were greater than 0.2, indicating that any uncertainty associated with these quantities significantly affects the GWP results. The stable C content in biochar has the most significant effect on the GWP. Notably, the SR for the N content in biochar was greater than 0.2 for PT=300°C and urea ammonium nitrate fertiliser substitution, suggesting that there was interaction effects between the N content and PT.

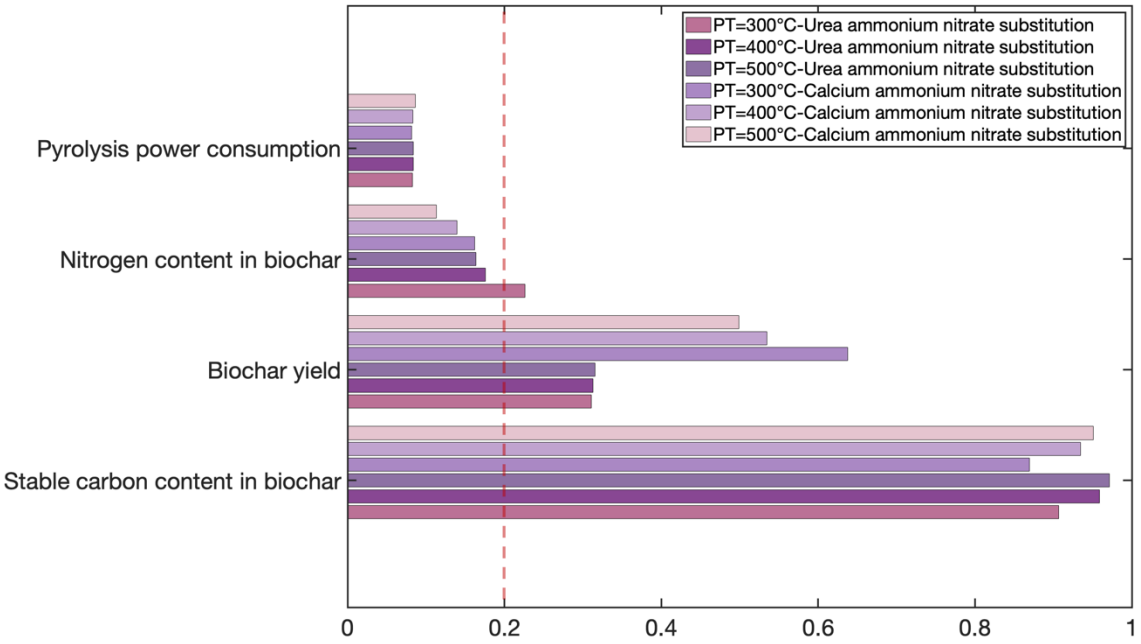

Fig. 4-11. One-way parameter sensitivity analysis quantifying SR, with sensitivity plots showing the effect of each parameter on GWP.

In assessing the impact of biochar production and soil application on GWP, while this study focused on biochar yield, N content and C content, it did not fully consider the ash content of biochar. Ash is the sum of the inorganic components of biochar and has an impact on the physical and chemical properties of biochar. For example, the presence of ash may affect the pore structure, water holding capacity and thermal stability of biochar. In addition, high ash content may lead to changes in soil pH, which may indirectly affect the effectiveness of biochar as a N fertiliser substitute. In order to have a more comprehensive understanding of the effects of biochar application in soil on GWP, ash content could be considered in future study.

4.4 Summary

This work developed an environmental impact assessment framework by combining data-driven ML modeling and LCA, which facilitated our understanding of the influences of the biochar production and application conditions towards GWP. Five different models were compared with MLP-NN outperforming in biochar yield and C content predictions while GPR in biochar N content predictions. Based on the ML predictions on biochar yields, and C and N contents, the GWPs for biochar production and soil application were analysed across different PT conditions and fertiliser displacement scenarios. It was shown that that the two N fertiliser substitution scenarios had GWPs of –606.858 and –632.938 $kgCO_2$-eq/t feedstock, respectively. The outcome of LCA was most sensitive to the stable C content in biochar and biochar yields, suggesting the importance of accurate biochar production prediction.

Chapter 5 Machine Learning-Assisted Multi-Objective Optimization and Multi-Criteria Decision Making Combined with Life Cycle Assessment: An Integrated Framework

In Chapter 4, the predictive capabilities of ML models for biochar pyrolysis production are revealed and these prediction results are applied to the LCA to assess the GWP impact. This work provides the basis to be able to further explore the integration of the ML model with MOO and MCDM in Chapter Five. Through this framework, it not only able to exploit the predictive ability of ML models, but also consider optimising multiple objectives and constraints when finding for optimal solutions. The core of Chapter 5 is to show how the integration of ML, MOO and MCDM can provide a more comprehensive and accurate framework for LCA approach. The advantage of this integrated approach is that it not only suggests optimal solutions, but also enhances the understanding in terms of the environmental impacts of biochar pyrolysis production and its soil applications. Therefore, Chapter 5 will specifically address how this integrated framework can be utilised to achieve better GWP results to drive environmentally friendly forward in the field of environmental optimization of biochar pyrolysis production and its soil applications.

5.1 Introduction

For biochar production, the yield or multiple properties are expected to be optimised simultaneously rather than optimising a single objective. However, some of the properties of biochar are mutually exclusive. For example, as the PT increases, the yield and N content decreases while the C content increases. This creates a great variety of parameter combinations to be explored. Therefore, an advanced strategy was developed in this study to conduct a MOO of biochar yield and properties (C and N content). The methodology is based on ML-assisted prediction combined

with MOO to obtain the optimal design parameters of the production process and feedstock selection. GA-based Non-dominated Sorting Genetic Algorithm II (NSGA-II) is an effective MOO method. This strategy was originally proposed by Deb *et al*. [164]. NSGA-II is designed not to use archives but to implement elitism and does not rely on specific shared parameters. To preserve the diversity of solutions, this method utilises the congestion distance metric as the core mechanism. For each solution, the crowding distance is computed by finding the distance to the nearest solution along each objective function, and then the crowding distance is used to modify the fitness of each solution. Particularly noteworthy is its efficient computational properties. Due to the above features. the NSGA-II is often chosen as the method for dealing with MOO problems. The solutions it produces are also known as Pareto optimal solutions [18]. Furthermore, MCDM is the decision-making method that aims to determine the best option by considering multiple criteria in the selection process. It has a wide range of tools (*i.e.*, Simple Additive Weighting (SAW), Multi-Attributive Border Approximation Area Comparison (MABAC), Grey Relational Analysis (GRA), Technique for Order of Preference by Similarity to Ideal Solution (TOPSIS), and Preference Ranking On the Basis of Ideal-average Distance (PROBID) *etc.*) that can be applied in different fields, varying from finance to engineering design [19]. Biochar production challenges with their multidimensional characteristics and multiple conflicting objectives make the use of the MCDM effective method. It can provide support when considering multiple conflicting decision criteria simultaneously. Ultimately, three targets (yield, C, N content of biochar) were optimised, which will directly affect the carbon sequestration potential and soil application of biochar.

This work develops an integrated framework that combines the ML model with the MOO-MCDM; the optimised parameters are input to LCA to analyse the holistic environment impact for biochar

soil application. LCA is defined as the systematic analysis of the potential environmental impacts of a product or service throughout its life cycle. Overall, the MOO aims to maximise the yield, C content and N content of biochar to fully enhance its carbon reduction potential for soil applications. The ML models in Chapters 3 and 4 provided the necessary predicted data (biochar yield, and C and N contents) support for the LCA. The optimised biochar parameters combined with the LCA to analysis GWP of optimal scenario were compared against the GWP of baseline scenario of Chapter 4. This study fully proposed an integrated ML-MOO-MCDM-LCA framework that provides a sustainable assessment and optimization strategy for biochar production pyrolysis systems considering environmental objectives.

5.2 Methods

The whole framework consists of three main components, *i.e.*, ML models, MOO-MCDM and LCA. The first step is to analyse the dataset used for model training and construct different ML models to find the optimal predictive model for biochar production. Then model prediction accuracy analysis is performed through evaluation metrics. In the second step, a clear definition of the MOO problem is required, which involves identifying the objective, specifying the decision variables, and setting its corresponding boundaries and constraints. Subsequently, an appropriate solution strategy or algorithm is selected for the defined MOO problem. The choice of this strategy is crucial, and it should have a broad search capability to ensure that the true Pareto optimal solution space of the problem can be fully explored and represented. Furthermore, a multi-criteria decision analysis of the non-dominated solution is performed using several selected MCDM methods. The recommended solutions and their corresponding decision variable values are analysed to filter a representative Pareto-optimal solution for implementation. For the third step, the optimal solutions are combined with the LCA for a systematic environmental analysis. And

breakdown the GWP impacts for different phases of biochar production and soil application. A holistic flowchart of ML-MOO-MCDM for the biochar production system is shown in Fig. 5-1.

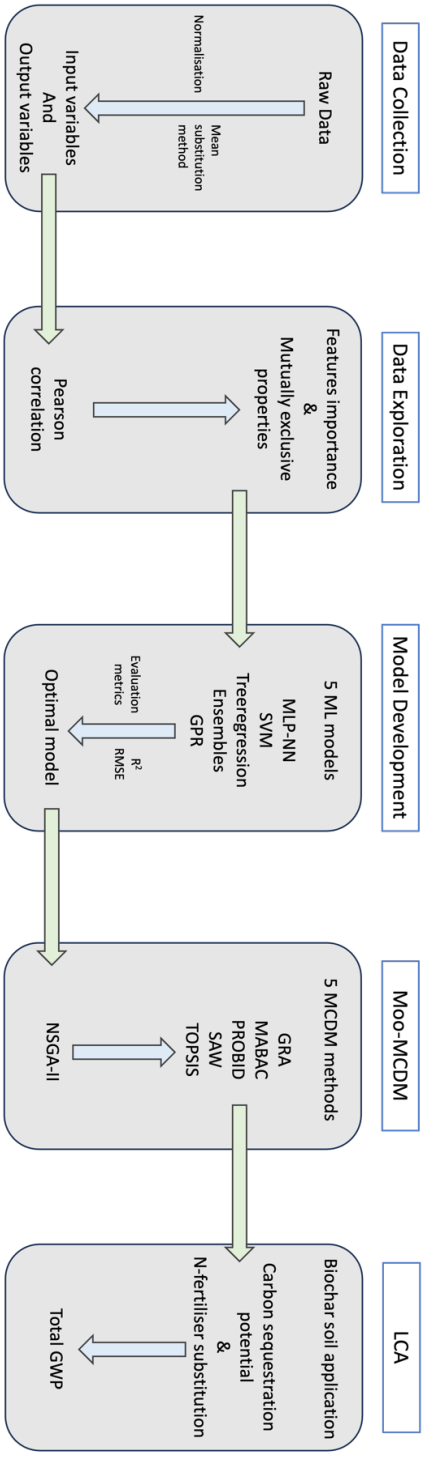

Fig. 5-1. A holistic framework of ML-MOO-MCDM for biochar production design.

5.2.1 Machine Learning Development

Referring to Chapter 4.2.1.1, the dataset was pre-processed by normalisation due to it contains different ranges of variables. The missing values of the input features were handled by the mean substitution method [141]. Furthermore, *PCC* was employed to assess the relationship between any two variables in this dataset. Five ML models were developed for biochar yield and property prediction. These were MLP-NN, SVM, tree regression, ensembles, and GPR. Information on model development is detailed in Chapter 4.2.1.2. Two metrics R^2 and *RMSE* were applied for the evaluation of the model performance accuracy (detailed in Chapter 4.2.1.3).

5.2.2 Multi-Objective Optimization

This research employs the NSGA-II algorithm to address MOO, notably aiming to optimise biochar yield, as well as its C and N content. The NSGA-II is a state-of-the-art evolutionary algorithm specifically designed to solve complex MOO problems. The approach is fundamentally derived from the principles of Genetic Algorithm (GA), which mimic the evolutionary processes of natural selection and genetics. NSGA-II extends these principles to efficiently handle the nuances of MOO.

A distinguishing feature of NSGA-II is its non-dominance sorting mechanism. The algorithm classifies solutions into different "frontiers" based on the concept of Pareto dominance. A solution is considered to dominate another if it is at least equal on all objectives and superior on at least one objective. The forefront consists of programmes that are not dominated by any other programme, and subsequent fronts follow a similar hierarchical structure. In NSGA-II, a "solution" is a candidate solution generated by the algorithm during the optimisation process. Each solution represents a set of possible values for the decision variables in the optimisation space.

Diversity among solutions is maintained by calculating the crowding distance, which is a measure of how densely populated a solution is in the target space. A larger crowding distance indicates a sparser cluster of solutions, which is desirable for exploring a variety of potential solutions and goal tradeoffs.

The NSGA-II selection process uses a binary tournament approach that considers both solution rank (based on non-dominated ordering) and crowding distance. This dual consideration ensures that high-quality solutions are retained, while also ensuring a diversity of solutions. The selected solutions are then subjected to crossover and mutation operations, thus facilitating the exploration of the new solution space.

An integral part of NSGA-II is the Elite Strategy, which retains the best solutions from current and previous generations. This approach ensures that high quality solutions are not lost as generations increase. The combined population is then sorted and pruned to maintain a constant size, focusing on retaining the optimal solutions.

The ultimate goal of NSGA-II is to converge towards the Pareto-optimal frontier, which represents the set of best solutions considering all objectives. The algorithm aims to balance the goals of convergence (finding the optimal solution) and diversity (exploring multiple solutions) and is therefore particularly effective for MOO challenges.

Incorporating NSGA-II into research provides a robust and efficient method for navigating the complex optimization landscape to find the best solution that balances multiple (often conflicting) objectives.

Overall, the NSGA-II incorporation of a crowding-based ranking system fosters population diversity and maintains convergence towards the true Pareto front. It offers both efficient exploration of solution spaces and the preservation of solution diversity. Therefore, NSGA-II was selected as the appropriate solution for this study due to its excellent capabilities and fit with the identified research objectives.

Succinctly, following the start-up phase of acquiring initial trial solutions, the NSGA-II algorithm is scheduled through two main procedures. The first phase is characterised using a tournament selection mechanism combined with crossover and mutation processes to foster offspring solutions from the existing population. After that, the algorithm starts to characterise the upcoming population by performing a non-dominated ordering of parent and offspring solutions. The basis of such ordering lies in the comparative evaluation of their objective values, as well as in the evaluation of the crowding distance, a metric designed to quantify the sparsity of a given solution. This study has implemented NSGA-II in the Python environment. The constraints applied to this MOO are defined by the equations shown below. The Lower Bound (LB) and Upper Bound (UB) for each input decision variable are defined by the minimum and maximum values of the original dataset, as detailed in Table 5-1.

$$0 < C + H + O + N < 100\% \quad (5.1)$$

$$0 < VM + FC + Ash < 100\% \quad (5.2)$$

where, C, H, O, and N represent the respective contents of carbon, hydrogen, oxygen, and nitrogen. Meanwhile, VM, FC, and Ash are indicative of the VM, FC, and mineral ash content, respectively.

Table 5-1. UB and LB on input decision variables for pyrolysis of biochar.

Decision Variables	UB	LB	Unit
FC	27.80	5.58	%
VM	87.82	68.20	%
Ash	15.00	0.43	%
C	53.42	35.70	%
H	7.77	4.10	%
O	48.88	32.88	%
N	0.01	9.61	%
PT	550	300	°C
HR	20	5	°C/min
RT	90	10	min

5.2.3 Multi-Criteria Decision Making

The NSGA-II algorithm results in a range of different obtained Pareto optimal frontiers. Selecting a comprehensive, compromise solution from these different optimal solutions is an MCDM problem. It aims to rank all optimal solutions and ultimately suggest the one with the highest-ranking score for implementation. This study employs multiple MCDM methods, including GRA, MABAC, PROBID, SAW, and TOPSIS. Non-dominated solutions are evaluated using these MCDM methods and analysed regarding their corresponding values to the solution and the

decision variables. Finally, the Pareto-optimal solutions are selected for implementation. This procedure can be elaborated into several sub-steps, as detailed in Fig. 5-2.

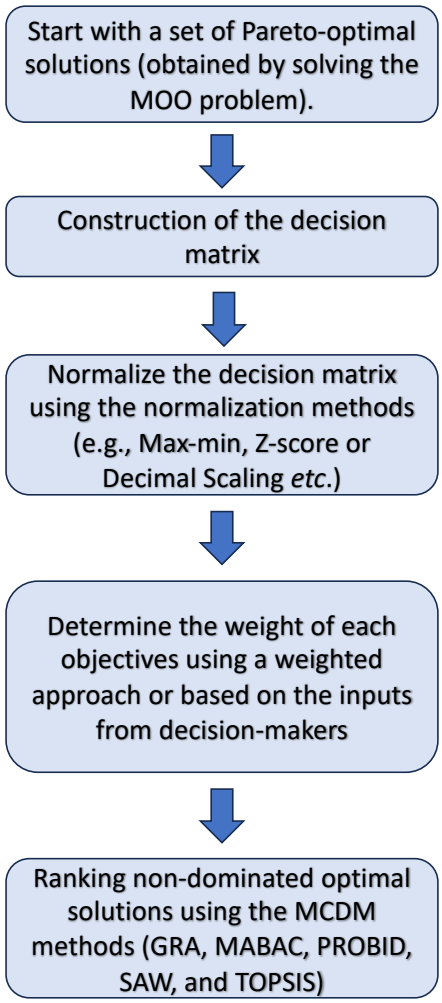

Fig. 5-2. The procedure of MCDM.

GRA measures the degree of similarity between sequences by developing a grey correlation scale. One of its main advantages is its ability to deal effectively with uncertainty and incomplete information, meaning minimal data preprocessing is required. However, a potential disadvantage is that the choice of grey correlation coefficients and weighted sequences can significantly impact the results [165].

MABAC ranks alternatives by comparing their distance from the virtual ideal alternative. This approach allows for considering positive and negative biases, effectively classifying alternatives into preferred groups. Nevertheless, it does require the decision maker to define such virtual ideal alternatives and may need to be more effective for problems involving large datasets [166].

PROBID is a ranking method that evaluates and ranks alternatives based on pairwise comparisons. A clear advantage is its ability to consider preference and indifference thresholds, proving robust to changes in the decision matrix. However, the method can be computationally intensive, especially if there are many alternatives, and may require expert judgment to set specific thresholds [167].

SAW calculates a weighted sum of attribute values for each decision scheme. Its main advantages are its simplicity, ease of computation, and having a transparent ranking mechanism. However, it operates under the attribute independence assumption and requires normalisation of the decision matrix [168].

TOPSIS ranks alternatives based on the distance from ideal and anti-ideal solutions. A key advantage is its comprehensive approach, which considers both best and worst-case scenarios and applies to different types of decision matrices. Nevertheless, as with other methods, there is a requirement to normalise the decision matrix and how the weights are determined affects the final ranking [169].

5.2.4 Life Cycle Assessment

This study presents an approach to assess the GWP of biochar production and biochar soil application by combining Pareto-optimal solutions from five MOO-MCDM methods with LCA. The environmental impact is measured in $kgCO_2$-eq/t feedstock. The structure of this LCA consists of four key stages: objective and scope definition, LCI, LCIA and life cycle interpretation. For a full understanding of these steps, refer to Chapter 4.2.2. Ultimately, the GWP results from the optimization parameters of this work will be compared with the results of the study presented in Chapter 4.

5.3 Results and Discussion

5.3.1 MOO-MCDM

Three key objectives were optimised: biochar yield, C content and N content. These components are directly linked to the application of biochar in soil. The overall goal was to maximise these three targets, thereby increasing biochar production while reducing GHG emissions. This reduction is achieved by improving soil sequestration and increasing the effect of N-fertiliser replacements.

In this study, the NSGA-II was used to deal with the MOO problem of biochar production. A series of parameters were set: a population size of 100, a total number of iterations of 200, a crossover rate of 0.9, and a mutation rate of 0.1. The algorithm terminates the iterations when there is no significant change in the Pareto frontier for 50 consecutive generations. By analysing the ML model prediction dataset, a set of 15 Pareto-optimal solutions were identified, as listed in Table 5-2. To deepen the differences between these scenarios, the solutions were plotted in a 3D diagram (see Fig. 5-3). This visualisation reveals the trade-offs between the three objectives. The graph

clearly demonstrates the distribution of the Pareto frontiers, proving the competitiveness between the solutions, with no one solution outperforming the other on all objectives.

Table 5-2. Optimal values of decision variables and objectives for pyrolysis of biomass using NSGA-II MOO method.

Decision Variables	Parato solutions														
Serial number	1.	2.	3.	4.	5.	6.	7.	8.	9.	10.	11.	12.	13.	14.	15.
FC (%)	13.42	10.16	7.49	10.06	18.00	11.19	17.67	18.00	16.72	17.14	11.73	18.00	10.16	10.06	7.49
VM (%)	71.94	76.86	86.09	76.87	78.70	87.76	75.28	78.70	82.74	81.26	87.82	78.70	76.86	76.87	86.09
Ash (%)	14.63	12.98	6.42	13.07	3.284	1.05	7.046	3.28	0.52	1.60	0.43	3.28	12.98	13.07	6.42
C (%)	38.62	40.06	43.92	40.06	48.12	44.47	45.92	48.12	49.10	47.66	50.52	48.12	40.06	40.06	43.92
H (%)	6.10	5.47	5.92	5.47	6.48	5.82	6.21	6.48	5.55	6.18	5.81	6.48	5.47	5.47	5.92
O (%)	32.88	40.23	42.54	40.23	43.51	48.88	40.09	43.51	44.90	46.01	43.44	43.51	40.23	40.23	42.54
N (%)	1.60	0.69	0.49	0.69	1.899	0.01	6.90	1.89	0.45	0.15	0.23	1.89	0.69	0.69	0.49

RT (min)	30	30	30	30	60	60	30	60	30	60	60	60	30	30	30
PT (°C)	300	300	350	350	400	400	500	500	500	500	500	500	500	500	550
HR (°C/min)	10	10	10	10	15	5	5	10	20	10	10	15	10	10	10
Objectives															
Biochar yield	70.24	71.03	45.77	49.83	32.52	32.57	30.45	23.20	19.74	26.63	23.85	25.07	38.30	38.34	31.94
C-biochar	45.35	45.30	59.33	48.24	64.06	61.20	64.78	81.15	83.33	78.52	83.48	73.71	54.34	54.28	69.96
N-biochar	2.20	0.81	0.71	0.90	0.81	1.38	7.98	0.90	1.72	0.40	0.74	0.89	0.90	0.90	0.73

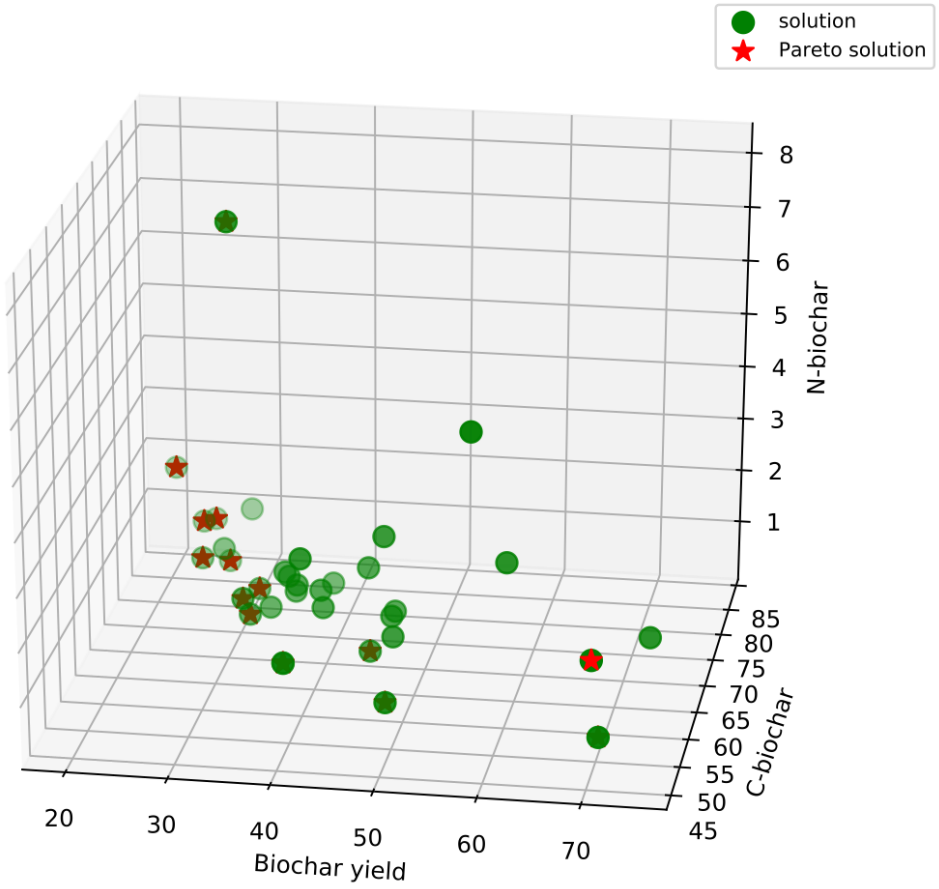

Fig. 5-3. Pareto-optimal solutions of biochar pyrolysis production.

For the Pareto optimal solutions, further optimization of either objective comes at the expense of the other. Therefore, an optimal solution needs to be selected from the 15 solutions. For this purpose, 1/3 weight was assigned to biochar yield, C content, and N content, respectively. The MCDM approach was applied, including GRA, MABAC, PROBID, SAW, and TOPSIS methods to identify the best solutions. Selected solutions by 5 different tools plotted in a 3D diagram was shown in Fig. 5-4.

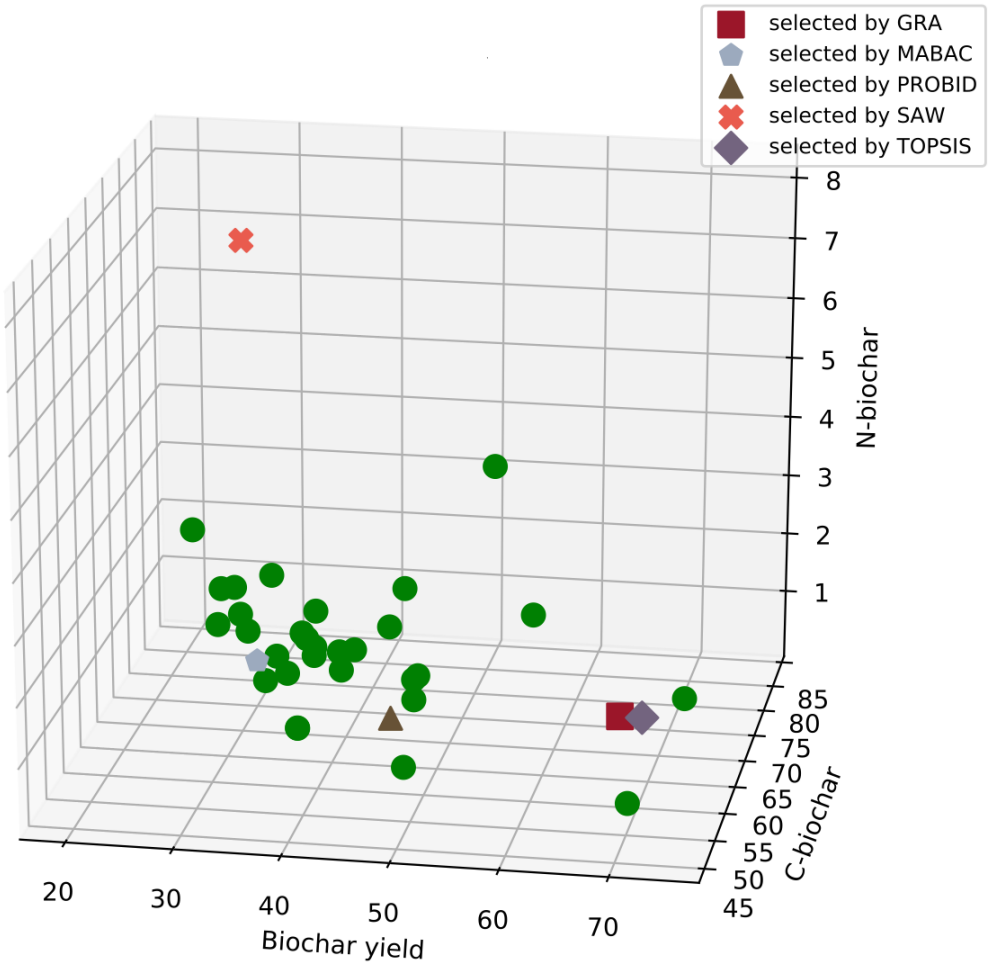

Fig. 5-4. The Pareto-optimal solutions of biochar pyrolysis production; Selected solution by GRA and TOPSIS (■◆); selected solution by MABAC (⬟); selected solution by PROBID (▲); selected solution by SAW (✖).

Table 5-3 shows the decision variables and objective values of the solutions selected by the different MCDM methods. Among the five MCDM methods applied in the study, both GRA and TOPSIS elected the same solution, implying that the solution has excellent performance under multiple methods. In addition, the SAW method selected the lowest biochar yield and the largest N content. MABAC had similar results to SAW, but the value of MABAC was smaller than SAW in several features such as VM, O, and RT. Based on the principle of majority and the

reasonableness of the solution, the research team recommended the solution selected by the GRA and TOPSIS methods. The underlying principles and assumptions of GRA and TOPSIS are inherently similar. Although they employ different mathematical frameworks, both techniques aim to evaluate the performance of alternatives against predefined criteria; GRA uses grey relational coefficients to measure the proximity or similarity between an alternative and a criterion, whereas TOPSIS identifies the best compromise by evaluating the proximity of an alternative to an ideal solution. When the dataset characteristics or the optimisation problem closely matched the assumptions and conditions of both methods, consistent solutions were produced in this study. When two methods (e.g. GRA and TOPSIS) agree in giving the best solution, this consistency usually has two main advantages. Firstly, it increases the reliability and stability of the decision because the best solution obtained remains consistent even when different methods and techniques are used, which means that the decision results are more credible. Second, consistent results increase the confidence of the decision maker because two independent methods point to the same optimal solution, which indicates that the solution has been validated from multiple perspectives, thus giving the decision maker more confidence in accepting and adopting the solution [170]. Furthermore, the solution by SAW was also explored because it has the maximum N content which is closely associated with the carbon saving related to fertiliser displacement. This analysis provides the optimal process condition that led to highest C and N content, which is expected to favour biochar soil application and GHG emission reduction.

Table 5-3. Optimal values of decision variables and objectives of selected solutions by GRA, MABAC, PROBID, SAW and TOPSIS.

Decision Variables	GRA	MABAC	PROBID	SAW	TOPSIS
FC	13.42966	11.19	7.49	17.6714	13.42966

VM	71.94008	87.76	86.09	75.28241	71.94008
Ash	14.63026	1.05	6.42	7.046192	14.63026
C	38.62	44.47	43.92	45.92	38.62
H	6.1	5.82	5.92	6.21	6.1
O	32.88	48.88	42.54	40.09	32.88
N	1.6	0.01	0.49	6.9	1.6
RT	30	60	30	30	30
PT(°C)	300	400	350	500	300
HR(°C/min)	10	5	10	5	10
Objectives					
Biochar yield	70.24	32.57	45.77	30.45	70.24
C-biochar	45.35	61.20	59.33	64.78	45.35
N-biochar	2.20	1.38	0.71	7.98	2.20

5.3.2 Life Cycle Assessment

The three main optimization objectives (biochar yield, C content and N content) directly affected the biochar carbon sequestration potential and N fertiliser substitution associated GWP. However, these effects were not related to the GWP associated with the pre-processing or pyrolysis unit, so they were not considered in this study (detailed in Chapter 4.3.3). Scenarios A_1 and A_2 depict the biochar's carbon sequestration potential coupled with the substitution of Urea ammonium nitrate and Calcium ammonium nitrate, respectively, at a PT of 300°C (biochar yield: 70.24%, C content: 45.35%, and N content: 2.20%). The optimal solutions used are from both GRA and TOPSIS methods. In contrast, scenarios B_1 and B_2 describe similar comparative contexts but at PT of 500°C (biochar yield: 30.45%, C content: 64.78%, and N content: 7.98%). The optimal solution employed are obtained from the SAW method. Notably, considering the long-term retention of biochar in soil and carbon sequestration effects, while the production of biochar reduces one-time CO_2 emissions, but its long-term retention capacity in soil has a positive impact on the carbon cycle and the reduction of GHG emissions. Carbon sequestration of biochar in soil has a significant negative impact on GWP (implication of environmental benefits) [83].

Fig. 5-5 and 5-6 reveal Scenario A_1, A_2, B_1, and B_2, where the optimised GWP potential (Optimal) is significantly lower than the original GWP potential (Original, referring to results in Chapter 4). This suggests that the environmental benefits of biochar soil application were significantly enhanced after optimization of the pyrolysis system using MOO-MCDM. Specifically, after optimization with MOO-MCDM in the four scenarios, all significantly reduced their GWP. This finding highlights the benefits of the MOO-MCDM approach in environmental decision optimization. Notably, the optimal solutions obtained using both GRA and TOPSIS methods are

consistent, which enhances the reliability of this result. Incorporating the optimal solution into the LCA model for environmental assessment ensures that the conclusions drawn are not only based on the theoretical optimal solution but are also feasible and meaningful in practical applications. In summary, adopting the optimal solution of MOO-MCDM optimization into the LCA model for the calculation can provide strong support and reference for decision-making in related fields, which can help to better design the process parameters and select the appropriate feedstock to achieve the environmental benefits in practical applications.

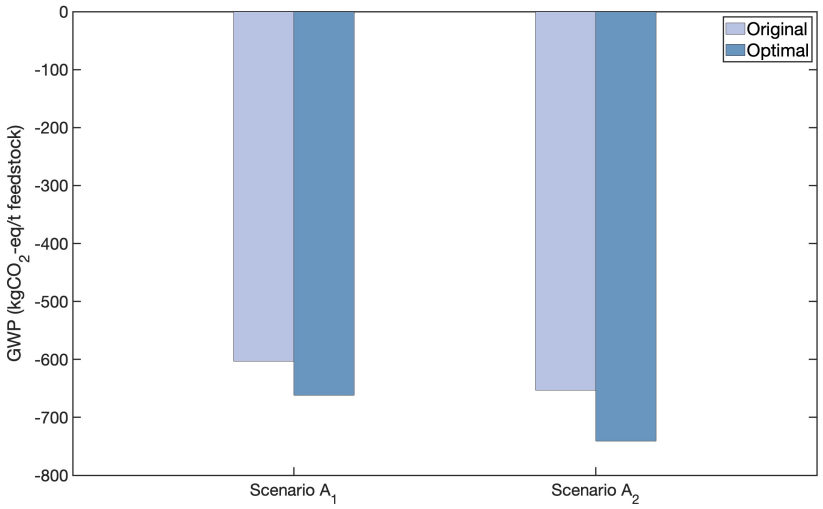

Fig. 5-5. GWP of Scenarios A_1 and A_2 depicting the biochar's carbon sequestration potential coupled with the substitution of Urea ammonium nitrate and Calcium ammonium nitrate, respectively, at a PT of 300°C (optimal solution obtained by GRA and TOPSIS).

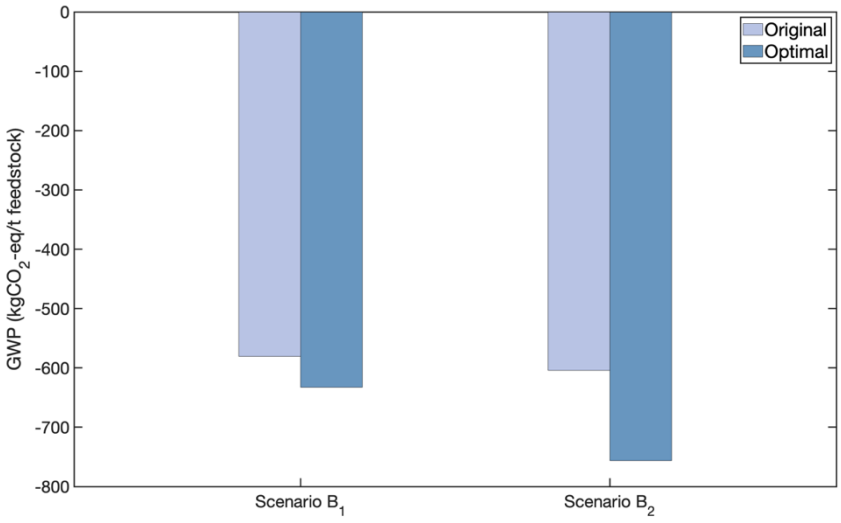

Fig. 5-6. GWP of Scenarios B_1 and B_2 depicting the biochar's carbon sequestration potential coupled with the substitution of Urea ammonium nitrate and Calcium ammonium nitrate, respectively, at a PT of 500°C (optimal solution obtained by SAW).

5.4 Summary

This study proposed a framework that combines ML with MOO-MCDM to apply optimal solutions to LCA. Five ML models including MLP-NN, SVM, GPR, tree and ensembles tree were developed to predict the biochar yield and properties. MOO-MCDM was essential for determining the optimal reaction conditions to optimise the C and N content and biochar yield. LCA further assessed the environmental impacts of biochar soil application. The optimal solutions from TOPSIS and GRA at 300°C and the SAW solution at 500°C were selected based on MOO-MCDM combined with best predictive ML model. The LCA showed that the GWP was more negative compared to the non-optimised (original) scenario, indicating an improvement in environmental benefits. Overall, an integrated ML-MOO-MCDM-LCA framework is fully presented in this study. A path is carved out to provide a sustainable assessment and optimization strategy for biochar production pyrolysis systems considering environmental objectives.

Chapter 6 Conclusion and Future plan

6.1 Conclusions

The pursuit of sustainable waste management and carbon sequestration solutions has driven biochar to the forefront of environmental research. As the emergency of mitigating climate change increases, the conversion of agricultural wastes into biochar through pyrolysis offers a promising pathway for not only recycling wastes, but biochar can also serve as a substitute for N fertiliser and carbon sequestration. The main objective of this study is to develop a systematic framework to optimise the biochar production and the environmental benefits of biochar soil application, including the development of biochar prediction ML models, and their integration with LCA and MOO approaches. The framework serves as a useful tool for designing biochar production and soil application from greater environmental benefits.

The second chapter of the thesis assessed how various agricultural wastes and pyrolysis conditions influence the resulting biochar's properties and yield based on a comprehensive literature review. It covered the state-of-the-art research in biochar production and its applications, with a focus on ML, LCA and MOO-MCDM approaches. This chapter also highlighted the environmental feasibility of applying LCA to biochar various applications. ML-assisted modelling and the emerging strategy of MOO-MCDM proved to be useful in predicting the outcome of biochar production, which is a key factor in optimising the design of the system and the implementation of the biochar application.

Data-driven ML models for predicting biochar yield and composition were developed and compared. It was shown that the MLP-NN model achieved a higher prediction accuracy in biochar

yield and composition prediction. The importance of process parameters such as pyrolysis temperature, C content and N content were discussed in detail, paving the way for future research into the optimization of data-driven biochar production processes.

Afterwards, an environmental impact assessment framework was developed by combining the data-driven ML modelling with LCA. Five different ML models were developed and compared: the MLP-NN model outperformed the others in predicting biochar C content, while the GPR model performed well in predicting N content. Finally, the GWP reduction associated with biochar production and soil application (N fertiliser substitution and carbon sequestration) was quantified, emphasising the application potential of the ML-LCA combined framework.

Finally, an integrated ML-MOO-MCDM-LCA framework for optimising biochar production conditions was presented. It was demonstrated based on the development of several ML models for predicting biochar production and the application of MOO-MCDM in finding optimal pyrolysis conditions. The use of optimal process condition in LCA to assess the environmental impacts of biochar application in soils was presented, demonstrating that optimised conditions can achieve greater environmental benefits than non-optimised scenarios.

Collectively, the drive for environmentally sustainable solutions to agricultural waste management has led to the exploration of biochar as a multifunctional product with the potential to address multiple global challenges, including waste reduction, soil enhancement and carbon sequestration. This research begins with an understanding of the roots of biochar, examining its historical development, mechanisms of production through pyrolysis, and its emerging role in contemporary

environmental applications. This thesis demonstrates the synergistic potential of combining ML, LCA and optimization frameworks to address the complexities of biochar production from agricultural waste towards soil application. The potential of biochar as a scalable, impactful solution for a sustainable agriculture is emphasised. As such, this work contributes to the existing knowledge base and opens avenues for innovative applications, policy implications and future research in environmental sustainability and low carbon development.

6.2 Recommendations for Future Research

Future research should introduce the economic consideration into the frameworks developed for a more comprehensive evaluation of the feasibility of biochar production and soil application. The theoretical framework guiding biochar production and applications should also evolve to include socio-economic factors which are key to its adoption by farmers and industry, thus providing a more comprehensive understanding of its utility and dissemination. An interdisciplinary approach that incorporates environmental science, economics, and social science should be promoted to generate a more comprehensive strategy for biochar adoption. Such an approach should consider not only production and environmental aspects, but also the socio-economic impacts of biochar, ensuring a balanced and sustainable application of this promising technology. Research should keep addressing the modelling of the influences of the chemical constituents in biochar towards its environmental impacts upon applications. Predictive models should be extended to include more diverse input characteristics, with the exploration of a wider range of biochar applications. Also, unresolved questions remain, especially regarding the long-term stability of biochar in different soils and climates and its interaction with the soil microbiota. Finally, methodologically, the development of more sophisticated models that can be adapted to dynamic agricultural conditions and integrate real-time data analyses is crucial. The potential integration of blockchain

technology could significantly enhance data integrity in ML applications. Moreover, future work also includes using the framework developed in this study to apply to a wider range of scenarios. Whilst the focus of this thesis has been on biochar, this framework could be applied to other bioenergy aspects in the future. This could lead to valuable insights and breakthroughs for a wide range of fields, potentially enhance the impact and significance of the research.

References

1. Maibach EW, Sarfaty M, Mitchell M, Gould R. Limiting global warming to 1.5 to 2.0°C—A unique and necessary role for health professionals. PLoS Med. 2019;16:e1002804–e1002804.

2. Tripathi N, Hills CD, Singh RS, Atkinson CJ. Biomass waste utilisation in low-carbon products: harnessing a major potential resource. NPJ Clim Atmos Sci. 2019;2:35.

3. Wang K, Tester JW. Sustainable management of unavoidable biomass wastes. Green Energy and Resources. 2023;1:100005.

4. Chungcharoen T, Srisang N. Preparation and characterization of fuel briquettes made from dual agricultural waste: Cashew nut shells and areca nuts. J Clean Prod. 2020;256:120434.

5. Oluseun Adejumo I, Adebukola Adebiyi O. Agricultural Solid Wastes: Causes, Effects, and Effective Management. Strategies of Sustainable Solid Waste Management. IntechOpen; 2021.

6. Li C, Hayashi J, Sun Y, Zhang L, Zhang S, Wang S, et al. Impact of heating rates on the evolution of function groups of the biochar from lignin pyrolysis. J Anal Appl Pyrolysis. 2021;155:105031.

7. Ippolito JA, Cui L, Kammann C, Wrage-Mönnig N, Estavillo JM, Fuertes-Mendizabal T, et al. Feedstock choice, pyrolysis temperature and type influence biochar characteristics: a comprehensive meta-data analysis review. Biochar. 2020;2:421–38.

8. Liu R, Sarker M, Rahman MdM, Li C, Chai M, Nishu, et al. Multi-scale complexities of solid acid catalysts in the catalytic fast pyrolysis of biomass for bio-oil production – A review. Prog Energy Combust Sci. 2020;80:100852.

9. Yousaf B, Liu G, Ubaid Ali M, Abbas Q, Liu Y, Ullah H, et al. Decisive role of vacuum-assisted carbonization in valorization of lignin-enriched (Juglans regia-shell) biowaste. Bioresour Technol. 2021;323:124541.

10. Liu C, Liu X, He Y, An X, Fan D, Wu Z. Microwave-assisted catalytic pyrolysis of apple wood to produce biochar: Co-pyrolysis behavior, pyrolysis kinetics analysis and evaluation of microbial carriers. Bioresour Technol. 2021;320:124345.

11. Nzediegwu C, Arshad M, Ulah A, Naeth MA, Chang SX. Fuel, thermal and surface properties of microwave-pyrolyzed biochars depend on feedstock type and pyrolysis temperature. Bioresour Technol. 2021;320:124282.

12. Wang J, Wang S. Preparation, modification and environmental application of biochar: A review. J Clean Prod. 2019;227:1002–22.

13. Li Y, You S. Biochar soil application: soil improvement and pollution remediation. Biochar in Agriculture for Achieving Sustainable Development Goals. Elsevier; 2022. p. 97–102.

14. Li S, Harris S, Anandhi A, Chen G. Predicting biochar properties and functions based on feedstock and pyrolysis temperature: A review and data syntheses. J Clean Prod. 2019;215:890–902.

15. Sun J, He F, Pan Y, Zhang Z. Effects of pyrolysis temperature and residence time on physicochemical properties of different biochar types. Acta Agric Scand B Soil Plant Sci. 2017;67:12–22.

16. Qian C, Li Q, Zhang Z, Wang X, Hu J, Cao W. Prediction of higher heating values of biochar from proximate and ultimate analysis. Fuel. 2020;265:116925.

17. Supraja KV, Kachroo H, Viswanathan G, Verma VK, Behera B, Doddapaneni TRKC, et al. Biochar production and its environmental applications: Recent developments and machine learning insights. Bioresour Technol. 2023;387:129634.

18. Marler RT, Arora JS. Survey of multi-objective optimization methods for engineering. Structural and Multidisciplinary Optimization. 2004;26:369–95.

19. Wang Z, Li J, Rangaiah GP, Wu Z. Machine learning aided multi-objective optimization and multi-criteria decision making: Framework and two applications in chemical engineering. Comput Chem Eng. 2022;165:107945.

20. Bebbington J, Unerman J. Achieving the United Nations Sustainable Development Goals. Accounting, Auditing & Accountability Journal. 2018;31:2–24.

21. Luo L, Wang J, Lv J, Liu Z, Sun T, Yang Y, et al. Carbon Sequestration Strategies in Soil Using Biochar: Advances, Challenges, and Opportunities. Environ Sci Technol. 2023;57:11357–72.

22. Gao Y, Fang Z, Van Zwieten L, Bolan N, Dong D, Quin BF, et al. A critical review of biochar-based nitrogen fertilizers and their effects on crop production and the environment. Biochar. 2022;4:36.

23. Pryshlakivsky J, Searcy C. Life Cycle Assessment as a decision-making tool: Practitioner and managerial considerations. J Clean Prod. 2021;309:127344.

24. Hellweg S, Milà i Canals L. Emerging approaches, challenges and opportunities in life cycle assessment. Science (1979). 2014;344:1109–13.

25. Matuštík J, Hnátková T, Kočí V. Life cycle assessment of biochar-to-soil systems: A review. J Clean Prod. 2020;259:120998.

26. Tomczyk A, Sokołowska Z, Boguta P. Biochar physicochemical properties: pyrolysis temperature and feedstock kind effects. Rev Environ Sci Biotechnol. 2020;19:191–215.

27. Ji M, Wang X, Usman M, Liu F, Dan Y, Zhou L, et al. Effects of different feedstocks-based biochar on soil remediation: A review. Environmental Pollution. 2022;294:118655.

28. Usman ARA, Abduljabbar A, Vithanage M, Ok YS, Ahmad M, Ahmad M, et al. Biochar production from date palm waste: Charring temperature induced changes in composition and surface chemistry. J Anal Appl Pyrolysis. 2015;115:392–400.

29. Leng L, Xiong Q, Yang L, Li H, Zhou Y, Zhang W, et al. An overview on engineering the surface area and porosity of biochar. Science of The Total Environment. 2021;763:144204.

30. Alhashimi HA, Aktas CB. Life cycle environmental and economic performance of biochar compared with activated carbon: A meta-analysis. Resour Conserv Recycl. 2017;118:13–26.

31. Leng L, Huang H. An overview of the effect of pyrolysis process parameters on biochar stability. Bioresour Technol. 2018;270:627–42.

32. Liew YW, Arumugasamy SK, Selvarajoo A. Potential of Biochar as Soil Amendment: Prediction of Elemental Ratios from Pyrolysis of Agriculture Biomass Using Artificial Neural Network. Water Air Soil Pollut. 2022;233:54.

33. Pariyar P, Kumari K, Jain MK, Jadhao PS. Evaluation of change in biochar properties derived from different feedstock and pyrolysis temperature for environmental and agricultural application. Science of The Total Environment. 2020;713:136433.

34. Liu Z, Niu W, Chu H, Zhou T, Niu Z. Effect of the Carbonization Temperature on the Properties of Biochar Produced from the Pyrolysis of Crop Residues. Bioresources. 2018;13.

35. Shariff A, Noor NM, Lau A, Ali MAM. A comparative study on biochar from slow pyrolysis of corn cob and cassava wastes. International Journal of Biotechnology and Bioengineering. 2016;10:767–71.

36. Bhattacharjee N, Biswas AB. Pyrolysis of orange bagasse: Comparative study and parametric influence on the product yield and their characterization. J Environ Chem Eng. 2019;7:102903.

37. Wang L, Olsen MNP, Moni C, Dieguez-Alonso A, de la Rosa JM, Stenrød M, et al. Comparison of properties of biochar produced from different types of lignocellulosic biomass by slow pyrolysis at 600 °C. Applications in Energy and Combustion Science. 2022;12:100090.

38. He X, Liu Z, Niu W, Yang L, Zhou T, Qin D, et al. Effects of pyrolysis temperature on the physicochemical properties of gas and biochar obtained from pyrolysis of crop residues. Energy. 2018;143:746–56.

39. Ahmed N, Zeeshan M, Iqbal N, Farooq MZ, Shah SA. Investigation on bio-oil yield and quality with scrap tire addition in sugarcane bagasse pyrolysis. J Clean Prod. 2018;196:927–34.

40. Rout T, Pradhan D, Singh RK, Kumari N. Exhaustive study of products obtained from coconut shell pyrolysis. J Environ Chem Eng. 2016;4:3696–705.

41. Biswas B, Pandey N, Bisht Y, Singh R, Kumar J, Bhaskar T. Pyrolysis of agricultural biomass residues: Comparative study of corn cob, wheat straw, rice straw and rice husk. Bioresour Technol. 2017;237:57–63.

42. Hong Z, Zhong F, Niu W, Zhang K, Su J, Liu J, et al. Effects of temperature and particle size on the compositions, energy conversions and structural characteristics of pyrolysis products from different crop residues. Energy. 2020;190:116413.

43. Sellin N, Krohl DR, Marangoni C, Souza O. Oxidative fast pyrolysis of banana leaves in fluidized bed reactor. Renew Energy. 2016;96:56–64.

44. dos Reis Ferreira RA, da Silva Meireles C, Assunção RMN, Reis Soares R. Heat required and kinetics of sugarcane straw pyrolysis by TG and DSC analysis in different atmospheres. J Therm Anal Calorim. 2018;132:1535–44.

45. Ahmed MJ, Hameed BH. Adsorption behavior of salicylic acid on biochar as derived from the thermal pyrolysis of barley straws. J Clean Prod. 2018;195:1162–9.

46. Mukhambet Y, Shah D, Tatkeyeva G, Sarbassov Y. Slow pyrolysis of flax straw biomass produced in Kazakhstan: Characterization of enhanced tar and high-quality biochar. Fuel. 2022;324:124676.

47. Intani K, Latif S, Kabir AKMR, Müller J. Effect of self-purging pyrolysis on yield of biochar from maize cobs, husks and leaves. Bioresour Technol. 2016;218:541–51.

48. Ghysels S, Estrada Léon AE, Pala M, Schoder KA, Van Acker J, Ronsse F. Fast pyrolysis of mannan-rich ivory nut (Phytelephas aequatorialis) to valuable biorefinery products. Chemical Engineering Journal. 2019;373:446–57.

49. Tripathi M, Sahu JN, Ganesan P. Effect of process parameters on production of biochar from biomass waste through pyrolysis: A review. Renewable and Sustainable Energy Reviews. 2016;55:467–81.

50. Tan H, Lee CT, Ong PY, Wong KY, Bong CPC, Li C, et al. A Review On The Comparison Between Slow Pyrolysis And Fast Pyrolysis On The Quality Of Lignocellulosic And Lignin-Based Biochar. IOP Conf Ser Mater Sci Eng. 2021;1051:12075.

51. Zhang X, Zhang P, Yuan X, Li Y, Han L. Effect of pyrolysis temperature and correlation analysis on the yield and physicochemical properties of crop residue biochar. Bioresour Technol. 2020;296:122318.

52. Foong SY, Chan YH, Cheah WY, Kamaludin NH, Tengku Ibrahim TNB, Sonne C, et al. Progress in waste valorization using advanced pyrolysis techniques for hydrogen and gaseous fuel production. Bioresour Technol. 2021;320:124299.

53. Li X, Peng B, Liu Q, Zhang H. Microwave pyrolysis coupled with conventional pre-pyrolysis of the stalk for syngas and biochar. Bioresour Technol. 2022;348:126745.

54. Li L, Rowbotham JS, Christopher Greenwell H, Dyer PW. An Introduction to Pyrolysis and Catalytic Pyrolysis: Versatile Techniques for Biomass Conversion. New and Future Developments in Catalysis. Elsevier; 2013. p. 173–208.

55. Sekar M, Mathimani T, Alagumalai A, Chi NTL, Duc PA, Bhatia SK, et al. A review on the pyrolysis of algal biomass for biochar and bio-oil – Bottlenecks and scope. Fuel. 2021;283:119190.

56. dos Santos KJL, dos Santos GE de S, de Sá ÍMGL, Ide AH, Duarte JL da S, de Carvalho SHV, et al. Wodyetia bifurcata biochar for methylene blue removal from aqueous matrix. Bioresour Technol. 2019;293:122093.

57. Garcìa-Pèrez M, Chaala A, Roy C. Vacuum pyrolysis of sugarcane bagasse. J Anal Appl Pyrolysis. 2002;65:111–36.

58. Lam SS, Lee XY, Nam WL, Phang XY, Liew RK, Yek PNY, et al. Microwave vacuum pyrolysis conversion of waste mushroom substrate into biochar for use as growth medium in mushroom cultivation. Journal of Chemical Technology & Biotechnology. 2019;94:1406–15.

59. Kong L, Zhang L, Gu J, Gou L, Xie L, Wang Y, et al. Catalytic hydrotreatment of kraft lignin into aromatic alcohols over nickel-rhenium supported on niobium oxide catalyst. Bioresour Technol. 2020;299:122582.

60. Oh S, Lee J, Lam SS, Kwon EE, Ha J-M, Tsang DCW, et al. Fast hydropyrolysis of biomass Conversion: A comparative review. Bioresour Technol. 2021;342:126067.

61. Wang A, Song H. Maximizing the production of aromatic hydrocarbons from lignin conversion by coupling methane activation. Bioresour Technol. 2018;268:505–13.

62. Zhang J, Zheng N, Wang J. Comparative investigation of rice husk, thermoplastic bituminous coal and their blends in production of value-added gaseous and liquid products during hydropyrolysis/co-hydropyrolysis. Bioresour Technol. 2018;268:445–53.

63. Ethaib S, Omar R, Kamal SMM, Awang Biak DR, Zubaidi SL. Microwave-Assisted Pyrolysis of Biomass Waste: A Mini Review. Processes. 2020;8:1190.

64. Morgan HM, Bu Q, Liang J, Liu Y, Mao H, Shi A, et al. A review of catalytic microwave pyrolysis of lignocellulosic biomass for value-added fuel and chemicals. Bioresour Technol. 2017;230:112–21.

65. Xiang W, Zhang X, Cao C, Quan G, Wang M, Zimmerman AR, et al. Microwave-assisted pyrolysis derived biochar for volatile organic compounds treatment: Characteristics and adsorption performance. Bioresour Technol. 2022;355:127274.

66. Mendonça FG de, Cunha IT da, Soares RR, Tristão JC, Lago RM. Tuning the surface properties of biochar by thermal treatment. Bioresour Technol. 2017;246:28–33.

67. Gabhane JW, Bhange VP, Patil PD, Bankar ST, Kumar S. Recent trends in biochar production methods and its application as a soil health conditioner: a review. SN Appl Sci. 2020;2:1307.

68. Zhou Y, Qin S, Verma S, Sar T, Sarsaiya S, Ravindran B, et al. Production and beneficial impact of biochar for environmental application: A comprehensive review. Bioresour Technol. 2021;337:125451.

69. Zheng X, Zhou Y, Liu X, Fu X, Peng H, Lv S. Enhanced adsorption capacity of MgO/N-doped active carbon derived from sugarcane bagasse. Bioresour Technol. 2020;297:122413.

70. Du J, Zhang L, Liu T, Xiao R, Li R, Guo D, et al. Thermal conversion of a promising phytoremediation plant (Symphytum officinale L.) into biochar: Dynamic of potentially toxic elements and environmental acceptability assessment of the biochar. Bioresour Technol. 2019;274:73–82.

71. Yang C, Liu J, Lu S. Pyrolysis temperature affects pore characteristics of rice straw and canola stalk biochars and biochar-amended soils. Geoderma. 2021;397:115097.

72. Zhao B, O'Connor D, Zhang J, Peng T, Shen Z, Tsang DCW, et al. Effect of pyrolysis temperature, heating rate, and residence time on rapeseed stem derived biochar. J Clean Prod. 2018;174:977–87.

73. Li Y, Xing B, Ding Y, Han X, Wang S. A critical review of the production and advanced utilization of biochar via selective pyrolysis of lignocellulosic biomass. Bioresour Technol. 2020;312:123614.

74. Yaashikaa PR, Senthil Kumar P, Varjani SJ, Saravanan A. Advances in production and application of biochar from lignocellulosic feedstocks for remediation of environmental pollutants. Bioresour Technol. 2019;292:122030.

75. Fazeli Sangani M, Abrishamkesh S, Owens G. Physicochemical characteristics of biochars can be beneficially manipulated using post-pyrolyzed particle size modification. Bioresour Technol. 2020;306:123157.

76. Liao W, Thomas S. Biochar Particle Size and Post-Pyrolysis Mechanical Processing Affect Soil pH, Water Retention Capacity, and Plant Performance. Soil Syst. 2019;3:14.

77. Chen J, Li S, Liang C, Xu Q, Li Y, Qin H, et al. Response of microbial community structure and function to short-term biochar amendment in an intensively managed bamboo (Phyllostachys praecox) plantation soil: Effect of particle size and addition rate. Science of The Total Environment. 2017;574:24–33.

78. Abbas Q, Liu G, Yousaf B, Ali MU, Ullah H, Munir MAM, et al. Contrasting effects of operating conditions and biomass particle size on bulk characteristics and surface chemistry of rice husk derived-biochars. J Anal Appl Pyrolysis. 2018;134:281–92.

79. Pathomrotsakun J, Nakason K, Kraithong W, Khemthong P, Panyapinyopol B, Pavasant P. Fuel properties of biochar from torrefaction of ground coffee residue: effect of process temperature, time, and sweeping gas. Biomass Convers Biorefin. 2020;10:743–53.

80. Sessa F, Veeyee KF, Canu P. Optimization of biochar quality and yield from tropical timber industry wastes. Waste Management. 2021;131:341–9.

81. Melligan F, Auccaise R, Novotny EH, Leahy JJ, Hayes MHB, Kwapinski W. Pressurised pyrolysis of Miscanthus using a fixed bed reactor. Bioresour Technol. 2011;102:3466–70.

82. Arabiourrutia M, Lopez G, Artetxe M, Alvarez J, Bilbao J, Olazar M. Waste tyre valorization by catalytic pyrolysis – A review. Renewable and Sustainable Energy Reviews. 2020;129:109932.

83. Zhu X, Labianca C, He M, Luo Z, Wu C, You S, et al. Life-cycle assessment of pyrolysis processes for sustainable production of biochar from agro-residues. Bioresour Technol. 2022;360:127601.

84. Vieira FR, Romero Luna CM, Arce GLAF, Ávila I. Optimization of slow pyrolysis process parameters using a fixed bed reactor for biochar yield from rice husk. Biomass Bioenergy. 2020;132:105412.

85. Polin JP, Peterson CA, Whitmer LE, Smith RG, Brown RC. Process intensification of biomass fast pyrolysis through autothermal operation of a fluidized bed reactor. Appl Energy. 2019;249:276–85.

86. Garcia-Nunez JA, Pelaez-Samaniego MR, Garcia-Perez ME, Fonts I, Abrego J, Westerhof RJM, et al. Historical Developments of Pyrolysis Reactors: A Review. Energy & Fuels. 2017;31:5751–75.

87. Hu E, Tian Y, Yang Y, Dai C, Li M, Li C, et al. Pyrolysis behaviors of corn stover in new two-stage rotary kiln with baffle. J Anal Appl Pyrolysis. 2022;161:105398.

88. Campuzano F, Brown RC, Martínez JD. Auger reactors for pyrolysis of biomass and wastes. Renewable and Sustainable Energy Reviews. 2019;102:372–409.

89. Chen W, Fang Y, Li K, Chen Z, Xia M, Gong M, et al. Bamboo wastes catalytic pyrolysis with N-doped biochar catalyst for phenols products. Appl Energy. 2020;260:114242.

90. Cen K, Zhang J, Ma Z, Chen D, Zhou J, Ma H. Investigation of the relevance between biomass pyrolysis polygeneration and washing pretreatment under different severities: Water, dilute acid solution and aqueous phase bio-oil. Bioresour Technol. 2019;278:26–33.

91. Lee J, Kim K-H, Kwon EE. Biochar as a Catalyst. Renewable and Sustainable Energy Reviews. 2017;77:70–9.

92. Lee XJ, Lee LY, Gan S, Thangalazhy-Gopakumar S, Ng HK. Biochar potential evaluation of palm oil wastes through slow pyrolysis: Thermochemical characterization and pyrolytic kinetic studies. Bioresour Technol. 2017;236:155–63.

93. Xie R, Zhu Y, Zhang H, Zhang P, Han L. Effects and mechanism of pyrolysis temperature on physicochemical properties of corn stalk pellet biochar based on combined characterization approach of microcomputed tomography and chemical analysis. Bioresour Technol. 2021;329:124907.

94. Li J, Dai J, Liu G, Zhang H, Gao Z, Fu J, et al. Biochar from microwave pyrolysis of biomass: A review. Biomass Bioenergy. 2016;94:228–44.

95. Qu J, Wang S, Jin L, Liu Y, Yin R, Jiang Z, et al. Magnetic porous biochar with high specific surface area derived from microwave-assisted hydrothermal and pyrolysis treatments of water hyacinth for Cr(VI) and tetracycline adsorption from water. Bioresour Technol. 2021;340:125692.

96. Mahmoud Fodah AE, Ghosal MK, Behera D. Bio-oil and biochar from microwave-assisted catalytic pyrolysis of corn stover using sodium carbonate catalyst. Journal of the Energy Institute. 2021;94:242–51.

97. Leng L, Huang H, Li H, Li J, Zhou W. Biochar stability assessment methods: A review. Science of The Total Environment. 2019;647:210–22.

98. Xu Z, He M, Xu X, Cao X, Tsang DCW. Impacts of different activation processes on the carbon stability of biochar for oxidation resistance. Bioresour Technol. 2021;338:125555.

99. Zhang H, Liao W, Zhou X, Shao J, Chen Y, Zhang S, et al. Coeffect of pyrolysis temperature and potassium phosphate impregnation on characteristics, stability, and adsorption mechanism of phosphorus-enriched biochar. Bioresour Technol. 2022;344:126273.

100. Kozyatnyk I, Yacout DMM, Van Caneghem J, Jansson S. Comparative environmental assessment of end-of-life carbonaceous water treatment adsorbents. Bioresour Technol. 2020;302:122866.

101. Lefebvre D, Williams A, Kirk GJD, Meersmans J, Sohi S, Goglio P, et al. An anticipatory life cycle assessment of the use of biochar from sugarcane residues as a greenhouse gas removal technology. J Clean Prod. 2021;312:127764.

102. Haeldermans T, Campion L, Kuppens T, Vanreppelen K, Cuypers A, Schreurs S. A comparative techno-economic assessment of biochar production from different residue streams using conventional and microwave pyrolysis. Bioresour Technol. 2020;318:124083.

103. Ijaz M, Tahir M, Shahid M, Ul-Allah S, Sattar A, Sher A, et al. Combined application of biochar and PGPR consortia for sustainable production of wheat under semiarid conditions with a reduced dose of synthetic fertilizer. Brazilian Journal of Microbiology. 2019;50:449–58.

104. Zhu X, Li Y, Wang X. Machine learning prediction of biochar yield and carbon contents in biochar based on biomass characteristics and pyrolysis conditions. Bioresour Technol. 2019;288:121527.

105. Pathy A, Meher S, P B. Predicting algal biochar yield using eXtreme Gradient Boosting (XGB) algorithm of machine learning methods. Algal Res. 2020;50:102006.

106. Li Y, Gupta R, You S. Machine learning assisted prediction of biochar yield and composition via pyrolysis of biomass. Bioresour Technol. 2022;359:127511.

107. Chakraborty I, Sathe SM, Dubey BK, Ghangrekar MM. Waste-derived biochar: Applications and future perspective in microbial fuel cells. Bioresour Technol. 2020;312:123587.

108. Kant Bhatia S, Palai AK, Kumar A, Kant Bhatia R, Kumar Patel A, Kumar Thakur V, et al. Trends in renewable energy production employing biomass-based biochar. Bioresour Technol. 2021;340:125644.

109. Qu J, Zhang L, Zhang X, Gao L, Tian Y. Biochar combined with gypsum reduces both nitrogen and carbon losses during agricultural waste composting and enhances overall compost quality by regulating microbial activities and functions. Bioresour Technol. 2020;314:123781.

110. Akinfalabi S-I, Rashid U, Ngamcharussrivichai C, Nehdi IA. Synthesis of reusable biobased nano-catalyst from waste sugarcane bagasse for biodiesel production. Environ Technol Innov. 2020;18:100788.

111. Vamvuka D, Esser K, Komnitsas K. Investigating the Suitability of Grape Husks Biochar, Municipal Solid Wastes Compost and Mixtures of Them for Agricultural Applications to Mediterranean Soils. Resources. 2020;9:33.

112. You S, Li W, Zhang W, Lim H, Kua HW, Park Y-K, et al. Energy, economic, and environmental impacts of sustainable biochar systems in rural China. Crit Rev Environ Sci Technol. 2022;52:1063–91.

113. Han L, Ro KS, Wang Y, Sun K, Sun H, Libra JA, et al. Oxidation resistance of biochars as a function of feedstock and pyrolysis condition. Science of The Total Environment. 2018;616–617:335–44.

114. Vendra Singh S, Chaturvedi S, Dhyani VC, Kasivelu G. Pyrolysis temperature influences the characteristics of rice straw and husk biochar and sorption/desorption behaviour of their biourea composite. Bioresour Technol. 2020;314:123674.

115. Kung C-C, Kong F, Choi Y. Pyrolysis and biochar potential using crop residues and agricultural wastes in China. Ecol Indic. 2015;51:139–45.

116. Azzi ES, Karltun E, Sundberg C. Prospective Life Cycle Assessment of Large-Scale Biochar Production and Use for Negative Emissions in Stockholm. Environ Sci Technol. 2019;53:8466–76.

117. Rajabi Hamedani S, Kuppens T, Malina R, Bocci E, Colantoni A, Villarini M. Life Cycle Assessment and Environmental Valuation of Biochar Production: Two Case Studies in Belgium. Energies (Basel). 2019;12:2166.

118. Kaczor Z, Buliński Z, Werle S. Modelling approaches to waste biomass pyrolysis: a review. Renew Energy. 2020;159:427–43.

119. Wang Z, Peng X, Xia A, Shah AA, Huang Y, Zhu X, et al. The role of machine learning to boost the bioenergy and biofuels conversion. Bioresour Technol. 2022;343:126099.

120. Khan M, Ullah Z, Mašek O, Raza Naqvi S, Nouman Aslam Khan M. Artificial neural networks for the prediction of biochar yield: A comparative study of metaheuristic algorithms. Bioresour Technol. 2022;355:127215.

121. Wang Z, Tan WGY, Rangaiah GP, Wu Z. Machine learning aided model predictive control with multi-objective optimization and multi-criteria decision making. Comput Chem Eng. 2023;179:108414.

122. Duro JA, Kumar Saxena D, Deb K, Zhang Q. Machine learning based decision support for many-objective optimization problems. Neurocomputing. 2014;146:30–47.

123. Lu J, Wang Q, Zhang Z, Tang J, Cui M, Chen X, et al. Surrogate modeling-based multi-objective optimization for the integrated distillation processes. Chemical Engineering and Processing - Process Intensification. 2021;159:108224.

124. Anand A, Kumar V, Kaushal P. Biochar and its twin benefits: Crop residue management and climate change mitigation in India. Renewable and Sustainable Energy Reviews. 2022;156:111959.

125. Cao C, Wei L, Su M, Wang G, Shen J. Low-cost adsorbent derived and in situ nitrogen/iron co-doped carbon as efficient oxygen reduction catalyst in microbial fuel cells. Bioresour Technol. 2016;214:348–54.

126. Behera B, Selvam S M, Dey B, Balasubramanian P. Algal biodiesel production with engineered biochar as a heterogeneous solid acid catalyst. Bioresour Technol. 2020;310:123392.

127. Asgari S, Moazamigoodarzi H, Tsai PJ, Pal S, Zheng R, Badawy G, et al. Hybrid surrogate model for online temperature and pressure predictions in data centers. Future Generation Computer Systems. 2021;114:531–47.

128. Abd El Aziz M, Hemdan AM, Ewees AA, Elhoseny M, Shehab A, Hassanien AE, et al. Prediction of biochar yield using adaptive neuro-fuzzy inference system with particle swarm optimization. 2017 IEEE PES PowerAfrica. IEEE; 2017. p. 115–20.

129. Chen D, Liu D, Zhang H, Chen Y, Li Q. Bamboo pyrolysis using TG–FTIR and a lab-scale reactor: Analysis of pyrolysis behavior, product properties, and carbon and energy yields. Fuel. 2015;148:79–86.

130. Crombie K, Mašek O. Pyrolysis biochar systems, balance between bioenergy and carbon sequestration. GCB Bioenergy. 2015;7:349–61.

131. Crombie K, Mašek O, Sohi SP, Brownsort P, Cross A. The effect of pyrolysis conditions on biochar stability as determined by three methods. GCB Bioenergy. 2013;5:122–31.

132. Lee Y, Park J, Ryu C, Gang KS, Yang W, Park Y-K, et al. Comparison of biochar properties from biomass residues produced by slow pyrolysis at 500°C. Bioresour Technol. 2013;148:196–201.

133. Liu X, Zhang Y, Li Z, Feng R, Zhang Y. Characterization of corncob-derived biochar and pyrolysis kinetics in comparison with corn stalk and sawdust. Bioresour Technol. 2014;170:76–82.

134. Liu Z, Han G. Production of solid fuel biochar from waste biomass by low temperature pyrolysis. Fuel. 2015;158:159–65.

135. Liu Z, Niu W, Chu H, Niu Z. Process optimization for straws pyrolysis and analysis of biochar physiochemical properties. Transactions of the Chinese Society of Agricultural Engineering. 2018;34:196–203.

136. Liu Z, Zhang F, Liu H, Ba F, Yan S, Hu J. Pyrolysis/gasification of pine sawdust biomass briquettes under carbon dioxide atmosphere: Study on carbon dioxide reduction (utilization) and biochar briquettes physicochemical properties. Bioresour Technol. 2018;249:983–91.

137. Patra BR, Nanda S, Dalai AK, Meda V. Slow pyrolysis of agro-food wastes and physicochemical characterization of biofuel products. Chemosphere. 2021;285:131431.

138. Tag AT, Duman G, Ucar S, Yanik J. Effects of feedstock type and pyrolysis temperature on potential applications of biochar. J Anal Appl Pyrolysis. 2016;120:200–6.

139. Ucar S, Ozkan AR. Characterization of products from the pyrolysis of rapeseed oil cake. Bioresour Technol. 2008;99:8771–6.

140. Zhang Y, Ma Z, Zhang Q, Wang J, Ma Q, Yang Y, et al. Comparison of the physicochemical characteristics of bio-char pyrolyzed from moso bamboo and rice husk with different pyrolysis temperatures. Bioresources. 2017;12:4652–69.

141. Ascher S, Sloan W, Watson I, You S. A comprehensive artificial neural network model for gasification process prediction. Appl Energy. 2022;320:119289.

142. Bakyani AE, Sahebi H, Ghiasi MM, Mirjordavi N, Esmaeilzadeh F, Lee M, et al. Prediction of CO2–oil molecular diffusion using adaptive neuro-fuzzy inference system and particle swarm optimization technique. Fuel. 2016;181:178–87.

143. Asgari S, MirhoseiniNejad S, Moazamigoodarzi H, Gupta R, Zheng R, Puri IK. A gray-box model for real-time transient temperature predictions in data centers. Appl Therm Eng. 2021;185:116319.

144. Marx S, Chiyanzu I, Piyo N. Influence of reaction atmosphere and solvent on biochar yield and characteristics. Bioresour Technol. 2014;164:177–83.

145. Asgari S, Gupta R, Puri IK, Zheng R. A data-driven approach to simultaneous fault detection and diagnosis in data centers. Appl Soft Comput. 2021;110:107638.

146. Cao H, Xin Y, Yuan Q. Prediction of biochar yield from cattle manure pyrolysis via least squares support vector machine intelligent approach. Bioresour Technol. 2016;202:158–64.

147. IPCC. Climate Change and Land. https://www.ipcc.ch/site/assets/uploads/2019/11/SRCCL-Full-Report-Compiled-191128.pdf. 2019.

148. You S, Wang X. On the Carbon Abatement Potential and Economic Viability of Biochar Production Systems. Biochar from Biomass and Waste. Elsevier; 2019. p. 385–408.

149. El-Naggar A, Lee SS, Rinklebe J, Farooq M, Song H, Sarmah AK, et al. Biochar application to low fertility soils: A review of current status, and future prospects. Geoderma. 2019;337:536–54.

150. You S, Ok YS, Tsang DCW, Kwon EE, Wang C-H. Towards practical application of gasification: a critical review from syngas and biochar perspectives. Crit Rev Environ Sci Technol. 2018;48:1165–213.

151. Thers H, Djomo SN, Elsgaard L, Knudsen MT. Biochar potentially mitigates greenhouse gas emissions from cultivation of oilseed rape for biodiesel. Science of The Total Environment. 2019;671:180–8.

152. Mohammadi A, Cowie A, Anh Mai TL, de la Rosa RA, Kristiansen P, Brandão M, et al. Biochar use for climate-change mitigation in rice cropping systems. J Clean Prod. 2016;116:61–70.

153. Yang Q, Mašek O, Zhao L, Nan H, Yu S, Yin J, et al. Country-level potential of carbon sequestration and environmental benefits by utilizing crop residues for biochar implementation. Appl Energy. 2021;282:116275.

154. Ipharmachine. Cone Mill Machine CFZ-150. https://www.ipharmachine.com/granulator-cfz-150. 2023.

155. TG-MACHINES. Rotary Disc Dryer – RDD. https://tg-machines.com/images/biblioteka/282/zalaczniki/rendering_rotary_disc_dryer_ver._1.3_en.pdf. 2022.

156. Bestongroup. Beston Pyrolysis Plant. https://www.bestongroup.net. 2022.

157. IPCC. Appendix 4 Method for Estimating the Change in Mineral Soil Organic Carbon Stocks from Biochar Amendments: Basis for Future Methodological Development. https://www.ipcc-nggip.iges.or.jp/public/2019rf/pdf/4_Volume4/19R_V4_Ch02_Ap4_Biochar.pdf. 2019.

158. Brentrup F, Hoxha A, Christensen B. Carbon footprint analysis of mineral fertilizer production in Europe and other world regions [Internet]. 2016. Available from: https://www.researchgate.net/publication/312553933

159. Han Z, Lin H, Xu P, Li Z, Wang J, Zou J. Impact of organic fertilizer substitution and biochar amendment on net greenhouse gas budget in a tea plantation. Agric Ecosyst Environ. 2022;326:107779.

160. Kaur N, Kieffer C, Ren W, Hui D. How much is soil nitrous oxide emission reduced with biochar application? An evaluation of meta-analyses. GCB Bioenergy. 2023;15:24–37.

161. Food and Agriculture Organization. Optimizing Nitrogen use on the farm. https://www.fao.org/3/Y5146E/y5146e09.htm#:~:text=%3E%20e.g.%202%20t%20ha,1%20required. 2003.

162. Kumar R, Karmakar S, Minz A, Singh J, Kumar A, Kumar A. Assessment of Greenhouse Gases Emission in Maize-Wheat Cropping System Under Varied N Fertilizer Application Using Cool Farm Tool. Front Environ Sci. 2021;9.

163. Gupta R, McRoberts R, Yu Z, Smith C, Sloan W, You S. Life cycle assessment of biodiesel production from rapeseed oil: Influence of process parameters and scale. Bioresour Technol. 2022;360:127532.

164. Deb K, Pratap A, Agarwal S, Meyarivan T. A fast and elitist multiobjective genetic algorithm: NSGA-II. IEEE transactions on evolutionary computation. 2002;6:182–97.

165. Zhang S, Liu S, Zhai R. An extended GRA method for MCDM with interval-valued triangular fuzzy assessments and unknown weights. Comput Ind Eng. 2011;61:1336–41.

166. Wang J, Wei G, Wei C, Wei Y. MABAC method for multiple attribute group decision making under q-rung orthopair fuzzy environment. Defence Technology. 2020;16:208–16.

167. Wang Z, Rangaiah GP, Wang X. Preference Ranking on the Basis of Ideal-Average Distance Method for Multi-Criteria Decision-Making. Ind Eng Chem Res. 2021;60:11216–30.

168. Wang P, Zhu Z, Wang Y. A novel hybrid MCDM model combining the SAW, TOPSIS and GRA methods based on experimental design. Inf Sci (N Y). 2016;345:27–45.

169. Chakraborty S. TOPSIS and Modified TOPSIS: A comparative analysis. Decision Analytics Journal. 2022;2:100021.

170. Lolli F, Ishizaka A, Gamberini R, Rimini B, Messori M. FlowSort-GDSS – A novel group multi-criteria decision support system for sorting problems with application to FMEA. Expert Syst Appl. 2015;42:6342–9.